The Role of FGFR3 in Mesenchymal Stromal Cells

Amy Wells

MSc by Research

University of York

Biology

December 2021

Abstract

Fibroblast growth factor (FGF) signalling regulates all stages of skeletal development, from embryonic mesenchymal condensation to adult bone homeostasis. Mutations in FGF receptors (FGFRs) are a common cause of skeletal disorders, as their signalling is indispensable for normal bone development. The unique function of FGFR3 as an inhibitor of postnatal bone growth underlies the pathology of several skeletal dysplasias. However, the effects of FGFR3 mutations in mesenchymal stromal cells (MSCs), the progenitors from which the skeletal system develops, are understudied.

This project aimed to understand the role of FGFR3 on a cellular level using an FGFR3-knockout (FGFR3-KO) MSC line. Wild type (WT) and FGFR3-KO MSCs were compared to determine the effects of FGFR3 deletion on MSC proliferation, morphology, migration, transcriptome, and secretome.

FGFR3-KO MSCs had an increased proliferative and migratory capability, but a decreased differentiation capacity compared to WT MSCs. Transcriptomic analysis showed markedly altered expression of transcripts encoding proteins associated with the actin cytoskeleton, extracellular region, and extracellular matrix ($q<0.0001$ for all). Accordingly, FGFR3-KO MSCs showed an altered morphology characterised by a round cell shape with broad lamellipodia. FGFR3-KO MSCs secreted greater numbers of extracellular vesicles, which were larger than those produced by WT MSCs. Conditioned media from FGFR3-KO MSCs, but not WT MSCs, promoted wound healing of WT MSCs ($p<0.0001$ and $p=0.0769$ respectively), demonstrating an altered secretome. Finally, FGFR3-KO MSCs were resistant to serumstarvation, and proliferated in the absence of FBS supplementation, unlike WT MSCs.

The striking phenotype and behaviours of FGFR3-KO MSCs described in this thesis demonstrates the importance of FGFR3 signalling in MSCs. This serves to advance the understanding of signalling pathways in MSCs, as well as the cellular mechanisms underlying FGFR3-related disorders.

List of Contents

List of Tables

List of Figures

Acknowledgements

Firstly, I would like to thank my supervisor Paul Genever, for his guidance and support throughout this project. I would also like to thank Dani Ungar for his feedback and suggestions as a member of my thesis advisory panel.

I am grateful to all the members of the Genever group for providing the warmest welcome to the lab and sharing their knowledge and encouragement throughout the year. I would particularly like to thank Alasdair, for imparting his cell culture wisdom from day one; Jordan, my chondrogenesis partner in crime; and Savvas, an unfaltering source of support and expert on everything EVs!

Thank you to all of my friends, who have been wonderful supporters, especially Cam with his insightful conversation and enthusiasm for all things FGFs, and Sophie with a constant belief in me and my work. Most of all, I am thankful for my partner Harry, whose support has kept me going through the highs and lows of the year.

Declaration

I declare that this thesis is a presentation of original work and I am the sole author. All experiments were performed by the author with the exception of the RNA-seq data, which was collected by Alice Carstairs, a previous PhD student in the Genever lab, andprocessed by members of staff at the University of York Bioscience Technology Facility. All subsequent pathway and enrichment analysis of the RNA-seq data was performed by the author. Additionally, the ptychographic study of migration was performed by AliceCarstairs, and nanoparticle tracking analysis was performed by Savvas Ioannou.
Subsequent data analysis for both was performed by the author. Transmission electron microscopy preparation was carried out by Clare Steele-King of the University of York Bioscience Technology Facility and imaging was conducted alongside the author. Thiswork has not previously been presented for an award at this, or any other, University.
All sources are acknowledged as references.

Chapter 1: Introduction

1.1 Fibroblast Growth Factor Signalling

Fibroblast growth factors (FGFs) and their receptors (FGFRs) play crucial roles in embryonic development and adult tissue homeostasis by initiating a variety of intracellular signalling pathways. In humans, there are 22 FGF ligands, which interact with 4 receptors belonging to the receptor tyrosine kinase superfamily. FGFR1, 2 and 3 have multiple isoforms, generating receptor variants that are differentially expressed throughout tissues, and have differential ligand binding affinity (Miki et al., 1992; Hughes, 1997). This enables FGF signalling to have a huge range of context-dependent functions, determined by the tissue, cell type, and ligand-receptor pairing.

In embryonic development, FGF signalling mediates growth, survival, differentiation and patterning, and thus drives developmental events from early mesoderm induction through to formation of organ systems (Turner and Grose, 2010). In adult tissues, FGF signalling often reactivates developmental pathways to allow tissue repair and regeneration, playing key roles in the wound response by regulating processes such as migration and proliferation (Floss et al., 1997; Meyer et al., 2012). However, the fact that FGFs underpin so many biological processes means that their disrupted signalling is a major cause of human disease. FGFR mutations are unusually common. Three of the highest germline point mutation rates described in humans occur in FGFRs: G380R in FGFR3, P250R in FGFR3, and S252W in FGFR2, causing achondroplasia, coronal craniosynostosis, and Apert syndrome respectively (Wilkie, 1997). A wide range of FGFR mutations have been reported in many other diseases, including a variety of cancers, where oncogenic function is often a result of overactive or overexpressed FGFRs, which may occur due to gene amplification, translocation, single nucleotide polymorphisms, or aberrant splicing (Helsten et al., 2016).

1.2 Fibroblast Growth Factor Receptor Family

FGFRs are located on the plasma membrane, and upon interaction with their ligands, dimerise, resulting in autophosphorylation of intracellular tyrosine residues. This leads to activation of many signalling pathways, including JAK/STAT, PLCγ, PI3K and MAPK/ERK (Eswarakumar et al., 2005) (Fig. 1.1). All secreted (canonical) FGFs require a heparin-based cofactor in order to confer signalling activity through FGFRs.

The heparin cofactor stabilises the FGF:FGFR complex and allows sustained activation of the receptor. Cofactors may be transmembrane proteins, such as syndecans, cell-surface anchored proteins, such as glypicans, or diffusible proteins in the extracellular matrix (ECM), such as perlecan and agrin. These heparan sulfate proteoglycans (HSPGs) can bind and tether FGFs to the cell surface immediately following their secretion, which supports local retention and activation of signalling (Shimokawa et al., 2011). HSPGs can serve as co-receptors, like heparin alone, to facilitate FGFR activity, but are also well-characterised as negative regulators of FGF signalling. Sequestration of FGF ligands by HSPGs in the extracellular space limits their diffusion distance and creates strong morphogenic gradients, typical of growth factor signalling (Yan and Lin, 2009). This sequestration is reversible, with HSPGs sometimes acting as a reservoir for FGF ligands until they are cleaved and released into the matrix by sheddases and heparinases (Kato et al., 1998; Hou et al., 2007). Finally, HSPGs can promote endocytosis of the activated FGF:FGFR complex (Elfenbein et al., 2012), leading to either lysosomal degradation, receptor recycling, or continued signalling from the surface of the endosomal membrane. This variety of regulatory pathways allows tight control of FGF signals.

Since the pathways downstream of each FGFR are largely overlapping, in many contexts there is redundancy or co-operative action between the receptors. However, each receptor has specific, and tightly regulated, spatial and temporal expression throughout development, indicating distinct functions (Hughes, 1997). Accordingly, unique phenotypes are seen when individual receptors are disrupted in mouse models (reviewed in Su et al., 2014). Further exemplifying this is the fact that different disorders, with distinct phenotypes, are caused by identical mutations in each FGFR. Within the linker region of immunoglobulin domains II and III, proline to arginine mutations cause Pfeiffer syndrome in FGFR1, Apert syndrome in FGFR2, and Muenke syndrome in FGFR3 (Wilkie, 1997). All three disorders are classed as skeletal dysostoses, as is the aforementioned coronal craniosynostosis. Dysostoses are skeletal disorders characterised by abnormalities in a specific group of bones, commonly those of the skull. FGFR mutations are also the cause of several skeletal dysplasias, such as the earlier mentioned achondroplasia, which differ from dysostoses in that abnormalities in bone and/or cartilage are more generalised throughout the skeleton (Krakow, 2015).

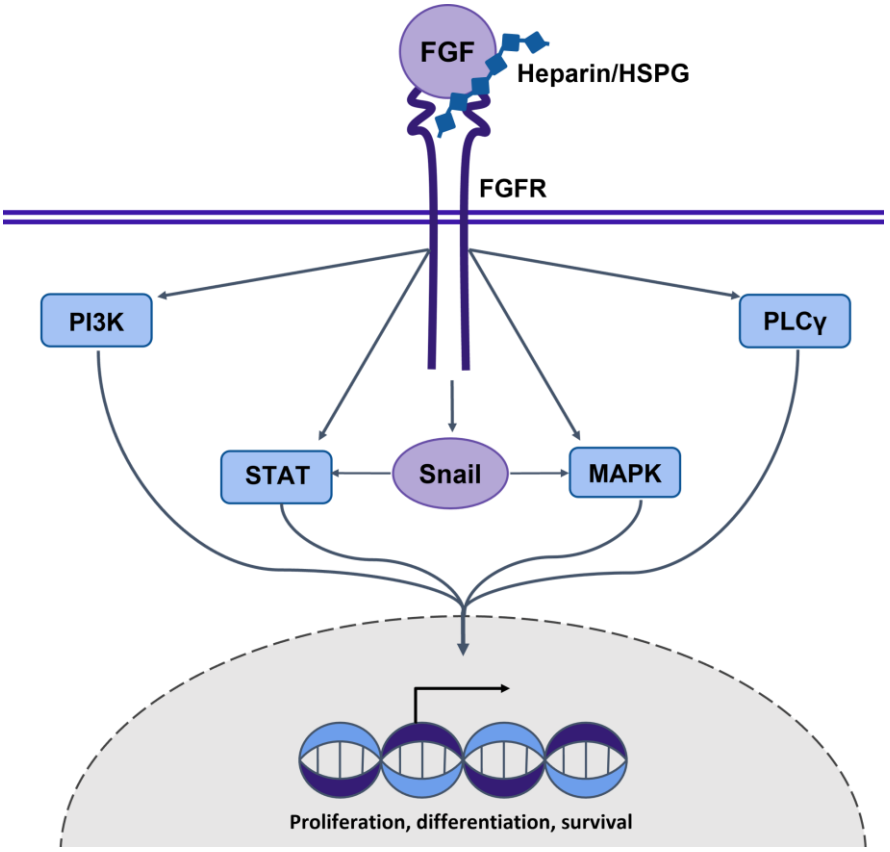

Figure 1.1 Overview of the FGF signalling pathway. Binding of an FGF ligand, along with a heparin-based cofactor, to an FGFR causes activation of intracellular signalling pathways. These are primarily PI3K, PLC$_\gamma$, STAT, and MAPK. The STAT and MAPK pathways may be activated directly or through mediators such as Snail. These signalling cascades result in changes to gene expression that regulate cell behaviours such as proliferation, differentiation, and survival.

1.3 FGF Signalling in Skeletal Development

1.3.1 The roles of FGFRs throughout skeletal development

Due to the skeletal disorders caused by mutations in FGFRs, it is no surprise FGF signalling is required for normal skeletal development. Indeed, FGF signalling regulates all stages of bone formation and growth, as well as mineral homeostasis (Wöhrle et al., 2011) and remodelling in adult bones (Behr et al., 2010).

Bone formation occurs by two distinct mechanisms, but both begin with condensation of mesenchymal cells. The initiation and maintenance of mesenchymal condensation relies on FGF signalling; precise spatial and temporal coordination of FGF/FGFR expression regulates mesenchymal proliferation, survival, and competence to

differentiate (Revest et al., 2001; Verheyden et al., 2005; Yu and Ornitz, 2008). Intramembranous ossification is the direct formation of bone from condensed mesenchyme, requiring signalling primarily through FGFR1 and 2, and produces the bones of the skull, face, and clavicles. The rest of the skeleton is formed by endochondral ossification, which sees cells in the condensed mesenchyme differentiate into chondrocytes. These chondrocytes express matrix proteins such as aggrecan and Type II collagen, forming a cartilaginous template that will later become bone. Once the template is formed, the chondrocytes rapidly proliferate, driven by activation of FGFR3, to drive growth of the skeletal elements. FGFR3 expression then decreases in favour of FGFR1 expression, enabling the proliferating chondrocytes to differentiate into hypertrophic chondrocytes, which secrete Type X collagen (Linsenmayer et al., 1991). As hypertrophy occurs, chondrocytes secrete matrix metalloproteinases (MMPs) to facilitate vascular invasion of the cartilage template (Vu et al., 1998; Inada et al., 2004). This allows osteoprogenitor cells, expressing high levels of FGFR2, to establish the primary ossification centre. Throughout embryonic development, the primary ossification centre expands bidirectionally until the cartilage template is replaced with trabecular bone. This occurs by sequential proliferation, hypertrophy, and apoptosis of chondrocytes, until they reside solely in the growth plate, and the bone is populated by osteoblasts, osteoclasts, and endothelial cells.

Postnatally, the secondary ossification centre is established, and vasculature throughout the bone continues to grow, allowing remodelling of trabecular bone to form the marrow cavity (Ornitz and Marie, 2015). FGFR expression patterns remain largely unchanged, with FGFRs 1 and 2 expressed in trabecular bone, perichondrium and periosteum. FGFR1 is highly expressed in hypertrophic chondrocytes, and FGFR3 expression is most intense in the proliferating chondrocytes. However, a key change occurs in the role of FGFR3 after formation of the secondary ossification centre, whereby it stops functioning as a mitogenic signal and instead is an inhibitor of chondrocyte proliferation. This inhibitory activity underlies the pathology of the most common group of skeletal dysplasias- achondroplasias- in which constitutively active FGFR3 causes decreased chondrocyte proliferation during postnatal growth, resulting in skeletal dwarfism.

1.3.2 FGFR3 in skeletal development and dysplasia

The achondroplasia group of skeletal dysplasias comprises of four disorders: achondroplasia, hypochondroplasia, severe achondroplasia with developmental delay and acanthosis nigricans (SADDAN) and thanatophoric dysplasia. All four are caused by gain-of-function FGFR3 mutations, and their common feature is short stature due to disruption of long bone growth. Achondroplasia is the most common non-lethal skeletal dysplasia, although complications such as accumulation of cerebrospinal fluid in the brain can reduce life expectancy (Hunter et al., 1998). In 97% of cases, achondroplasia results from a substitution mutation of arginine for glycine within the transmembrane domain of FGFR3 (Gly380Arg), rendering the receptor capable of ligand-independent dimerisation (Rousseau et al., 1994; Bellus et al., 1995). The genetic homogeneity of the disorder is hypothesised to be the reason for little variability in the achondroplastic phenotype, which is characterised by short limbs and macrocephaly. Hypochondroplasia is a similar, but milder and more heterogeneous condition, caused by a number of different mutations. SADDAN dysplasia is caused by a Lys650Met substitution, and shares the restriction of bone growth seen in achondroplasia patients, but is accompanied by unique phenotypes, including tibial bowing, structural abnormalities of the brain, and progressive acanthosis nigricans (Tavormina et al., 1999). Interestingly, a substitution in the same position to (Lys650Glu) is one of the causes of thanatophoric dysplasia. Thanatophoric dysplasia is classified into two subtypes (TDI and TDII), and is the most common neonatal lethal skeletal dysplasia. Those that survive birth often suffer respiratory difficulties, leading to a high infant mortality rate (Tavormina et al., 1995).

Despite these dramatic phenotypes and complications caused by FGFR3 mutation, understanding of the mechanisms behind these disorders is limited, and thus options for therapies are poor. The mechanisms by which these mutations lead to activation of FGFR3, and how this leads to dysplasia phenotypes, have been extensively studied. It is understood FGFR3 is a negative regulator of skeletal growth, unlike FGFRs 1 and 2, which are considered mitogenic, and their loss causes undergrowth of the bones, particularly the limbs (Perantoni et al., 2005). Accordingly, a rare loss-of-function FGFR3 mutation causes camptodactyly, tall stature, and hearing loss (CATSHL) syndrome, which has been identified in just three families worldwide to date, and one of its defining features is overgrowth of long bones.

FGFR3 inhibits both chondrocyte proliferation and differentiation postnatally, leading to a decrease in matrix production and bone growth, and thus much research has focused

on the downstream signalling of FGFR3 in chondrocytes specifically. However, FGFR3 mutations also result in at least three craniosynostosis syndromes, which are characterised by premature ossification, indicating a role for FGFR3 in osteogenesis as well as chondrogenesis. Indeed, FGFR3-null mice show osteopenia (Valverde-Franco et al., 2003).

Both chondrocytes and osteoblasts, along with other cellular components of the skeletal system, are derived from mesenchymal stem/stromal cells (MSCs), and whilst there is a wealth of - albeit conflicting - research into the effects of FGFR3 in chondrocytes, our understanding of its impacts in their MSC progenitors is lacking. Therapeutic approaches in development for achondroplasia disorders focus on remedying chondrocyte behaviour. However, a small body of research suggests overactivation of FGFR3 has disruptive effects on MSCs, and thus the pathogenesis of achondroplasia likely begins before chondrocytes are even formed, and would likely remain even if chondrocyte behaviour could be corrected. Su et al. (2010) found that an activating FGFR3 mutation decreased proliferation in MSCs. In their murine model, this decrease in proliferation, along with decreased bone mineralisation and increased resorption, recapitulated the achondroplasia phenotype. However, the extent to which these effects can be attributed to FGFR3 were clouded by an upregulation of FGFR1 in this model, and it has been proposed that FGFR1 may indirectly contribute to the pathogenesis of skeletal disorders in mouse models (Valverde-Franco et al., 2003). To elucidate the function of FGFR3 in MSCs a more effective model is required, however a number of factors confounds their use.

1.4 Mesenchymal Stromal Cells

1.4.1 Uses and complications

MSCs are multipotent cells capable of self-renewal and differentiation into adipogenic, chondrogenic and osteogenic lineages. Functions outside of ‘stemness’ have also been characterised, including immunomodulation (Nauta and Fibbe, 2007) and haematopoietic support (Majumdar et al., 2000). As such, they hold promising therapeutic potential, and show regenerative and anti-inflammatory effects in many disease models and clinical trials (Horwitz et al., 2002; Rojas et al., 2005).

However, the many possible uses of MSCs are hindered in a number of ways. Primary MSCs can be isolated from a wide range of tissue sources, and their therapeutic

potential is dependent on both the source and the isolation method used (Bortolotti et al., 2015). Even when isolated from the same donor tissue, MSCs are highly heterogeneous populations, with distinct subtypes of cells that have varying functions (James et al., 2015). For example, MSCs from endosteal bone marrow showed reduced expression of cell cycle inhibitors and therefore increased proliferative capacity, compared to MSCs from central bone marrow from the same murine donor (Siclari et al., 2013). This was accompanied by greater immunosuppressive activity in an inflammatory bowel disease model, thus demonstrating the differing therapeutic potential of MSCs. As well as this, there is debate over the classification and characterisation of MSCs, and it is likely that uncharacterised MSC subtypes still remain (Rostovskaya and Anastassiadis, 2012). ISCT criteria distinguish MSCs from other cell types by their expression (or lack of expression) of surface proteins, adherence to plastic, and differentiation capacity (Dominici et al., 2006). However, these are described as “minimal criteria”, and rightly so, since isolation of MSCs by these criteria produce nonclonal, heterogenous cultures, which as described above, have varied therapeutic uses due to their differing proliferation, differentiation, and migration rates (Squillaro et al., 2016). For cellular therapies, a consistent set of MSCs would be required, with clearly defined properties and little variation. This is hard to obtain with primary MSCs, and limited further by short lifespans before replicative senescence occurs.

1.4.2 Immortalised clonal MSC lines

To overcome the short, finite lifespan of primary MSCs, hTERT overexpression has been used to produce stable, immortal cell lines. This also allows for clonal isolation of MSC subtypes, enabling their thorough characterisation, as reported by James et al. (2015). These subtypes vary in their differentiation and immunomodulatory capacity, and have distinct molecular and biophysical markers. Of the subtypes characterized by James et al., the cell line Y201, derived from adult bone marrow stromal cells, are described as having ‘typical’ MSC characteristics, including strong tripotency, a fibroblastoid morphology and a migratory phenotype. Immortalised MSC lines also reduce the effect of passage, with Y201 cells shown to maintain growth for over 100 population doublings, compared to primary MSCs, which show senescence-associated growth arrest after 24-40 doublings, dependent on donor age (Stenderup et al., 2003).

As well as immortalised cell lines reducing the need to extract MSCs from primary sources and minimising heterogeneity, they have the potential to be genetically

modified to model disease pathologies at the cellular level. Their immortalisation provides a theoretically limitless supply of clonal cells, and thus boasts many advantages as a model system. This underpinned the rationale for the creation of an immortalised, clonal, FGFR3-knockout (KO) cell line, derived from the Y201 line.

1.4.3 FGFR3-KO MSCs

To elucidate the role FGFR3 plays in MSCs, Y201 cells (hereafter referred to as wild type cells) were edited by use of CRISPR/Cas9 to generate a mutation in the FGFR3 gene (Carstairs, 2017). This mutation introduces a premature stop codon, predicted to generate a truncation of the protein within the third immunoglobulin domain, therefore containing no kinase domain to confer signalling activity (Fig. 1.2). RNA-seq and western blot results supported that FGFR3 expression was lost as a result of the mutation. These FGFR3-knockout cells (FGFR3-KOs) showed an increased migratory response, but altered collective cell migration (Carstairs, 2017). Collective cell migration is the pattern bywhich large numbers of cells move during processes such as gastrulation and wound healing, allowing the maintenance of strong cell:cell interactions (Collins and Nelson, 2015). The cells will typically follow a group of leader cells, which produce MMPs to clear a path for the following cells (Parri and Chiarugi, 2010). WT MSCs migrate collectively, with leading cells protruding into the wound space, forming an arc shape as they move, and follower cells lined up behind the leaders. This coordination appears lost in FGFR3-KOs, with no clear leader or follower cells, and no distinct patterns of movement observed. This loss of coordination indicates a change to cell:cell communication, with the signals for leader-follower behaviour either no longer being produced, or not being responded to. One such signalling event involved in directing migration is the release of extracellular vesicles (EVs), which can act on neighbouring cells to promote chemotaxis (Kriebel et al., 2018). Indeed, many components of the MSC secretome have the capability to influence a wide range of cell behaviours, including migration, as well as proliferation and differentiation (Osugi et al., 2012; Ogata et al., 2018). The release of factors such as VEGF, MCP-1, and other cytokines, is key in driving these processes (Marolt Presen et al., 2019).

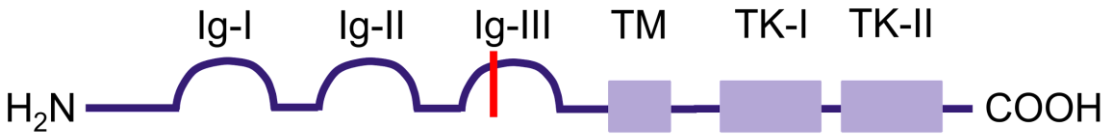

Figure 1.2. Schematic representation of the FGFR3 protein. Red line indicates where the premature stop codon in FGFR3-KO MSCs truncates the third immunoglobulin domain, meaning the downstream transmembrane and tyrosine kinase domains are lost.

1.5 The MSC Secretome

The secretome is comprised of all factors secreted by MSCs, including soluble molecules such as proteins, and lipid-delimited EVs, which themselves can carry a wide variety of bioactive molecules such as cytokines, RNAs, and lipids (Yáñez-Mó et al., 2015). EVs are considered to fall into different categories based on their size and biogenesis, the two main ones being exosomes and microvesicles. Exosomes are roughly 50-100nm in diameter and formed from the multivesicular body fusing with the plasma membrane, whereas microvesicles are 100-1000nm and formed by outward budding of the plasma membrane (Biancone et al., 2012). However, the distinction between subtypes of extracellular vesicles is clouded by challenges in isolating these particles- many experimental procedures struggle with yield, purity, or scalability- and therefore isolating a homogenous population for analysis is difficult (Xu, R. et al., 2016). Additionally, within the same subclass of EVs, distinct populations have been identified (Tauro et al., 2013). These share identical size and morphological properties, and expression of exosomal markers, but differing proteomic profiles and miRNA signatures (Ji et al., 2014). Research in the field is still emerging, but it is increasingly apparent that the classification of EVs is not clear-cut.

EVs transport bioactive cargo between cells, and also carry receptors on the vesicle surface that can elicit responses from target cells without fusion of the membranes, by juxtacrine signalling (Segura et al., 2007). EV cargo is determined by the cell type producing the EV, and itsphysiological/pathological state (Baffour et al., 2015). As such, the secretome of cells in a diseased state, such as tumour cells, have a drastically altered secretome in comparison to healthy cells (Graves et al., 2004; Safaei et al., 2005). It is therefore possible that FGFR3-KOs have a secretome that deviates from that of WT MSCs, which may shed insight into the secretome of skeletal

dysplasia cells. This secretome may be a driver of the disease pathology, and may impede the use of MSC therapies ifso. Conversely, the WT MSC secretome may be able to correct some of the altered behaviours of FGFR3-KOs. Indeed, EVs and other components of the MSC secretome have been shown to have therapeutic effects in an number of disease models, including skeletal disorders (Xu, J. et al., 2016; Marolt Presen et al., 2019), and have been hypothesised to be effective in achondroplasia (Sagar et al., 2018). Studies have shown EVs capable of resolving bone defects by increasing angiogenesis (Qi et al., 2016), osteogenesis (Qin et al., 2016), and cartilage formation (Zhang et al., 2016). MicroRNAs such as miR-196a have been proposed as one of the mediators of such therapeutic effects, but the full molecular mechanisms remain unclear. Regardless, the MSC secretome is now a focus of therapeutic research, as the regenerative properties of MSCs have been largely attributed to paracrine effects, leading to the suggestion to rename them ‘medicinal signaling cells’ (Caplan, 2017).

1.6 Project Aims

This project aims to undertake a thorough comparison of WT and FGFR3-KO MSCs, in order to understand the role of FGFR3 in MSC behaviour.

The specific aims of this project will be to:

- Compare the morphology, growth, migration, and gene expression of WT and FGFR3-KO cells, and investigate the mechanisms by which any differences between the cell lines arise.
- Isolate and characterise EVs from FGFR3-KOs.
- Determine the effects of FGFR3-KO EVs and the wider FGFR3-KO secretome on MSC behaviours, including morphology, migration and proliferation.

Chapter 2: Materials and Methods

2.1 Cell Culture

2.1.1 MSC Culture

Y201 hTERT MSCs described by James et al. (2015) were used as a Wild Type control to the FGFR3-KO cells and are referred to as WT cells throughout. FGFR3-KO MSCs were generated by Carstairs (2017) using CRISPR/Cas9 modification of the WT line. Cryopreserved stocks of both cell lines were provided by Paul Genever.

WT and FGFR3-KO MSCs were cultured in Dulbecco's Modified Eagle Medium (DMEM) (Gibco), supplemented with 10% Fetal bovine serum (FBS) and 1% penicillin/streptomycin (P/S), and incubated at 37℃ and 5% CO_2. Cells were washed with Phosphate Buffered Saline (PBS) and passaged using Trypsin-EDTA 0.05% upon reaching approximately 80% confluency.

2.1.2 CFU-F Assay

WT and FGFR3-KO cells were plated at 10 cells per cm^2 in six well plates in DMEM containing 20% Hyclone FBS and 1% P/S. Plates were incubated for 10 days, with media changes every 3-4 days, and stained with crystal violet at the end of the timecourse. For crystal violet staining, cells were washed with PBS before 0.5% crystal violet in dH_2O with 20% MeOH was applied for 20 minutes at room temperature.

2.1.3 Population Doubling Time Calculations

Population doubling time was determined by seeding equal numbers of WT and FGFR3-KO MSCs in T25 flasks, and counting cell number each day for 4 days. Cells were counted using Countess II Automated Cell Counter (Invitrogen) using trypan blue cell exclusion dye to discount dead cells. Doubling time was calculated using the formula:

$$t * log(Nf/Ni)$$

Where *t* is time in days between counts, *Nf* is the final number of cells counted, and *Ni* is the initial number of cells.

For cumulative population doublings, cells were counted at each passage for 50 days of continuous culture, and the number of population doublings between each count was calculated using the formula:

$$log(Nf/Ni)$$

Where *Nf* is the final number of cells counted, and *Ni* is the initial number of cells seeded. 500,000 cells were reseeded after each count for both WT and FGFR3-KO MSCs.

2.2 Morphological Analyses

2.2.1 Cell Seeding and Treatments

For initial morphological analysis in section 3.1.2, WT and FGFR3-KO cells were seeded in a 24 well plate at 4000 cells per cm². For morphological analysis at different confluencies in section 3.3.1, WT and FGFR3-KO cells were seeded at 7000, 14000, 21000, 28000, and 35000 cells per cm², with complete confluency seen at 35000 cells/cm². In both cases, cells were allowed to adhere overnight before washing with PBS and staining with crystal violet.

To examine the dependence of morphology on the Rac signalling pathway, WT and FGFR3-KO cells were seeded at 4000 cells per cm² in a 24 well plate, and allowed to adhere overnight. Media was removed and Rac inhibitor NSC23766 (Selleck) in DMSO was added to fresh media to a final concentration of 1µM. After 1 hour, this was replaced with fresh media. This pulse treatment cycle was done once a day for four days, and on the final day cells were washed with PBS and stained with crystal violet.

For serum free morphological analysis, WT and FGFR3-KO cells were seeded at 2000 cells per cm² in a 24 well plate and allowed to adhere overnight. Media was then replaced with serum-free media containing 1% P/S, and cells incubated for a further 48 hours before washing with PBS and staining with crystal violet.

2.2.2 Phalloidin Staining of the Actin Cytoskeleton

WT and FGFR3-KO cells were seeded on 10mm circular glass coverslips in 24 well plates at 4000 cells per cm² and allowed to adhere overnight. Coverslips were washed with PBS and fixed with 4% paraformaldehyde for 20 minutes at 37°C and 5% CO_2. Cells were washed again with PBS and treated with Alexa Fluor 594 Phalloidin (Invitrogen) at 1:1000 dilution in PBS; for 1 hour in the dark at room temperature. Cells were washed three times with PBS then counterstained with 2µg/ml DAPI for 5 minutes before a further three PBS washes. Coverslips were mounted onto slides with Vectashield

Mounting Medium (Vector Laboratories) and sealed with nail varnish before imaging the following day with a Zeiss 710LSM confocal microscope.

2.2.3 CellProfiler Pipeline Design

CellProfiler (McQuin et al., 2018) was used to determine cell size and shape metrics from brightfield images of crystal violet stained cells and confocal images of Phalloidin stained cells. Images were coloured to grey, and the 'Identify Primary Objects' function used to segment the cells with Two-Class Otsu thresholding. Cell size and shape metrics were exported and the following formulas used for downstream analysis:

Length:width ratio:

$$Major\ axis\ length/minor\ axis\ length$$

Roundness:

$$(4 * Area)/(\pi * Major\ axis^{2})$$

2.2.4 Anti-Arp3 Immunofluorescence

Cells were seeded and fixed as described in section 2.2.2, then permeabilised with 0.1% Triton X-100 for 30 minutes before washing three times with PBS. Cells were blocked with 1% bovine serum albumin for 1 hour, before Anti-Arp3 (Sigma) was applied at 1:200 dilution in 1% BSA for 2 hours at room temperature. Cells were washed in PBS. Goat anti-mouse Alexa Fluor 647 conjugated secondary antibody (Thermofisher) was applied at 1:200 alongside Alexa Fluor 594 Phalloidin (Invitrogen) at 1:1000 in PBS for 1 hour, at room temperature in the dark. Cells were washed in PBS and counterstained with DAPI, mounted and imaged as above.

2.3 Characterisation of Extracellular Vesicles

2.3.1 Conditioned Media Collection and Extracellular Vesicle Isolation

FBS-EV depleted media was generated by centrifugation of DMEM containing 20% FBS and 1% P/S at 100,000g for 18 hours at 4℃, using a Ty45i rotor in a Beckman Coulter Optima L-100XP Ultracentrifuge. This FBS-EV depleted media was then diluted with serum-free media containing 1% P/S, to a final concentration of 10% FBS.

WT and FGFR3-KO cells were seeded at 500,000 and 400,000 cells respectively per T175 flask in FBS-EV depleted media and cultured until reaching approximately 90% confluency. Cells were washed three times with PBS, and FBS-EV depleted media was replaced with serum-free media. After 24 hours, media was collected, fresh serum free media added, and collected after a further 24 hours. Cells were detached and counted to determine EV yield per million cells at the time of media collection. This conditioned media (CM) was stored at -70℃.

CM was centrifuged at 300g for 5 minutes to remove cells and debris. The supernatant was either used for CM treatments or to isolate EVs. For EV isolation, the media was centrifuged at 2000g for 20 minutes, the supernatant transferred into Ty45i tubes, and the pellet resuspended in PBS. The resuspended pellet was transferred into a protein low-binding tube and centrifuged again at 2000g for 20 minutes. The supernatant was discarded and the pellet is the isolated 2k fraction. The transferred supernatant from the first 2000g spin was centrifuged at 10,000g for 45 minutes, and the new supernatant transferred into fresh Ty45i tubes. The pellet was resuspended and transferred into micro-ultracentrifuge tubes, and centrifuged in a TLA 100.3 rotor at 10,000g for 45 minutes to isolate the 10k fraction. The transferred supernatant from the first 10,000g spin was centrifuged at 100,000g for 90 minutes and the supernatant kept (for use as EV-negative media). The pellet was resuspended, transferred to micro-ultracentrifuge tubes, and centrifuged again at 100,000g for 90 minutes to isolate the 100k fraction. All pellets were thoroughly resuspended in particle-free PBS, and all centrifugations were performed at 4℃.

2.3.2 Nanoparticle Tracking Analysis

Nanoparticle tracking analysis (NTA) was conducted with the Nanosight LM14 equipped with a green laser (532nm) and sCMOS camera. Isolated EV fractions were diluted in sterile-filtered PBS to a concentration of 20-120 particles per frame. Five 60 second video recordings were taken of all events for further analysis. The experimental conditions were as follows: i) Measuring time: 5X 60s, ii) Blur: Auto, iii) Detection Threshold: 4-5, iv) Blur size: Auto, iv) Number of frames: 1499. Downstream analysis was performed using Nanosight NTA Software 3.4 Build 3.4.003 (Malvern Panalytical).

2.3.3 Transmission Electron Microscopy

EV isolation was performed as described in 2.3.1, except instead of resuspending the final pellets in PBS, pellets were resuspended in 2% PFA and kept at 4℃ overnight. EVs were then placed on glow discharged Formvar/Carbon-coated grids for 20

minutes, before fixation with 1% glutaraldehyde for 5 minutes. Grids were washed eight times with PBS, then incubated with 2% uranyl acetate for 5 minutes in the dark. Methylcellulose was centrifuged at 100,000g for 95 minutes before grids were incubated in methylcellulose-uranyl acetate for 10 minutes on ice. Excess liquid was drawn off on filter paper and samples allowed to dry before imaging.

2.4 Migration Assays

2.4.1 Scratch Wound Assays

WT and FGFR3-KO MSCs were seeded at 42,500 cells per cm^2 in a 48 well plate and allowed to adhere overnight. Wells were checked for confluency and even distribution of cells before washing with PBS and replacing media. A 200µl pipette tip was used to generate a scratch, ensuring even, consistent pressure was applied across the well, before washing again with PBS and replacing fresh media. Cells were imaged 0 and 24 hours after scratching, with marks made on the plate to ensure the same field of view was captured. The resulting images were overlaid to mark the initial size of the wound on every image in each field of view. ImageJ (Schindelin et al., 2012) was then used to quantify the initial and final wound area, and the percentage healing was calculated.

2.4.2 Ptychography Analysis

Cells were seeded in an Ibidi Culture-Insert Plate as per manufacturer's instructions, and allowed to adhere overnight before inserts were removed, creating a space in the centre of each well for cells to migrate into. Plates were imaged using Livecyte microscopy (Phasefocus), for 24 hours, kept at 37°C and 5% CO_2. Images were captured every 5 minutes and analysed using Cell Analysis Toolbox (CAT) Software (Phasefocus). The software segmented cells using an advanced fuzzy threshold algorithm to track individual cell metrics.

2.4.3 Secretome-Treated Scratches

Cells were seeded and scratched as described in 2.4.1. Treatments were applied immediately following scratching. Control wells were treated with DMEM supplemented with 1% P/S and, where specified, 10% FBS. CM, EVs and EV-ve media was collected as described in 2.3.1. The volume of EV suspension required for a 1x treatment dose of EVs was calculated using the equation:

$$\frac{v}{Ni/Nt}$$

Where *Ni* is the number of cells EVs were isolated from, *Nt* is the number of cells receiving the treatment, and *v* is the volume EVs were resuspended in. For results reported in section 4.2.1, individual cell metrics were collected using Livecyte microscopy, with images taken every 30 minutes for 24 hours, before analysis using CAT software. For subsequent CM-treated scratches, analysis was performed in ImageJ.

2.5 RNA-seq Analysis

RNA-seq data was collected by Alice Carstairs, generating a list of differentially expressed transcripts between WT and FGFR3-KO MSCs, defined as those with a *log2* fold change of >±1 and an adjusted *p* value of <0.05 (Carstairs, 2017). Transcripts were then divided into two gene lists corresponding to: upregulation or downregulation in FGFR3-KOs versus WT, and those which had <5FPKM reads in both cell lines were excluded. GO term analysis was performed in STRING (Szklarczyk et al., 2019), and KEGG pathway analysis conducted using Enrichr (Chen et al., 2013) and KEGG Mapper (Kanehisa and Sato, 2020). Data was exported and graphed using ggplot2 (Wickham, 2016) in RStudio (RStudio Team, 2020).

2.6 Alamar Blue Cell Viability Assay

WT and FGFR3-KO cells were seeded in 96 well plates, with one plate per timepoint, and allowed to adhere overnight. Alamar blue cell viability agent (Invitrogen) was then added to the day 0 plate, in fresh media at a final concentration of 10%. After 4 hours, fluorescence was measured using a Clariostar plate reader. For all experiments, treatments were applied on day 0 and alamar blue readings were taken at the same time each day for a further 3 days. For initial comparison of WT and FGFR3-KOs, cells were plated at 9375 cells per cm^2, and for all subsequent experiments were plated at 7812 cells per cm^2 to ensure cells did not reach full confluency before the end of the time course. Day 2 alamar blue plates were used for morphological analysis of CM-treated and U0126-treated MSCs, by washing the plates with PBS after the fluorescence readings were taken, and staining with crystal violet. All results were normalised to the fluorescence of control treatments at day 0, and reported as relative fluorescence.

2.7 Chondrogenic Differentiation

WT and FGFR3-KO cells were seeded into 1.5ml eppendorf tubes, with 200,000 cells per tube. They were centrifuged at 400g for 5 minutes to form a pellet and incubated overnight. Pellets were then loosened from the wall of the tubes by gentle tapping, and media changes were performed. Control pellets were cultured in normal cell culture medium. Chondrogenic pellets were cultured in DMEM without FBS, supplemented with 1% P/S, 1% Insulin-transferrin-sodium selenite, linoleic;oleic-BSA (ITS+3), 50µg/ml ascorbic acid, 40µg/ml proline, 10ng/ml transforming growth factor beta 3 (TGF-β3) and 0.1µM dexamethasone. Cells were incubated for 28 days, with media changed approximately every 3-4 days. Pellets were loosened before each media change to ensure full coverage of media. At 0 and 28 days, pellets were fixed in 95%methanol for 15 minutes for histological analysis, washed with PBS and stored at 4°Cprior to embedding. Pellets were embedded in OCT and cryosectioned into 15µm sections, transferred onto Superfrost microscope slides (Thermo Scientific), and stained with Alcian blue overnight. Slides were washed three times with dH_2O for 5 minutes, then with 70%, 90% and 100% ethanol for 2 minutes each. Slides were thendipped briefly in xylene ten times, laid flat and allowed to air dry before mounting coverslips with DPX.

Chapter 3: Results and Discussion: Characterisation of FGFR3-KO Cells

3.1 Assessment of typical MSC characteristics

3.1.1 Clonogenic and proliferative capacity

A defining feature of MSCs is their ability to form colonies when plated at low density. To determine if FGFR3-KOs maintain this ability, CFU-F assays were performed, and the number and size of colonies quantified. Both WT and FGFR3-KO MSCs were able to form colonies, with no significant difference in their colony forming efficiency (Fig. 3.1 A, $p = 0.9665$), indicating a similar adhesion and survival rate between the MSC lines. Furthermore, there was no significant difference in the average colony surface area (Fig. 3.1B, $p = 0.6760$), indicating FGFR3-KOs have equivalent clonogenic capacity to WT MSCs. Thus, the overall surface area covered by colonies was similar for both lines (Fig. 3.1C, $p = 0.5940$). However, within individual colonies there was a clear difference in the density of cells. FGFR3-KO colonies were close to, or at, confluency, whereas WT colonies were composed of sparsely distributed cells. This was evidenced by the deeper, more pronounced colour of the crystal violet stain in FGFR3-KO colonies (Fig. 3.2A, B), but was especially obvious when imaging at a single-colony level (Fig. 3.2C, D). Additionally, when imaging individual colonies, the striking morphological differences between the cells of each line became clear. WT cells had a typical fibroblastic shape, whereas FGFR3-KOs were rounder, with a number of particularly large cells.

Differences in colony density could be due to differences in either proliferation or migration. However, the overall size of colonies was similar, indicating the low density of WT cells is not due to increased migration, but rather reduced proliferation compared to FGFR3-KOs.

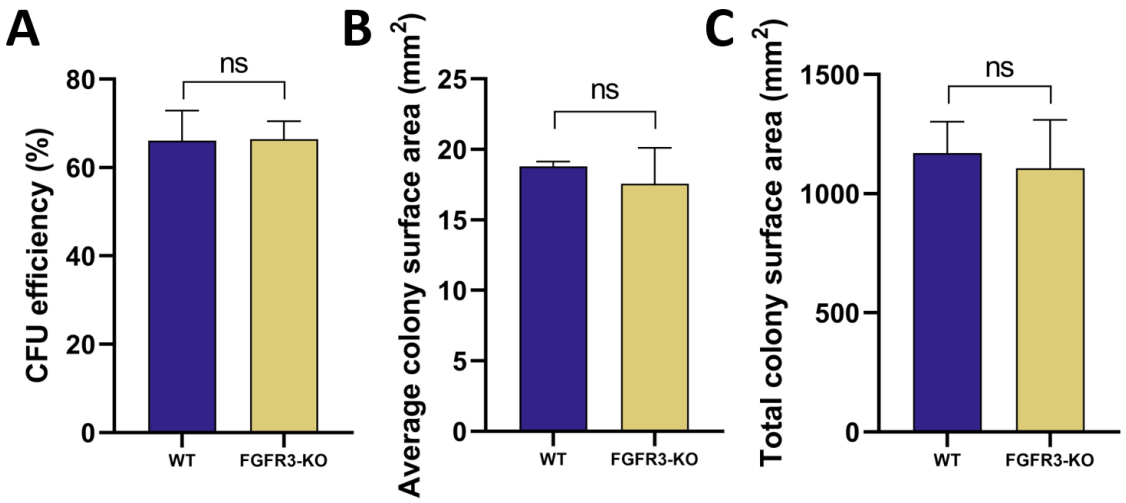

Figure 3.1. Comparison of the colony-forming capacity of WT and FGFR3-KO MSCs. CFU efficiency (A), average colony surface area (B) and total colony surface area (C) were not significantly different between the lines. Bars show mean +SEM, ns = p >0.05, as determined by t-tests (with Welch's correction for B), n = 3 biological replicates.

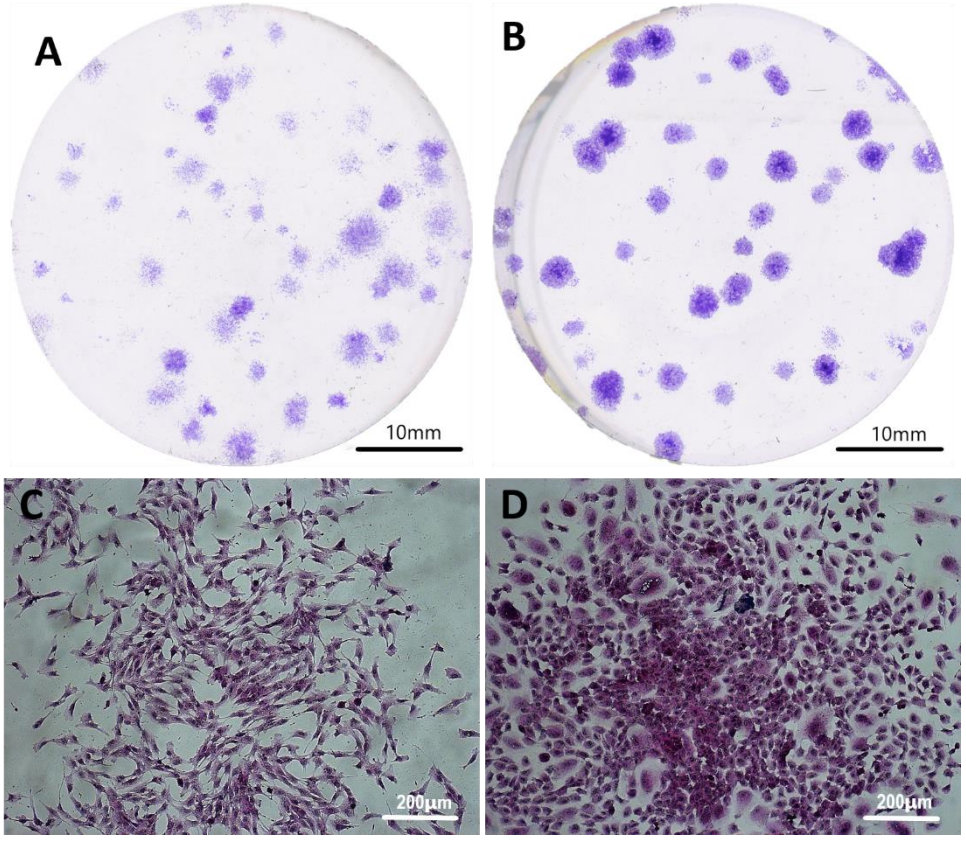

Figure 3.2. Crystal violet staining of WT and FGFR3-KO MSC colonies. Well-view of WT (A) and FGFR3-KO (B) CFU-F plates. Individual colony view of WT (C) and FGFR3-KO (D) cells.

Due to this increased confluency seen in FGFR3-KO colonies, the proliferation rates of the cell lines were compared. Equal numbers of WT and FGFR3-KO cells were seeded, and Alamar Blue Cell Viability reagent utilised to give an indication of cell number over 3 days. Fluorescence readings were taken each day, with increased fluorescence being indicative of increased cell number, and thus proliferation. FGFR3-KOs show a significantly increased fluorescence in comparison to WT cells on day 1 ($p=0.0461$), and this difference becomes more prominent on days 2 and 3 (Fig. 3.3A, $p<0.0001$ for both).

Although alamar blue fluorescence should be representative of cell number, metabolic differences between the cells may contribute to differential fluorescence. Cell counts were therefore also used as a measure of population growth. This allowed the determination of population doubling times of each cell line. In the 24 hours after seeding, FGFR3-KOs show a 75% increase in cell number compared to 18% for WT cells, indicating FGFR3-KOs begin to proliferate sooner after seeding. At each timepoint, FGFR3-KO MSCs showed a greater increase in cell number than WT MSCs. After four days, FGFR3-KOs had a significantly higher cell number than WT cells (Fig. 3.3B, $p<0.0001$). During the most rapid stage of growth, FGFR3-KOs have an average population doubling time of 18.6 hours, compared to 25.0 hours for WT cells.

Cumulative population doublings and cell number were also counted throughout long-term culture to show FGFR3-KO MSCs sustained this increased proliferation rate over time (Fig. 3.4A, B). At every timepoint, FGFR3-KOs had undergone more population doublings than WT cells, further supporting an increased proliferation rate of FGFR3-KOs.

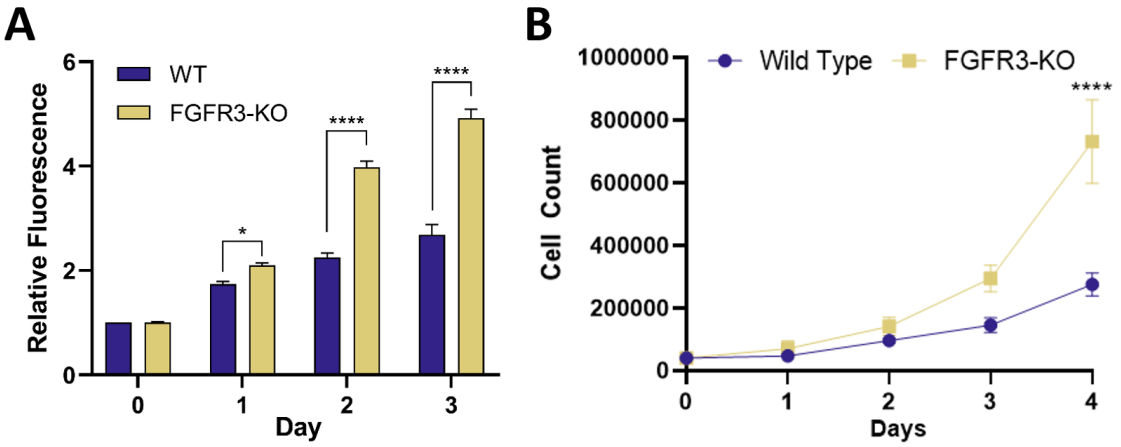

Figure 3.3. Comparison of WT and FGFR3-KO MSC proliferation rates. Alamar blue cell viability assay fluorescence readings at 600nm, relative to fluorescence of WT cells at day 0 (A). Cell counts of WT and FGFR3-KO MSCs (B). Bars show mean +SEM, n = 6 (A) and n = 3 (B). **** = p <0.0001, as determined by Sidak's multiple comparisons test.

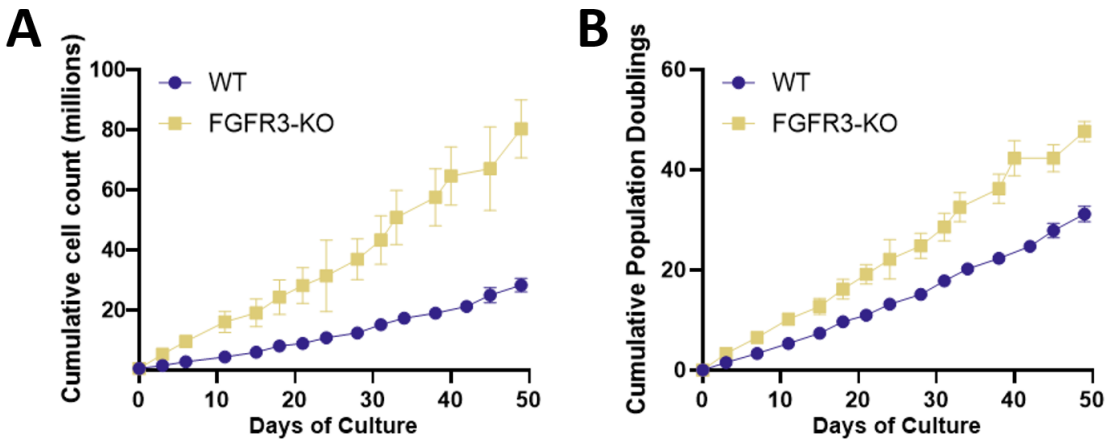

Figure 3.4. WT and FGFR3-KO MSC proliferation during continuous culture. Cumulative cell count (A) and population doublings (B) of WT and FGFR3-KO MSCs over time. Mean ± SEM plotted, n = 3 biological replicates.

3.1.2 Morphological changes in FGFR3-KO versus WT MSCs

As noted in the CFU-F assay, FGFR3-KOs appeared to have an altered morphology to WT cells. However, these cells were at different density levels, with FGFR3-KOs near-confluent and WT cells more sparsely distributed. To allow comparable analysis of morphology, cells were plated at equal densities of 4000 cells per cm², stained with crystal violet, and imaged (Fig. 3.5A, B). CellProfiler was then used to calculate cell shape metrics. Despite no alterations to cell volume between the lines (Carstairs,

2017), FGFR3-KO MSCs show a significantly reduced cell area (Fig. 3.5C). This likely indicates that WT cells have a lower sphericity index, whereby they cover a larger area by flattening more against the growth surface. However, there is a much wider range of cell areas seen in FGFR3-KOs, with a number of large, spread cells which appear to have broad lamellipodia. FGFR3-KOs show a decreased length to width ratio and an increased roundness index (Fig. 3.5D, E). A high length to width ratio is seen in the WT cells which show a typical elongated, fibroblastic morphology.

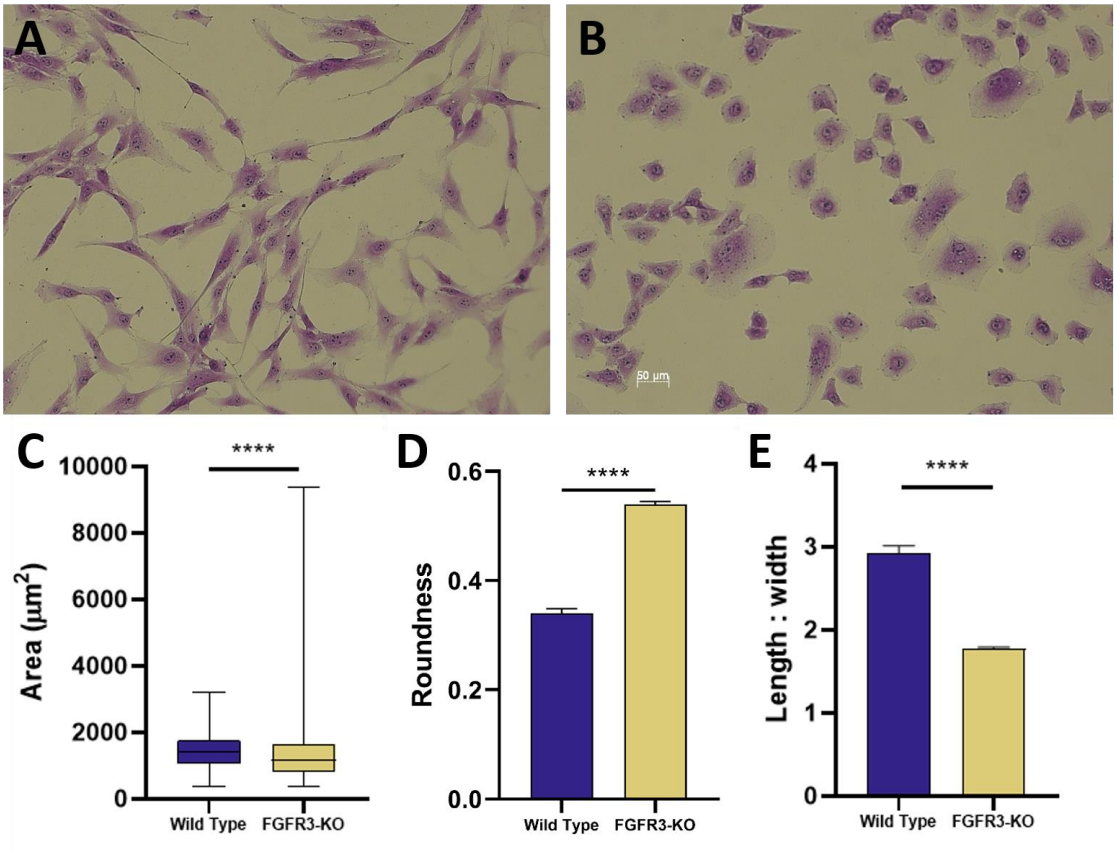

Figure 3.5. Comparison of WT and FGFR3-KO MSC morphologies. Crystal violet stained brightfield images of WT (A) and FGFR3-KO (B) MSCs. Area (C), showing median, inter-quartile, and min-max values. Length to width ratio (D), and roundness index (E), showing mean +SEM. **** = p <0.0001, as determined by Mann-Whitney test, n=1032 for WT, and n=345 for FGFR3-KO MSCs.

3.1.3 Differentiation capacity of FGFR3-KO MSCs

Previously, the FGFR3-KOs have been shown to be incapable of recapitulating WT MSC tripotency, as they are unable to differentiate into adipogenic or osteogenic lineages (Carstairs, 2017). To understand if FGFR3-KOs are fully nullipotent, they were stimulated to undergo chondrogenesis, with WT cells as a positive control. After 28 days, cells were cryosectioned and stained with Alcian blue.

Day 0 and day 28 basal controls showed only faint blue staining (Fig. 3.6A-D), indicating minimal proteoglycan content and therefore a lack of differentiation. This confirms that neither cell line spontaneously undergoes chondrogenesis in the absence of chondrogenic growth factors. Interestingly, there appears to be less staining in the FGFR3-KO basal day 0 controls than WT, indicating different basal levels of proteoglycan expression.

Chondrogenic-stimulated WT pellets showed strong positive staining, with distinct rings of staining around the exterior of the pellet (Fig. 3.6E). However, FGFR3-KO MSCs showed little, if any, chondrogenesis. Staining appears equivalent to that of the basal controls, and although there appeared to be slight staining around the exterior of some pellets, this was negligible in comparison to the clear bands seen in WT pellets (Fig. 3.6F).

WT basal pellets remained intact after 28 days, whereas FGFR3-KO basal pellets were fragile, and in some cases had fragmented. This may indicate weaker cell:cell and/or cell:matrix interactions in FGFR3-KO pellets, or may be caused by cell death within the pellet. Interestingly, despite an apparent lack of proteoglycan content shown by histological staining, chondrogenic-stimulated FGFR3-KO pellets were much sturdier than their basal counterparts, and appeared similar to WT chondrogenic pellets in size and shape. This may suggest that some changes in cell:cell interactions have occurred as a result of chondrogenic stimulation, allowing stability of the condensed pellet, but full differentiation has not occurred.

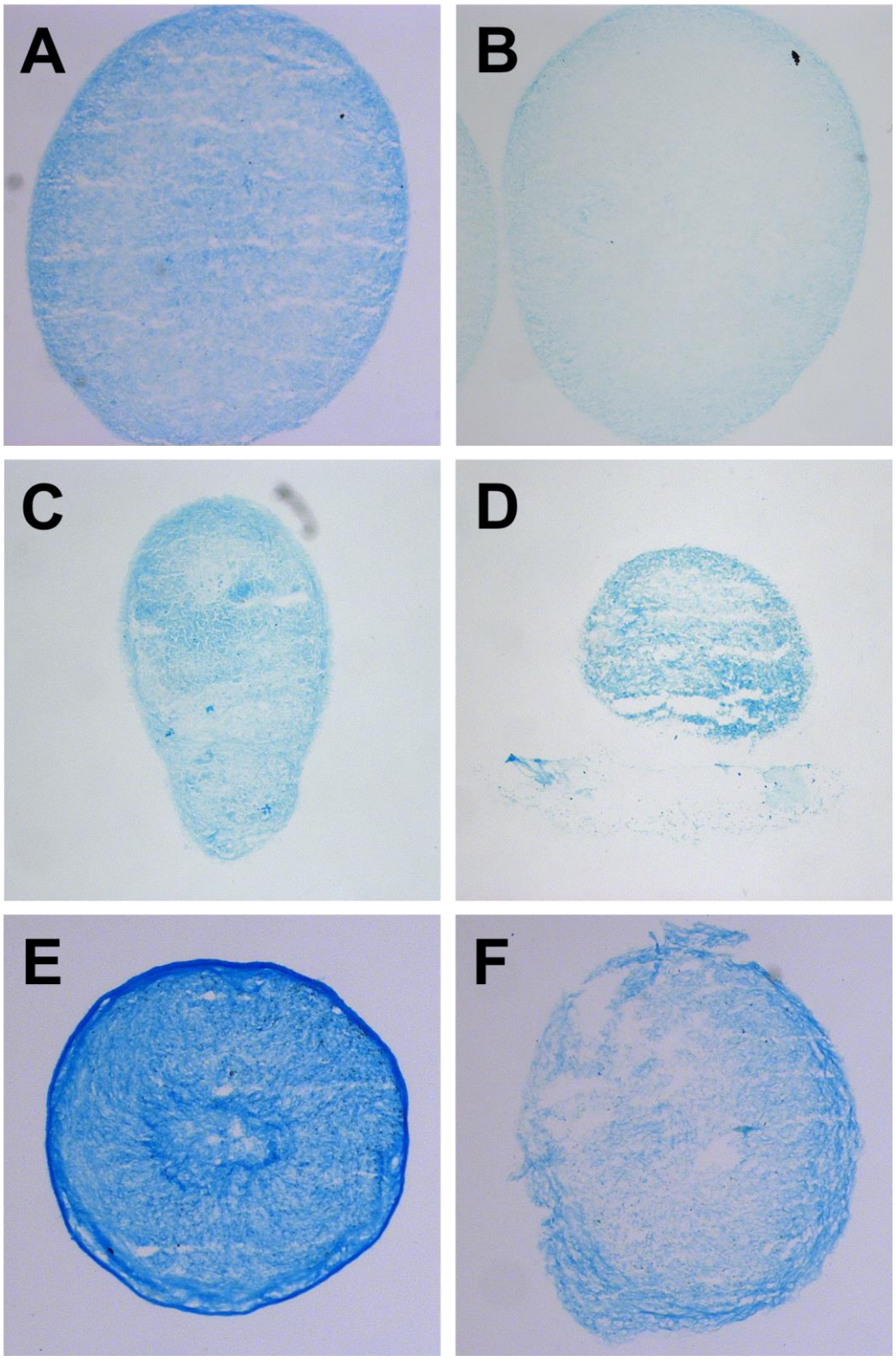

Figure 3.6. Chondrogenic differentiation of WT and FGFR3-KO MSCs. Representative brightfield images of Alcian Blue stained cryosections from day 0 basal WT (A) and FGFR3-KO (B) pellets, day 28 basal WT (C) and FGFR3-KO (D) pellets, and day 28 chondrogenic- stimulated WT (E) and FGFR3-KO (F) pellets.

3.2 Changes in gene expression as a result of FGFR3 knockout

These initial observations and experiments indicate FGFR3 is a key regulator of MSC behaviour, including proliferation, morphology and differentiation. To investigate the mechanisms by which these changes occurred, and to elucidate what other cell behaviours may be altered in these cells, previously conducted RNA-seq analysis (Carstairs, 2017) was subjected to bioinformatic interrogation. A total of 641 transcripts had significantly differential expression between WT and FGFR3-KO MSCs, with 274 transcripts upregulated in FGFR3-KOs and 367 downregulated.

Gene ontology (GO) and KEGG pathway analysis was performed on the differentially expressed transcripts to investigate if genes that participate in particular pathways or cell behaviours are enriched. A clear result from KEGG analysis is that the gene expression changes in FGFR3-KOs overlap with genes altered in cancers, including lung and bladder (Fig. 3.7A, B). In line with this, and in agreement with the increased proliferation rate observed in FGFR3-KOs, there was a highly significant enrichment for the GO term ‘regulation of cell population proliferation’, although this didn’t rank in the 10 most significant enrichments. Of the 641 genes differentially expressed in FGFR3-KOs, 103 belong to this GO term, meaning a vast number of pathways that regulate the cell cycle and proliferation have been impacted by loss of FGFR3. Additionally, transcripts encoding inflammation-related proteins were significantly upregulated in FGFR3-KOs. The most significant KEGG enrichment in the upregulated genes was ‘complement and coagulation cascades’ (Fig. 3.7B). As expected, there also was significant disruption to signalling pathways known to be downstream of FGFR3, such as PI3K signalling.

GO term Cellular Component analysis showed a significant enrichment for the actin cytoskeleton (Fig. 3.8A), meaning a number of transcripts encoding cytoskeletal proteins have altered expression in FGFR3-KO MSCs. This is in agreement with the altered morphology of FGFR3-KO MSCs, likely driven by changes in expression of cytoskeletal proteins. There was also significant enrichment for transcripts encoding proteins expressed extracellularly (Fig. 3.8B). Finally, GO Term Biological Processes analysis showed enrichment for processes predominantly relating to migration and tissue morphogenesis, and more broadly, ‘developmental process’ (Fig. 3.9).

Each of these findings was further interrogated, with the aim of narrowing down the specific genes and pathways altered in FGFR3-KO MSCs that may contribute to changes in cell behaviour. Genes with significantly differential expression in FGFR3-KOs that are mentioned in this chapter are summarised in supplementary Table 1.

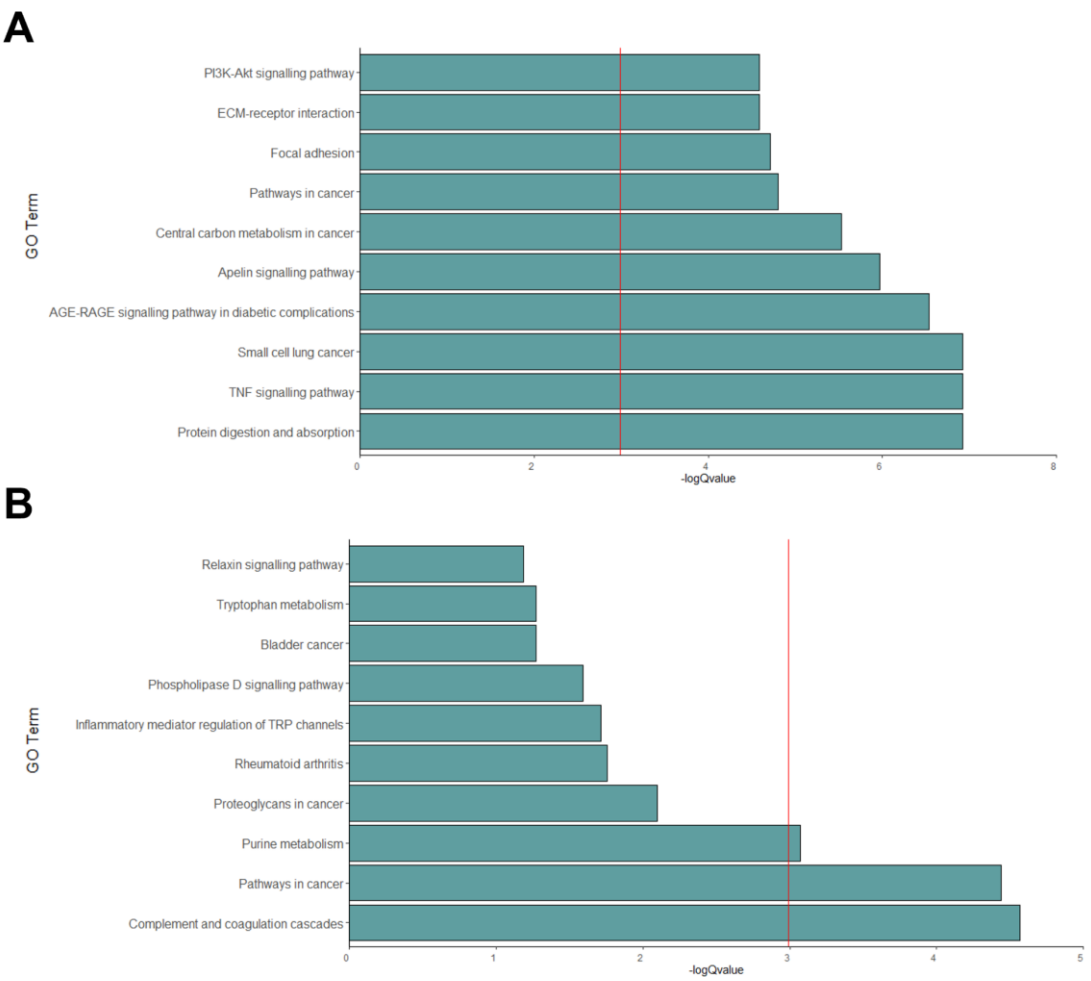

Figure 3.7. Top ten significantly enriched KEGG pathways for genes downregulated (A) and upregulated (B) in FGFR3-KO MSCs versus WT. All pathways have p values of <0.05, q value of 0.05 is indicated by red lines.

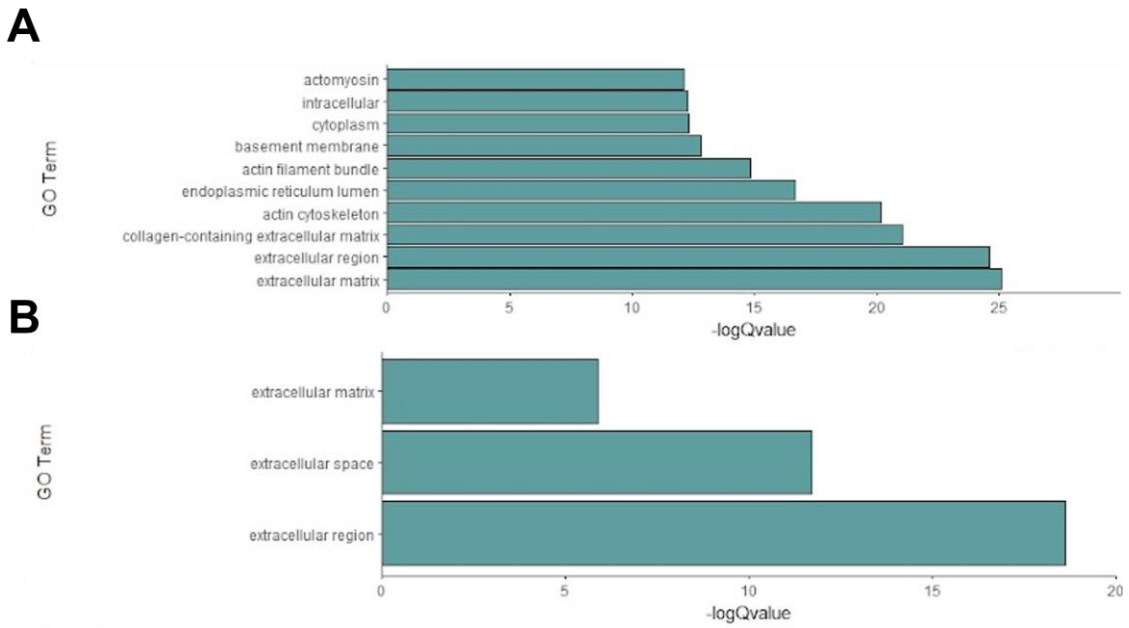

Figure 3.8. Top ten significantly enriched Cellular Component Gene Ontology (GO) terms for genes downregulated (A) and upregulated (B) in FGFR3-KO MSCs versus WT. All GO terms have Q values of <0.05.

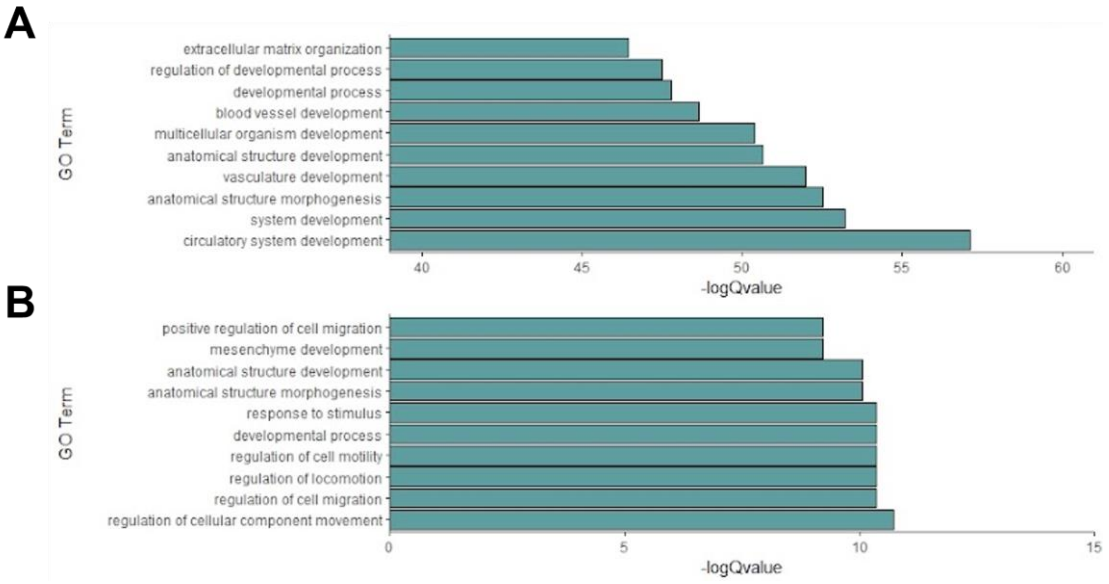

Figure 3.9. Top ten significantly enriched Biological Processes Gene Ontology (GO) terms for genes downregulated (A) and upregulated (B) in FGFR3-KO MSCs versus WT. All GO terms have Q values of <0.05.

3.2.1 Differential expression of transcripts encoding cytoskeletal proteins

Gene ontology analysis of the transcripts downregulated in FGFR3-KOs indicated there may be alterations in the cytoskeleton, with significant enrichments for the cellular components ‘actomyosin’, ‘actin filament bundle’, and ‘actin cytoskeleton’ (Fig. 3.8). KEGG Mapper was used to investigate the specific genes involved in these pathways that are differentially expressed (Fig. 3.10). Cross-linking protein actinin, actin alpha 2 (ACTA2), and both alpha and beta subunits of tropomyosin are all downregulated in FGFR3-KOs. Both the heavy and light chains of myosin 9 (Myosin IIA/ MYH9) show vastly decreased expression, along with myosin IB, and myosin light chain kinase (MLCK). Together, these changes are likely to impact the contractile ability of actomyosin filaments, the stability of focal adhesions, and the maintenance of filopodia and lamellipodia. This dramatic disruption to cytoskeletal composition likely drives the altered morphology observed in FGFR3-KO MSCs. Cell shape is tightly linked to cell function (Chen et al., 1997), therefore an altered morphology may predispose FGFR3-KO MSCs to different roles.

As well as alteration to cytoskeletal components themselves, a number of regulatory genes were disrupted by knockout of FGFR3. Two central mediators of cytoskeletal arrangement, Rho and Rac, have transcripts differentially expressed in FGFR3-KOs. RhoE is increased in FGFR3-KOs, whilst RhoB, RhoJ and Rac2 are decreased. As well as regulating cytoskeletal proteins, Rho proteins play roles in cell adhesion (Braga et al., 1997), and Rac regulates cell polarisation and secretion (Bretscher and Aguado-Velasco, 1998). As such, these cytoskeletal changes may have knock-on effects on processes such as migration, adhesion, and secretion.

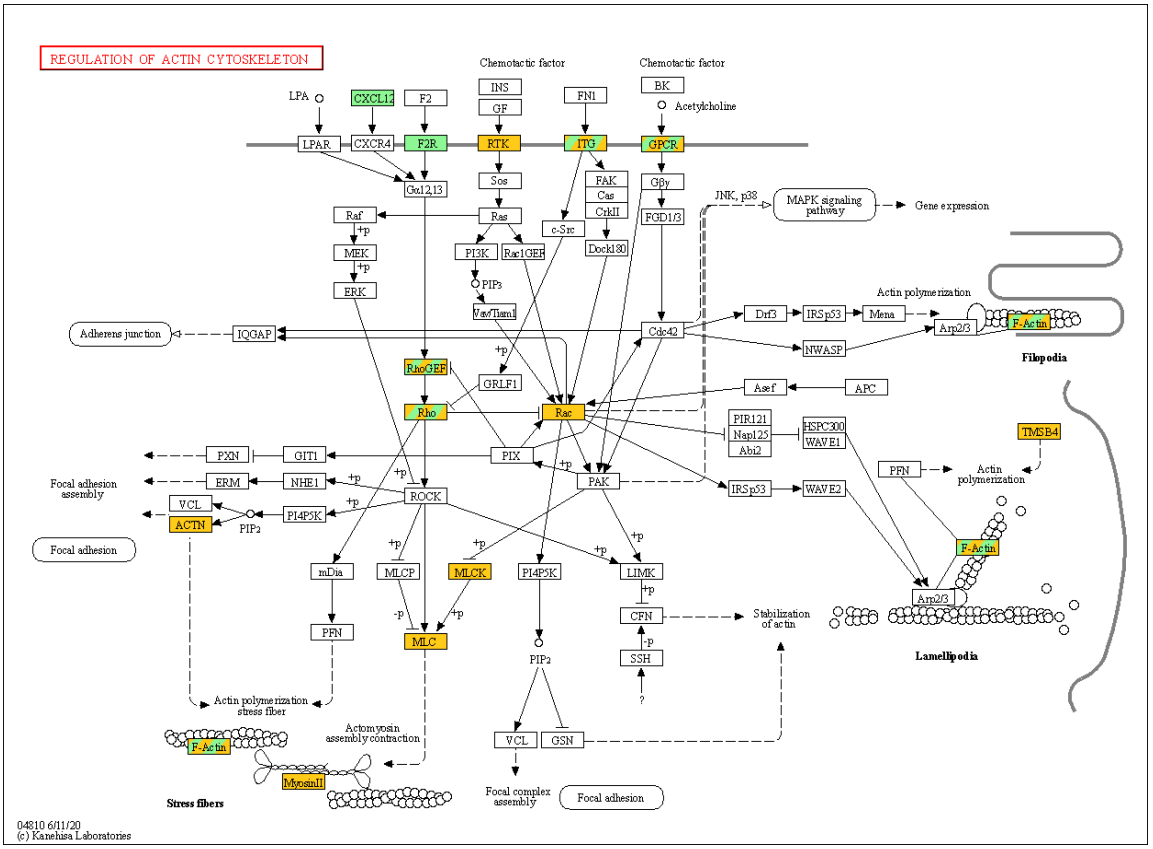

Figure 3.10. Differential expression of transcripts in FGFR3-KO MSCs that encode proteins involved in regulation of the actin cytoskeleton. KEGG Mapper diagram showing an overview of cytoskeletal signalling pathways. Transcripts significantly downregulated in FGFR3-KOs in comparison to WT MSCs are highlighted in orange, and transcripts upregulated are in green. Genes which have some transcript isoforms upregulated and other isoforms downregulated are denoted with striped highlights.

3.2.2 Differential expression of transcripts encoding proteins that regulate migration

Amongst the genes upregulated in FGFR3-KOs, the top ten most enriched biological process GO terms includes four relating to cell motility, including ‘positive regulation of cell migration’ (Fig. 3.9). This points towards an increased migratory capacity of FGFR3-KOs. For mesenchymal cell migration, careful regulation of cytoskeletal dynamics is required, including turnover of focal adhesions and contraction of acto-myosin filaments, to generate mechanical force. As such, the cytoskeletal changes previously discussed likely contribute to any differences in migratory capacity of FGFR3-KOs. Additionally, a number of chemotactic factors are upregulated in FGFR3-KOs. CXCL8 (IL-8) and CXCL12 (SDF-1), both chemokines normally

associated with inflammation (Matsuo et al., 2009), are potent chemoattractants that have significant increases in expression in FGFR3-KOs.

An essential stage of migration is the degradation of the extracellular matrix (ECM), in order to clear a path for cells to move into. This relies on the action of a number of protease families (Lu et al., 2011). Three matrix metalloproteinases (MMPs) were dramatically upregulated in FGFR3-KOs, MMPs 1, 2, and 11. These MMPs can act on most ECM proteins, including collagens, proteoglycans, and fibronectin, and their upregulation therefore suggests increased degradation of the ECM. However, two members of the A disintegrin and metalloproteinase with thrombospondin motifs (ADAMTS) protease family were downregulated, which contradicts this conclusion. ADAMTS 2 and 7 act on procollagens and cartilage oligomeric matrix protein (Thrombospondin-5). These changes may indicate FGFR3-KO MSCs have alterations to the remodelling of specific ECM proteins, rather than a global increase in degradation of the ECM. The altered ECM composition, which will be further discussed below, may impact the migratory ability of FGFR3-KO MSC, but it cannot be concluded that FGFR3-KOs are predisposed to a more migratory phenotype from this result alone.

3.2.3 Differential expression of transcripts encoding secreted proteins

In both the up- and downregulated genes in FGFR3-KO MSCs, one of the most significantly enriched Cellular Component GO terms was ‘extracellular region’. This encompasses all genes encoding proteins located outside the plasma membrane, including freely diffusible proteins, matrix components, and proteins packaged into extracellular organelles such as extracellular vesicles (EVs). No GO terms specifically linked to EV biogenesis were significantly enriched, which may suggest little difference in the secretion rate of EVs from FGFR3-KO relative to WT MSCs. However, EV cargo is reflective of the contents of the parent cell, thus, the differential gene expression of FGFR3-KOs would be expected to alter the contents of their EVs.

3.2.3.1 Extracellular matrix components

46 transcripts encoding ECM proteins were downregulated in FGFR3-KOs, and 21 were upregulated. Those downregulated included key ECM proteins such as aggrecan, perlecan, connective tissue growth factor, elastin, and collagens III, IV, V, XII, XV, and XVI, many of which show vast decreases in expression.

Although many ECM components were downregulated, there was also a significant enrichment for ECM gene upregulation in FGFR3-KOs. However, the upregulated genes with the highest fold changes included MMPs 1 and 2, and to a lesser extent, MMP11, all of which have roles in degrading the ECM. Combined, these results may indicate FGFR3-KO cells produce less extracellular matrix, or that it is more rapidly turned over and degraded.

3.2.3.2 Heparan sulfate proteoglycans

A number of proteoglycan binding genes were differentially expressed, with 'proteoglycan binding' being the eighth most enriched Molecular Function GO Term in the genes downregulated in FGFR3-KOs (Fig 3.11). 'Glycosaminoglycan binding' and, specifically, 'heparin binding' were also significantly enriched. Proteoglycans themselves were also downregulated- perlecan, agrin, aggrecan, biglycan, lumican, podocan and syndecan all show significant decreases in expression. Many of these proteoglycans are heparan sulfate proteoglycans (HSPGs), which are essential components of the FGF-FGFR complex (Lin et al., 1999). Heparan sulfate 6-O-sulfotransferase 1, an enzyme involved in synthesis of HSPGs is also downregulated. The effect of this dramatic remodelling to the HSPG landscape is difficult to predict given the diverse roles of HSPGs in regulating FGF signalling, but it is highly likely the activity of other FGFRs is disrupted.

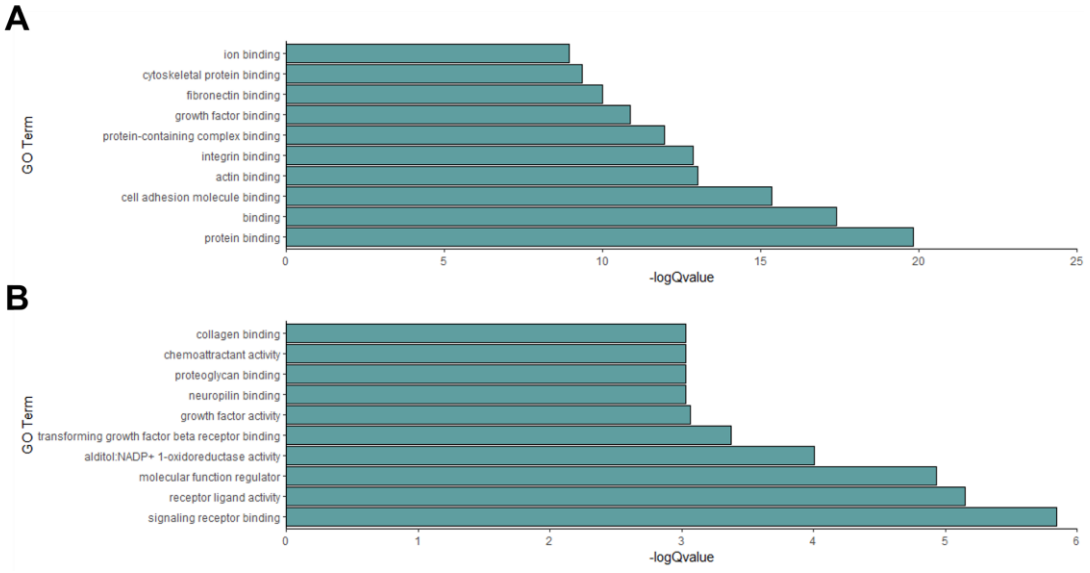

Figure 3.11. Top ten significantly enriched Molecular Functions Gene Ontology (GO) terms for genes downregulated (A) and upregulated (B) in FGFR3-KO MSCs versus WT.

3.2.4 Differential expression of transcripts encoding differentiation-related proteins

The dramatic decrease in proteoglycan expression provides an explanation for the reduced basal staining of FGFR3-KOs in the chondrogenic assay. This may have reduced the competency of FGFR3-KOs to differentiate into the chondrogenic lineage. However, the 'master regulator' of chondrogenesis, Sox9, is upregulated in FGFR3-KOs, as is transforming growth factor beta receptor 2 (TGFBR2), both of which normally promote chondrogenesis (Akiyama et al., 2002; Oka et al., 2007). However, neural cadherin (cadherin 2) is downregulated in FGFR3-KOs, which may be the reason for the fragility of FGFR3-KO basal pellets. One possibility is that FGFR3-KOs are able to undergo chondrogenic differentiation, but require an extended timecourse in order to overcome the disruption to the ECM in their basal state.

Whilst FGFR3 is known to inhibit endochondral ossification, its role in osteogenesis specifically is unclear and experimental models are highly conflicting. Previous osteogenic stimulation showed FGFR3-KO MSCs incapable of differentiating into osteoblasts (Carstairs, 2017). Indeed, a number of genes that either drive or mark osteogenesis showed decreased expression in FGFR3-KOs compared to WT, including Snail2 and periostin. Additionally, Twist2, an inhibitor of osteogenesis (Kronenberg, 2004), is upregulated.

Together, these data support a reduced differentiation capacity of FGFR3-KO MSCs. Although no genes or GO terms relating to adipogenesis were enriched, it is clear FGFR3 is key for the regulation of gene expression related to the maintenance of MSC tripotency.

3.2.5 Dysregulation to pathways downstream of FGFR3

Many intracellular signaling pathways are activated as a result of FGFR3 signalling, thus it would be expected that these are dysregulated in FGFR3-KOs. PI3K-Akt signalling is an enriched KEGG pathway in the genes downregulated in FGFR3-KOs (Fig. 3.7A), with components of the PI3K signalling pathway, such as Akt3, being significantly downregulated in the FGFR3-KOs. Thus it appears PI3K signalling in MSCs is at least partially dependent on FGFR3.

The MAPK pathway also acts downstream of FGFR3 signalling (Fig. 1.1), and is significantly enriched in both the genes upregulated and downregulated in FGFR3-KOs. It is therefore unclear whether MAPK signalling is more or less active in

FGFR3-KOs, and it is possible that other receptors are compensating for the loss of FGFR3 by activating MAPK through different adaptor proteins.

The STAT pathway has been implicated as one of the mechanisms through which FGFR3 mutations cause pathologies, although to a lesser extent than MAPK, since inhibition of overactive STAT signalling does not fully alleviate dysplasia phenotypes (Murakami et al., 2004). There seems to be no impact on the pathway in the RNA-seq data, however, a number of other pathways interact with STAT signalling, thus, FGFR3 knockout may indirectly alter STAT activity. Snail1 and Snail2 (Slug) are transcriptional effectors of FGFR3 (Frutos et al., 2007; Dale et al., 2006), and are both significantly downregulated in FGFR3-KO MSCs compared to WT. A correlation has been found between the levels of Snail1 and the activity of STAT1 (Frutos et al., 2007). Thus, with the reduced expression of Snail1 in FGFR3-KOs, it could be expected that STAT signalling is decreased. Similarly, a positive feedback mechanism between Snail1 and Erk1/2 has been proposed, whereby active Snail1 increases Erk1/2 phosphorylation and nuclear localisation, and activated Erk2 phosphorylates and stabilises Snail1 (Zhang et al., 2013). Therefore, signalling through Snail, STAT, and MAPK could all be decreased in FGFR3-KOs.

Integration of multiple signalling pathways is required throughout development, and the effect of FGF signalling is often dependent on the other signals present in the tissue. The interactions between FGF signalling and pathways such as Wnt, Notch, and TGFβ are well-studied (Chuang, Kawcak and McMahon, 2003; Akai, Halley and Storey, 2005; Mukherjee et al., 2005). Components of these pathways are differentially expressed in FGFR3-KOs, suggesting loss of FGFR3 may have knock-on effects beyond affecting the FGF pathway alone. Wnt signalling appears upregulated, indicated by an increase in the ligand Wnt5a and the Wnt receptor Frizzled-8, and downregulation of the Wnt inhibitor DKK3. Similarly, TGFBRs 2 and 3 are upregulated, perhaps indicating an attempt to compensate for the loss of FGFR3, or a role for FGFR3 in inhibiting these pathways in WT MSCs.

Altogether, this transcriptomic analysis shows the genetic landscape of FGFR3-KO MSCs is dramatically altered, and implicates FGFR3 as a regulator of key cell behaviours. The cytoskeleton and migratory ability of FGFR3-KO MSCs was next studied to confirm the effects of these transcriptomic changes, along with manipulation of signalling pathways to confirm their involvement in regulating these behaviours.

3.3 Cytoskeletal changes in FGFR3-KO MSCs

3.3.1 The effect of confluency on cell shape

As described in 3.1.2, FGFR3-KOs have a lower average cell area, with a lower length:width ratio and higher roundness than WT cells, which have a typical fibroblastic morphology. Transcriptomic analysis indicated alterations in cell:cell and cell:matrix interactions, so morphological characteristics were studied again at a range of cell confluencies, to investigate if cell density impacts their shape. WT MSCs maintain their fibroblastic morphology from 20-80% confluency (Fig. 3.12), with no significant differences in their area, roundness, or length to width ratio between 20 and 60%. Images of WT cells at 80% confluency were excluded from morphometric analysis due to difficulties in segmenting individual cells at high density. FGFR3-KO MSCs appear more sensitive to low cell densities, and take on a particularly small, rounded morphology at 20% confluency (Fig. 3.13). On the whole, at higher confluencies, FGFR3-KOs get larger, less round, and have a higher length to width ratio. The extension of large, broad lamellipodia does not appear dependent on the proximity of surrounding cells; examples of extreme spreading are seen in lone cells as well as cells surrounded by others.

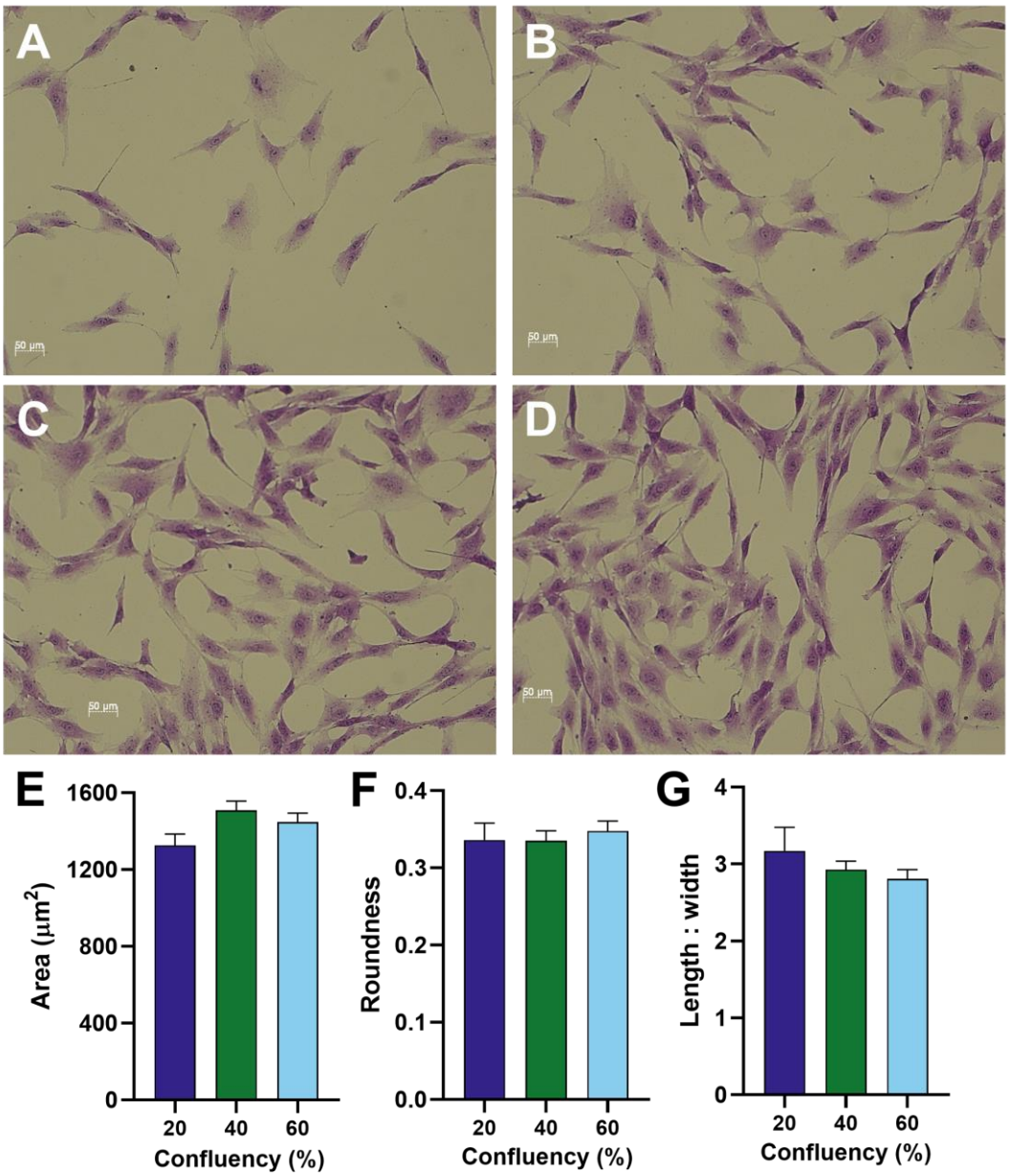

Figure 3.12. WT MSC morphology across varying confluency levels. Brightfield images of WT MSCs stained with crystal violet at 20, 40, 60, and 80% confluency (A-D). Quantification of cell area (E), roundness (F) and length:width ratio (G) at different confluencies. 80% was excluded from cell shape analysis due to difficulties in segmentation of individual cells. No significant differences in E-F as determined by Dunn's multiple comparisons test. Bars show mean +SEM.

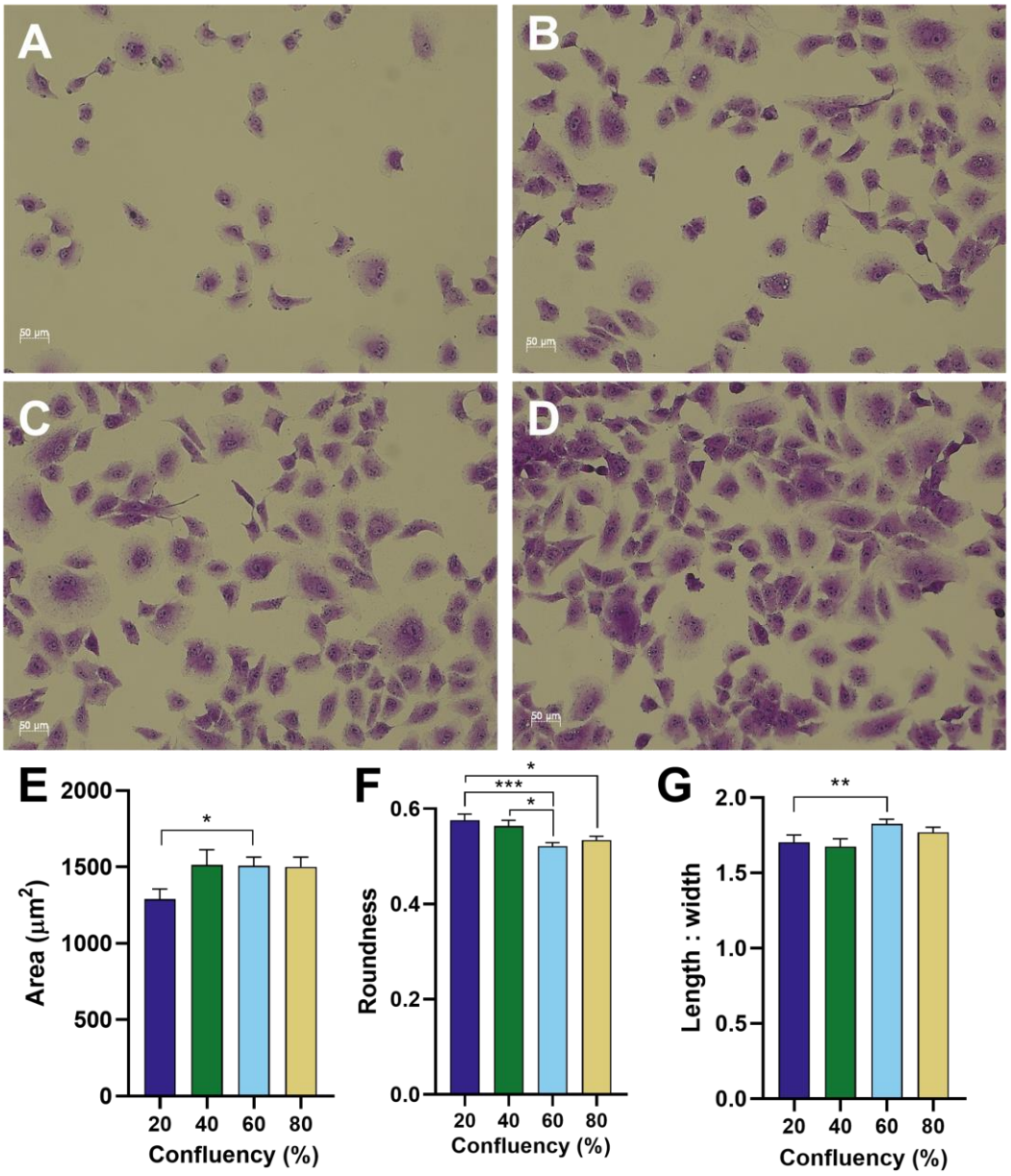

Figure 3.13. FGFR3-KO MSC morphology across varying confluency levels. Brightfield images of FGFR3-KO MSCs stained with crystal violet at 20, 40, 60, and 80% confluency (A-D). Quantification of cell area (E), roundness (F) and length:width ratio (G) at different confluencies. *** = p<0.001; ** = p<0.01; * = p<0.05; Dunn's multiple comparisons test. Bars show mean +SEM.

3.3.2 Phalloidin staining of the actin cytoskeleton

Due to the morphological changes in FGFR3-KOs, and the enrichment of actin cytoskeleton genes, fluorescence staining of the actin cytoskeleton was carried out to image the cells in greater detail. The arrangement of actin fibres in WT cells appeared striated, with stress fibres running from leading edge to tail, and some branched fibres at the leading edge (Fig. 3.14 A, B). In FGFR3-KOs, stress fibres appeared as thicker bundles, particularly prominent on the dorsal edge behind the lamella (Fig. 3.14 C, D). Additionally, FGFR3-KOs have a near-circular shape with prominent, broad transverse arcs and lamellipodia.

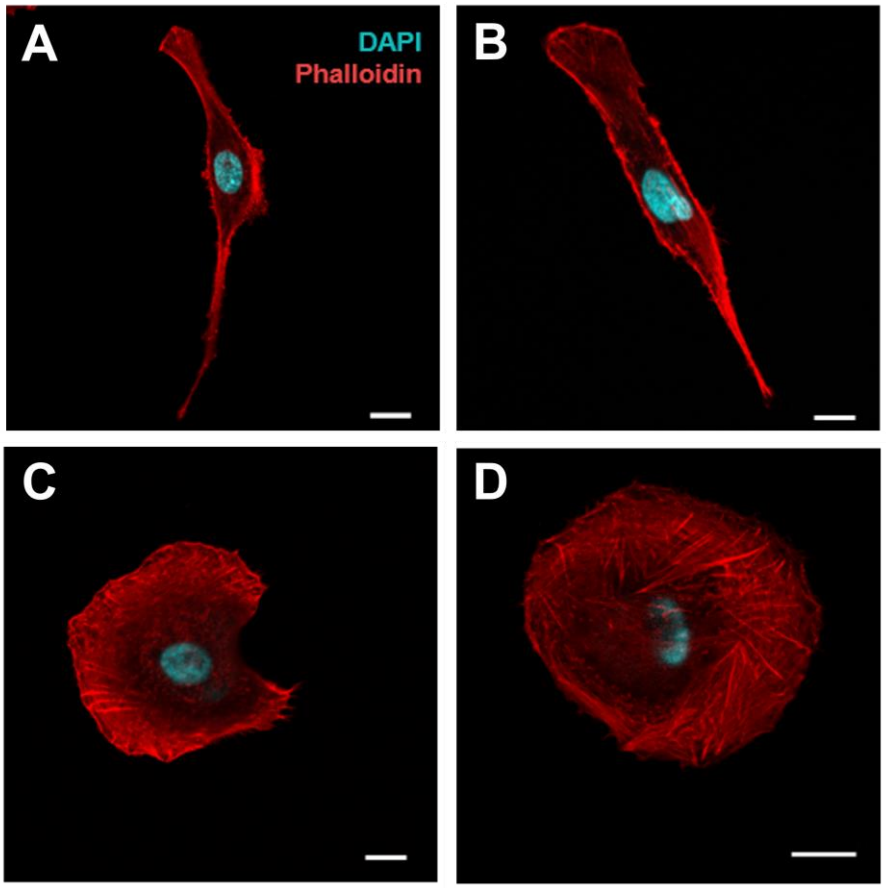

Figure 3.14. Visualisation of the WT and FGFR3-KO MSC actin cytoskeleton. Representative confocal images of WT (A, B) and FGFR3-KO (C, D) MSCs, stained with Alexa Fluor 594-conjugated Phalloidin, marking actin (red), and DAPI, marking nuclei (blue). Scale bars equivalent to 20µm.

Fluorescent images were also used to quantify cell shape metrics, since the distinct contrast of the actin cytoskeleton against the background and the high magnification allowed more precise measurements of single cells. WT MSCs had a significantly increased length:width ratio, and significantly lower roundness index, comparative to FGFR3-KO MSCs (Fig. 3.15). This is in agreement with previous metrics, but the differences noted when imaged at higher magnifications are even more pronounced.

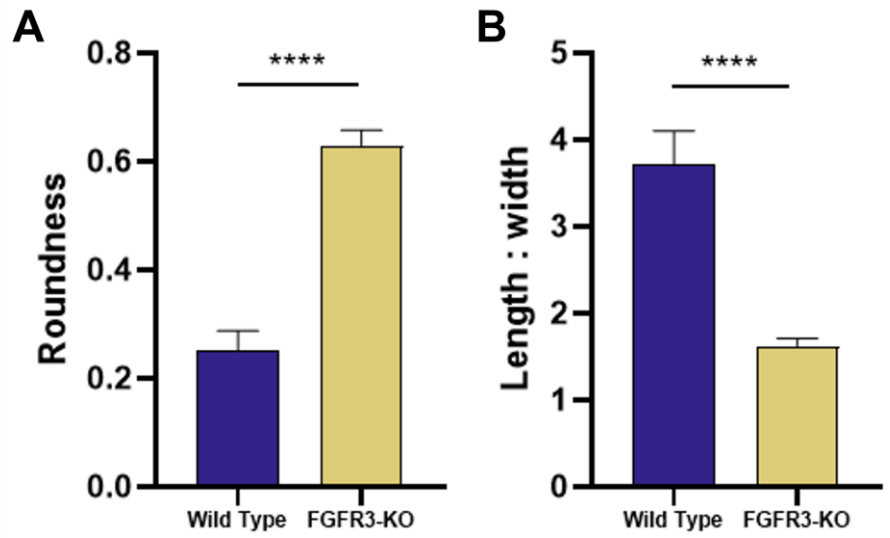

Figure 3.15. Comparison of WT and FGFR3-KO MSC actin cytoskeleton shape. Roundness (A) and length to width ratio (B) of WT and FGFR3-KO MSCs. **** = p<0.0001; Mann Whitney test.

3.3.3 Arp3 immunofluorescence

Due to its role in creating branched actin filaments, Arp3 protein is often enriched in the lamellipodia (Mejillano et al., 2004). Therefore, it was hypothesised FGFR3-KO MSCs may show a stronger localisation or increased level of Arp3 protein, allowing the formation of broad lamellipodia. However, there was widespread staining of Arp3 in FGFR3-KOs, perhaps contributing to the overall rounded shape of the cells, and there was no apparent enrichment in lamellipodia (Fig. 3.16). WT cells showed fewer, denser specks of Arp3 staining, many of which co-localised with actin.

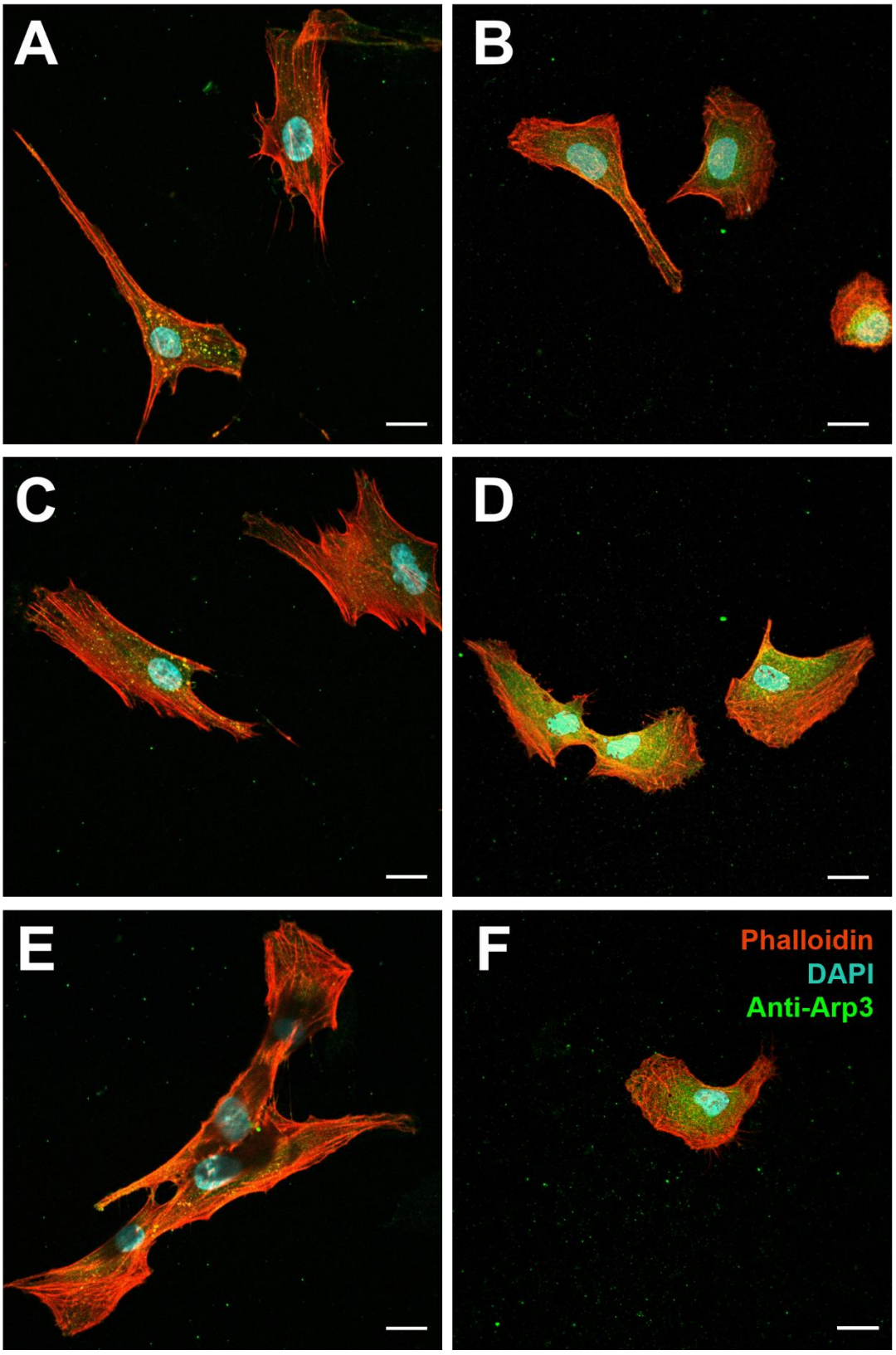

Figure 3.16. Visualisation of Arp3 protein in WT and FGFR3-KO MSCs.
Immunofluorescence of WT (A, C, E) and FGFR3-KO (B, D, F) MSCs, with staining for Arp3 (green) actin (red) and nuclei (blue). Scale bars = 20µm.

3.3.4 Dependence of MSCs on Rac signalling

The Rac pathway is upstream of Arp2/3, making Rac a driver of lamellipodial formation (Burridge and Wennerberg, 2004). The lack of strong Arp3 staining in lamellipodia suggests the FGFR3-KO morphology is Arp-independent. However, Rac is upstream of many other cytoskeletal signalling cascades, including MYH9, through mediators p21-activated kinase (PAK) and MLCK (Fig. 3.10), which may drive the altered cell shape of FGFR3-KOs. Thus, WT and FGFR3-KOs were treated with Rac inhibitor NSC23766 and their morphologies assessed.

Cells were treated at the recommended dosage of 10µM for 24 hours, but upon observation it was clear massive cell death had occurred in all treatment wells. This was confirmed by alamar blue cell viability assay, showing an 11 and 9% survival rate for WT and FGFR3-KO MSCs respectively, compared to the untreated controls. To optimise the treatment so that morphological changes could be observed without causing cell arrest, a variety of treatment doses and times were used. Dramatic cell death was observed with a 24 hour treatment even at low doses, across both cell lines (Fig. 3.17). Both lines showed a dose-dependent decrease in survival when treated for either 1 or 4 hours. There were no significant differences between the survival rate of the lines at any given treatment dose. Thus it appears Rac signalling is necessary for MSC survival, and FGFR3-KOs are equally as dependent on the pathway as their WT counterparts.

To allow sufficient time for morphological changes to occur, a pulse treatment was used, whereby the inhibitor was applied at a concentration of 1µM for 1 hour, then removed and fresh media applied each day for four days before staining the cells with crystal violet. WT cells showed a slight, but significant, decrease in cell area upon inhibitor treatment (Fig. 3.18A). Conversely, FGFR3-KOs showed a significant increase in cell area in the presence of the inhibitor. Neither cell line showed differences in roundness or length:width ratio upon inhibitor treatment, indicating they are not dependent on the Rac pathway for their morphology (Fig. 3.18 B, C).

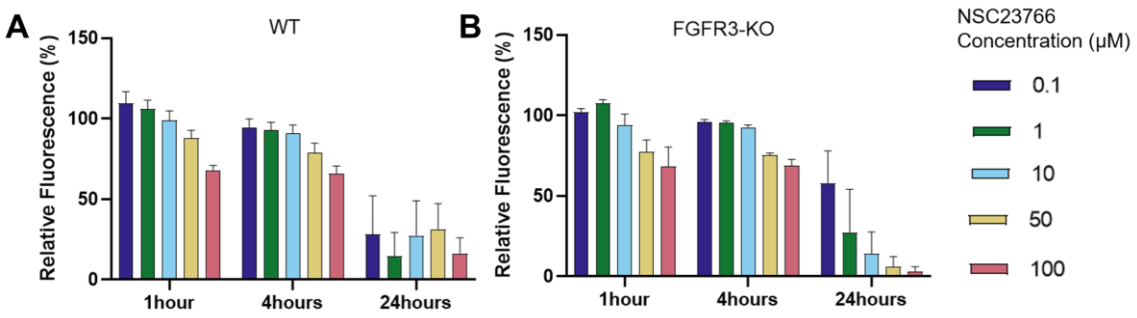

Figure 3.17. Dependence of WT and FGFR3-KO MSCs on Rac signalling for cell survival. WT and FGFR3-KO MSCs were treated with varying doses of Rac inhibitor NSC23766 for either 1, 4, or 24 hours, before use of Alamar blue cell viability assay. Relative fluorescence was calculated against untreated controls for each line.

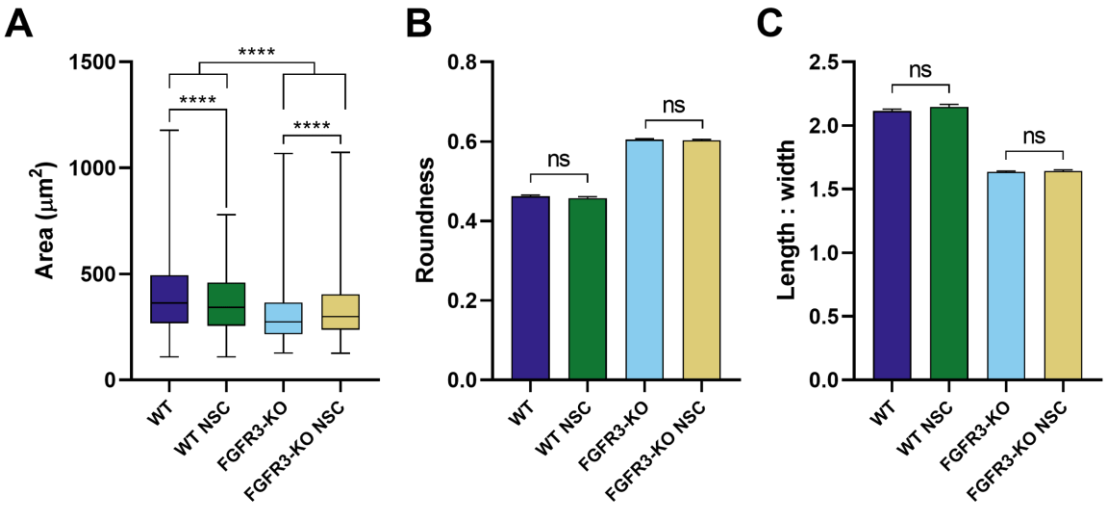

Figure 3.18. Dependence of WT and FGFR3-KO MSCs on Rac signalling for cell morphology. WT and FGFR3-KO MSC cell area (A), roundness (B) and length:width ratio (C) after pulse treatment with either vehicle or NSC23766. Boxplot shows 1-99 percentiles, and each quartile. Bars show mean +SEM. **** = $p<0.0001$, ns = $p>0.05$, Dunn's multiple comparisons test.

3.4 Dependence of MSCs on MAP Kinase pathway for survival and morphology

Transcriptomic analysis indicated significant disruption to the MAPK pathway in FGFR3-KOs. Signalling through MAPK regulates MSC survival and morphology, and aberrant signalling downstream of mutated FGFR3 is implicated in a number of pathologies (Raucci et al., 2004; Nowroozi et al., 2005). As such, the role of MAPK in FGFR3-KO MSCs was investigated. MEK inhibitor U0126 was applied at a concentration of 10μM to WT and FGFR3-KO MSCs for 3 days. Proliferation was monitored using alamar blue, and crystal violet staining was used to visualise morphology each day. Upon treatment with U0126, each cell line showed a distinct and different change in morphology (Fig. 3.19 A-D). Firstly, WT MSCs appear to form colonies, showing tight clustering of cells, which show a small but significant decrease in cell area. There is no significant change to WT roundness, or length:width ratio, but it is possible that these metrics may be less accurate due to the difficulty in identifying individual cells within these clusters. For FGFR3-KO MSCs, treatment with U0126 caused a significant decrease in cell area (Fig. 3.19E), with a noticeable reduction in the number of, and size of, cells that show extreme spreading. This may indicate aberrant MAPK activation in FGFR3-KOs drives their enlarged size and protrusion of lamellipodia. Indeed, cytoskeletal regulators such as myosin light chain kinase (MLCK) function downstream of MAPK.

Treatment with U0126 also impacted MSC proliferation. Both WT and FGFR3-KO cells showed a significant reduction in alamar blue fluorescence compared to untreated controls (Fig. 3.19F). However, both cell lines appear equally dependent on MAPK for proliferation, as there is a non-significant difference in the percentage reduction in fluorescence.

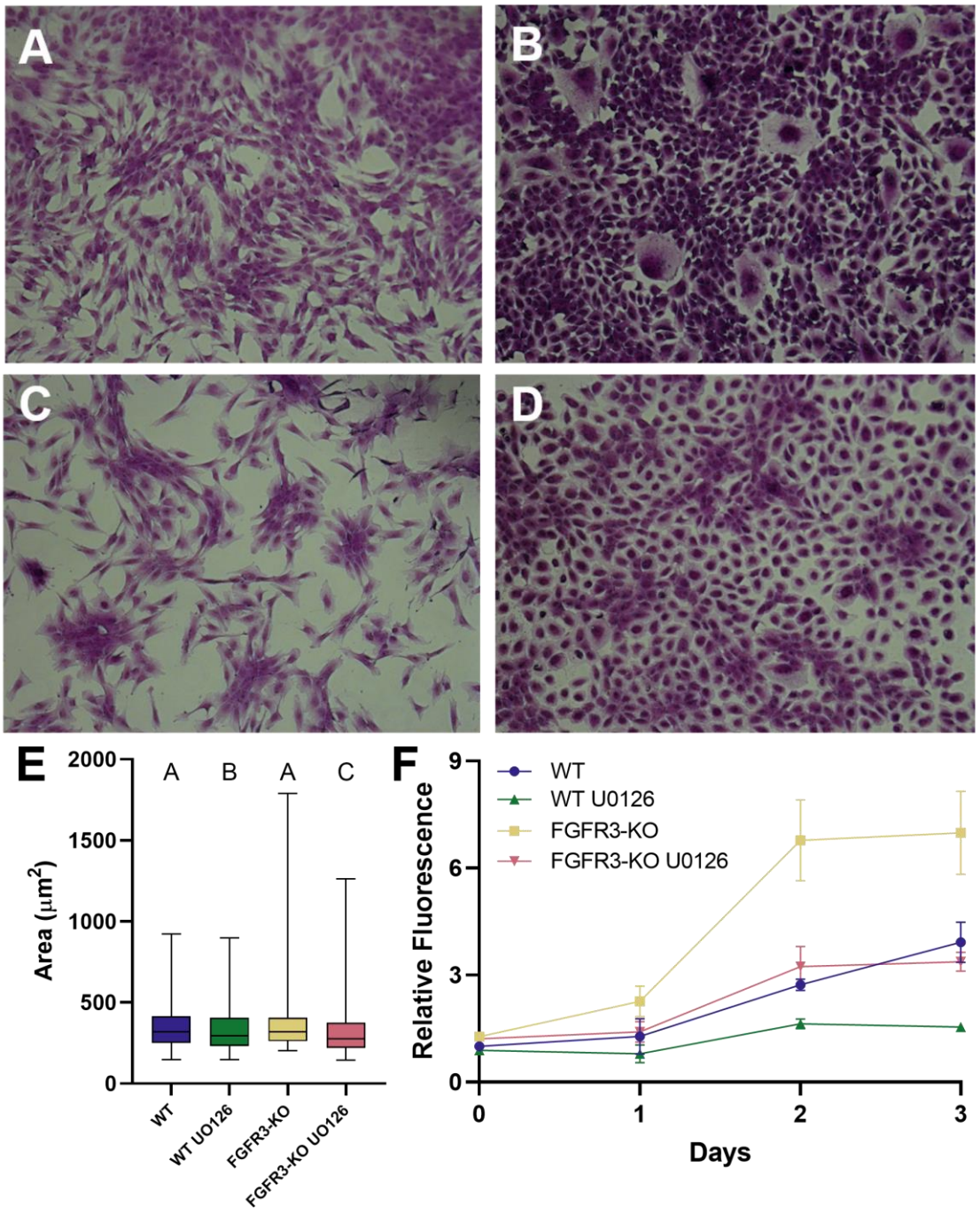

Figure 3.19. Dependence of WT and FGFR3-KO MSCs on MAPK signalling for cell morphology and proliferation. Brightfield images of crystal violet stained control WT (A) and FGFR3-KO (B) MSCs, and of U0126-treated WT (C) and FGFR3-KO (D) MSCs. Images were taken after 48 hours of control or inhibitor treatment, and cell area (E) calculated. Boxplot shows 1-99 percentile and each quartile, and boxes with different letters are significantly different from one another, $p < 0.05$, Dunn's multiple comparisons test. Alamar blue cell viability assay fluorescence readings at 600nm (F), relative to fluorescence of untreated WT cells at day 0, showing mean ±SEM.

3.5 Alterations in migratory behaviour of FGFR3-KO MSCs

3.5.1 Increased scratch wound healing capacity

Due to the enrichment in the RNA-seq analysis for migratory genes being differentially expressed in FGFR3-KOs, their migratory capacity was compared to WT MSCs. WT and FGFR3-KO cells were seeded into well plates, and a scratch generated with a pipette tip. Images were taken at 0 and 24 hours, and scratch closure was calculated as a percentage of the original wound size covered by cells. FGFR3-KOs had a significantly increased closure relative to WT MSCs, indicating an increased migratory capability (Fig. 3.20). However, a number of other factors may contribute to this increase in wound coverage, such as proliferation and cell morphology, both of which differ between the cell lines.

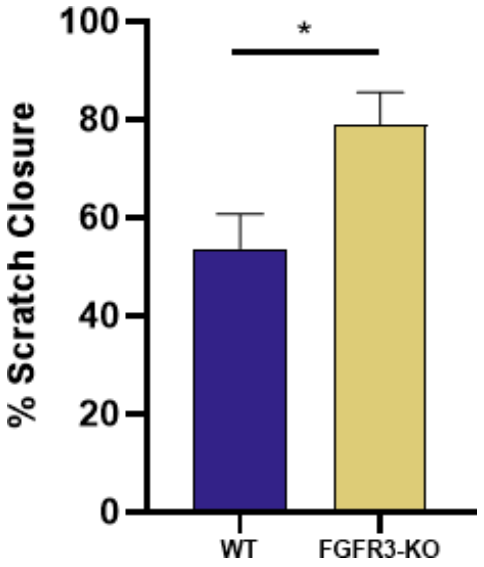

Figure 3.20. Scratch closure of WT and FGFR3-KO MSCs after 24 hours of wound healing. Bars show mean +SEM, * = $p<0.05$, t test, n = 5.

3.5.2 Individual cell migration metrics

To investigate which factors may drive the FGFR3-KOs altered migratory potential, data was analysed from a previous ptychographical experiment on the cell lines (Carstairs, 2017). FGFR3-KO and WT MSCs were plated in cell culture plates with a removable insert to create a space, enabling analysis of migration without generating a

wound in the cells. Cells were allowed to migrate for 24 hours, with single cell migratory metrics collected throughout the timecourse.

FGFR3-KOs covered a greater area at the end of the timecourse, despite on a single cell level having a reduced track length and velocity during migration (Fig. 3.21A-C). Additionally, FGFR3-KO MSCs show fewer cell divisions during the timecourse, suggesting increased proliferation is not the cause of the wound healing (Fig. 3.21D). However, despite normally having a smaller cell area than WT cells, during migration FGFR3-KOs show a significantly higher cell area, as well as a significantly decreased sphericity (Fig. 3.21E, F). This suggests FGFR3-KOs flatten and spread more than WT cells during migration, which aids them in covering a greater surface area. Further, FGFR3-KOs show a higher average directness, meaning they meander less than WT cells during migration, though this increase is statistically insignificant (Fig. 3.21G).

Image tracking of each well showed that WT MSCs undergo collective cell migration, in which a leader cell protrudes into the gap, and other cells follow. This creates a clear arc shape, maintaining cell:cell interactions (Fig. 3.21H). In contrast, FGFR3-KOs appear to migrate independently from each other, rather than following a leader cell, and thus swarm into the space (Fig. 3.21I). This ability to move unhindered by, and independently from, other cells may impact the direction of migration and likely contributes to the increased gap closure.

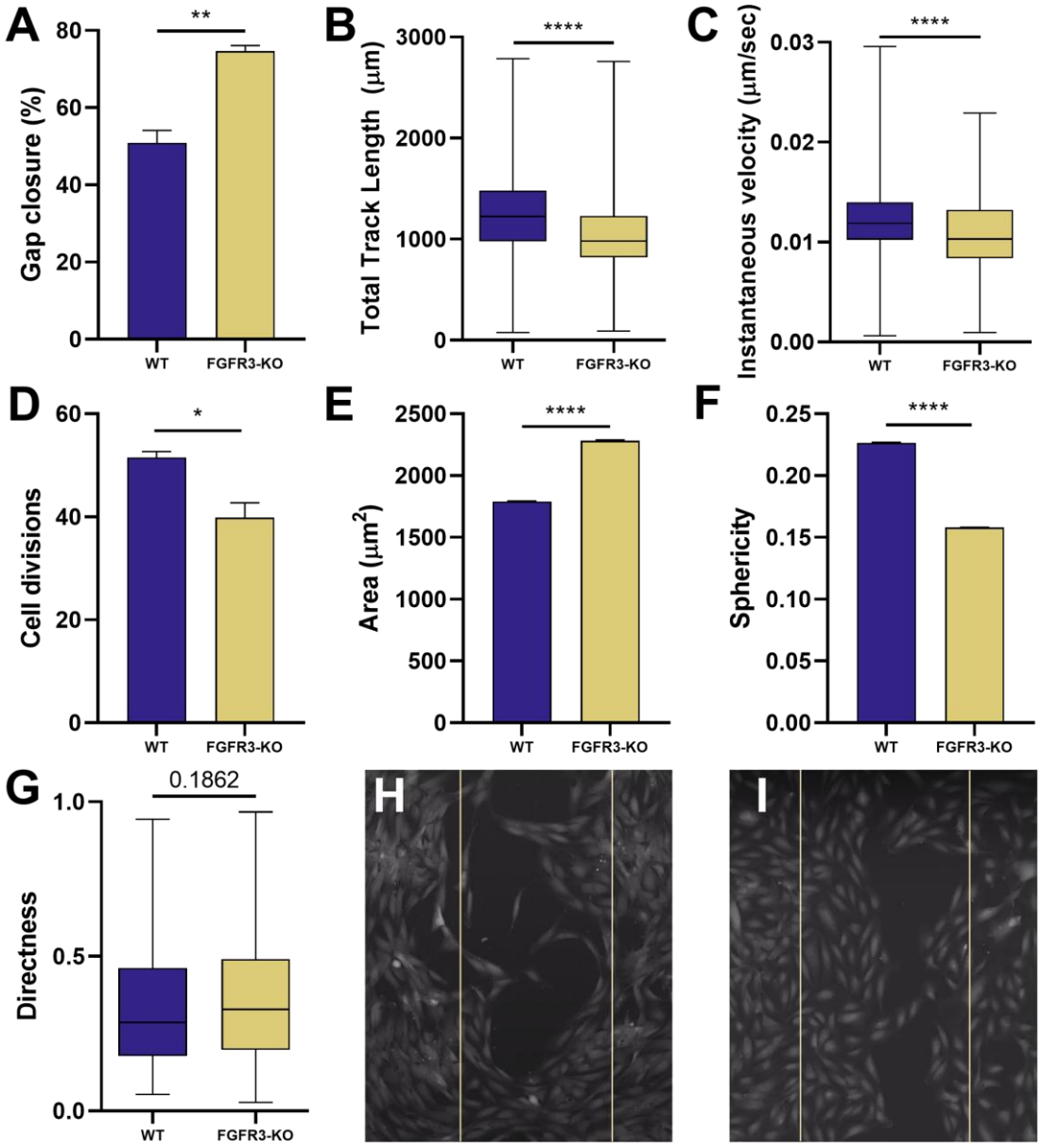

Figure 3.21. Migratory characteristics of WT and FGFR3-KO MSCs. Gap closure of WT and FGFR3-KO MSCs after 24 hours of migration (A). Total track length (B) and instantaneous velocity (C) of individual cells throughout migration. Number of cell divisions (D) within each field of view during migration. Area (E), sphericity (F) and directness (G) of individual cells throughout migration. Still images of WT (H) and FGFR3-KO (I) MSCs at the end of the 24 hour migration, with lines denoting the initial gap space. Boxplots show minimum, maximum, and quartile values. Bars show mean +SEM. **** = $p < 0.0001$; ** = $p < 0.01$; * = $p < 0.05$, as determined by Mann Whitney tests for A-C, E, F, and by t tests for D, G.

3.6 Summary

This disruption to leader-follower behaviour suggests altered cell:cell interactions and signalling. EVs, and the wider MSC secretome, are regulators of migration, and have been shown to regulate wound healing rate, directionality, and collective cell migration (Wysoczynski et al., 2019; Sagaradze et al., 2019; Shabbir et al., 2015). The MSC secretome also regulates proliferation and survival of a wide range of cell lines (Kim et al., 2012; Weil et al., 2009).

The composition and structure of the cytoskeleton regulates EV release (Beghein et al., 2018; Catalano and O'Driscoll, 2020)**,** so the quantity, shape, or properties of any EVs released by the FGFR3-KOs is likely to be altered as a result of their altered morphology. Accordingly, there was a significant enrichment for transcripts encoding proteins expressed in the extracellular vesicle amongst those differentially expressed in FGFR3-KO MSCs. For example, CD82, a tetraspanin enriched in exosomes (Andreu and Yáñez-Mó*,* 2014) was upregulated in FGFR3-KO MSCs. Thus, a number of proteins packaged into or associated with EVs have altered expression, and the functional effects of these vesicles may be affected as a result.

Therefore, the next two aims were broadly to elucidate if the FGFR3-KO secretome is altered from that of a WT MSC. Further, is this secretome sufficient to drive behaviours such as the altered migration and proliferation seen in FGFR3-KO cells, when applied to WT MSCs? As such, the EVs from WT and FGFR3-KO MSCs were next characterised, and the functional effects of each cell line's secretome studied.

Chapter 4: Results and Discussion: Characterisation and Functional Analysis of the FGFR3-KO MSC Secretome

4.1 Characterisation of extracellular vesicle size, yield, and morphology

4.1.1 Nanoparticle Tracking Analysis

Nanoparticle tracking analysis (NTA) was performed to assess the size and number of EVs secreted by WT and FGFR3-KO MSCs. EVs were isolated by differential centrifugation as described in 2.3.1, yielding fractions termed 2k, 10k, and 100k, each collected at increasing centrifugation speed.

In the 2k fraction, FGFR3-KO EVs had a broader size distribution than WT EVs, with a tendency towards larger diameters (Fig. 4.1A). The main population of WT 2k EVs had a diameter of 119nm, whereas the FGFR3-KOs had a broad main population, ranging between 127 and 150nm. The yield of EVs per million cells was $1.23x10^8$ and $3.10x10^8$ for WT and FGFR3-KO MSCs respectively. FGFR3-KOs therefore show an 2.52-fold increase in EV secretion in their 2k fraction.

In the 10k fraction, both lines showed peaks at 101nm, and a secondary peak at 147nm for WT MSCs and 141nm for FGFR3-KOs (Fig. 4.1B). Again, the yield in FGFR3-KOs was markedly increased. $2.98x10^8$ EVs per million cells were secreted by WT MSCs, and $9.29x10^8$ by FGFR3-KOs, meaning a 3.12-fold increase in secretion by FGFR3-KOs.

In the 100k fraction, FGFR3-KO EVs were, on average, larger than WT EVs. WT EVs had a modal population at 105.7nm, compared to 128nm for FGFR3-KO EVs (Fig. 4.1C). Interestingly, a small peak was observed at 72nm in the WT 100k fraction. EVs <100nm in diameter are typically classed as exosomes, though much controversy exists in the literature. By this definition, 14% of the WT 100k fraction could be classed as exosomes, compared to less than 1% in the FGFR3-KO fraction. Again, this supports a shift towards the secretion of larger EVs as a result of the removal of FGFR3. Per million cells, the 100k fraction contained $1.70x10^9$ and $4.85x10^9$ EVs for WT and FGFR3-KO MSCs respectively. Therefore, a 2.85-fold higher yield in FGFR3-KOs. The increase in yield in all three fractions may indicate a global change to the secretory pathway, rather than that biogenesis of a specific type of EV is upregulated. Since EVs are secreted and can be either uptaken by the parent cell, or surrounding cells, the higher yields may be caused either by increased production of EVs, or decreased uptake, or a combination of both.

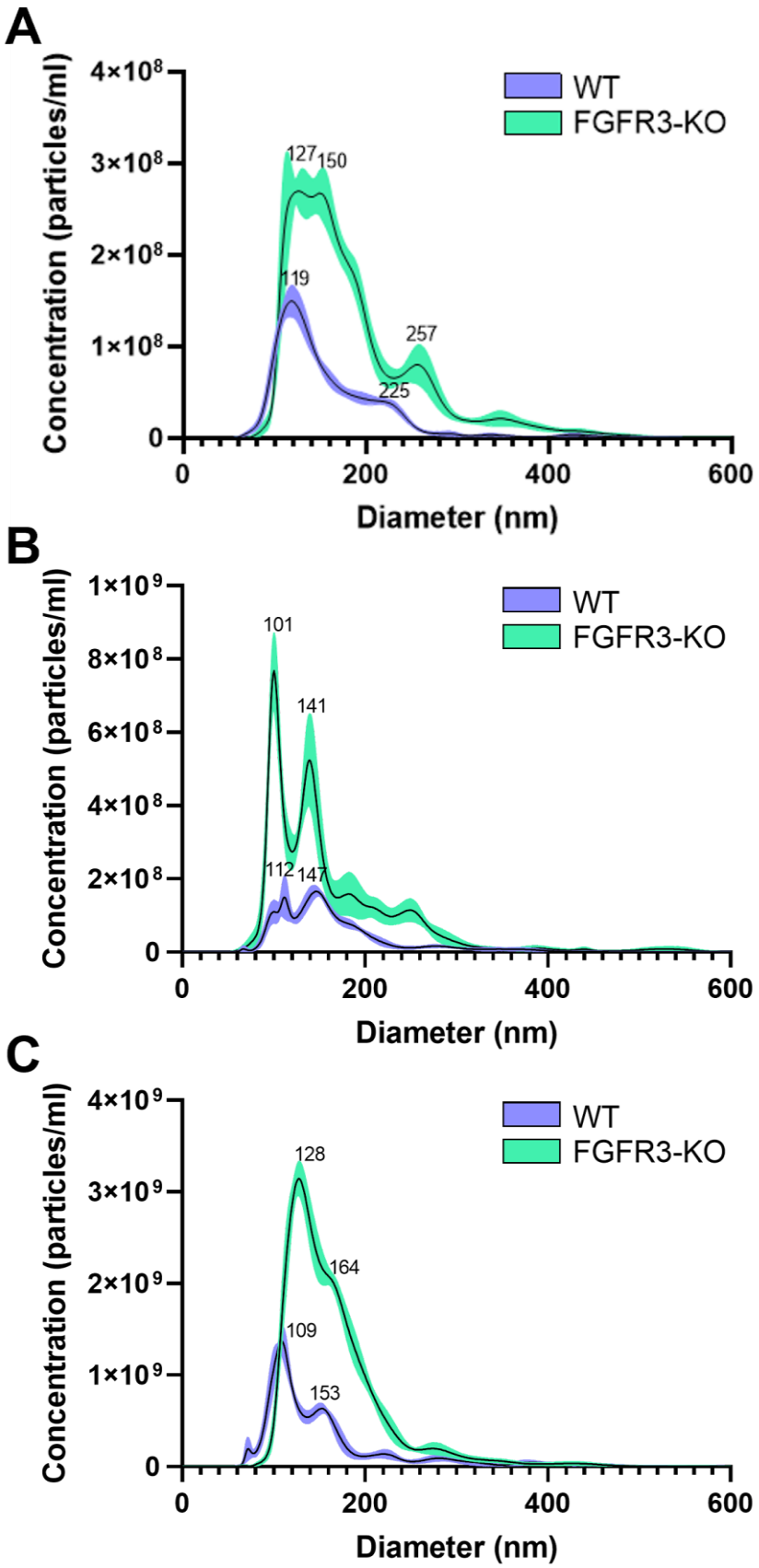

Figure 4.1. Nanoparticle tracking analysis (NTA) of extracellular vesicles (EVs) from WT and FGFR3-KO MSCs. Histogram overlays of EV size distribution for 2k (A), 10k (B), and 100k (C) fractions. Lines show mean ±SEM of 5 technical replicates.

EVs were isolated by differential centrifugation, resulting in three fractions with different densities. The 2k fraction was isolated at the lowest centrifugation speed and therefore theoretically contains the largest vesicles, and the opposite applies to the 100k fraction. However, the sedimentation of vesicles, and therefore the fraction into which they are isolated, is dependent on their size, density, and shape. Indeed, there is no trend towards a smaller size of EV in the 10k and 100k fractions (Fig. 4.2), regardless of the measure of average used or the cell line. The overlapping size distribution across different fractions indicates that density or shape contributes to the differential sedimentation rates more than EV size, for both WT and FGFR3-KO MSCs. Therefore, the amount of cargo carried in each EV is likely to differ, leading to heterogeneous populations.

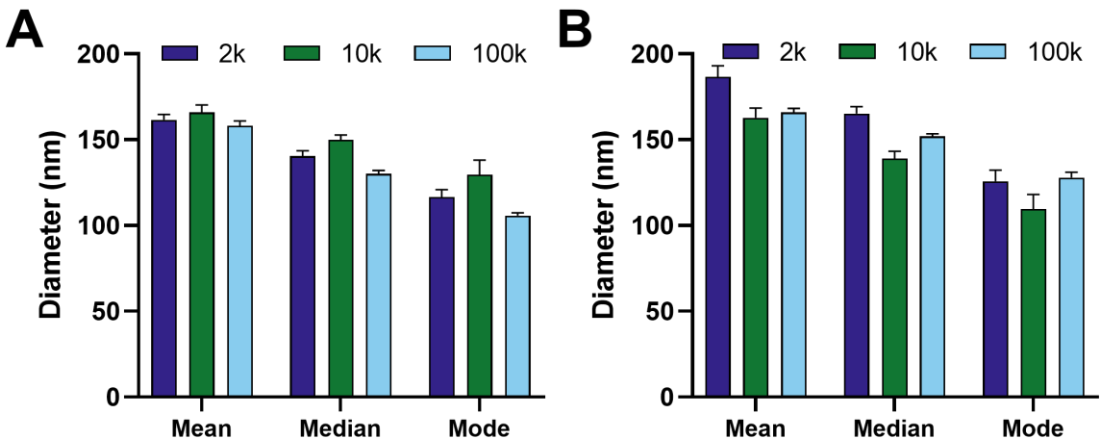

Figure 4.2. Visualisation of the average extracellular vesicle (EV) size in different isolation fractions. Mean, median, and mode diameter +SEM of EVs in the 2k, 10k, and 100k fraction for WT (A) and FGFR3-KO (B) MSCs.

4.1.2 Transmission Electron Microscopy

EV size was further investigated by TEM, which also allows study of EV morphology. Many EVs showed a typical ‘cup-shaped’ morphology, which is an artefact of the preparation process, caused by dehydration of the EVs (Fig. 4.3). Some EVs, however, remained intact, allowing their true spherical shape to be captured. FGFR3-KO EVs were much more abundant than WT ones, which was expected given the higher yields obtained in NTA calculations. That said, the number of WT EVs visualised by TEM was especially low compared to FGFR3-KO EVs. Whether there is a biological difference between the EVs that affected their attraction to the TEM grids, or simply an inefficient isolation/ TEM prep, is indeterminable. The high number of FGFR3-KO EVs per field of view allows the heterogeneity of EV size and shape to be clearly observed. Vesicles <50nm, as well as >500nm, were observed in the FGFR3-KO 100k fraction. In the 10k and 2k fractions, for both WT and FGFR3-KO MSCs, fewer EVs were observed. However, once again, WT EVs were consistently smaller than FGFR3-KO EVs. There appears a relationship between the size of EV and the morphology, whereby larger EVs seem more prone to collapsing into a cup-shape. Additionally, a number of large FGFR3-KO EVs had ruptured. This may be an artefact of the TEM preparation process, and therefore further study is required to compare the physical stability of the EVs.

From this TEM and NTA data, it is evident that FGFR3-KO EVs are larger than WT EVs, implying a novel role for FGFR3 in EV biogenesis. This may be indirect, as a result of the altered morphology and cytoskeleton, or through direct alteration to the secretory pathway. Next, the functional effects of EVs and the wider secretome were studied.

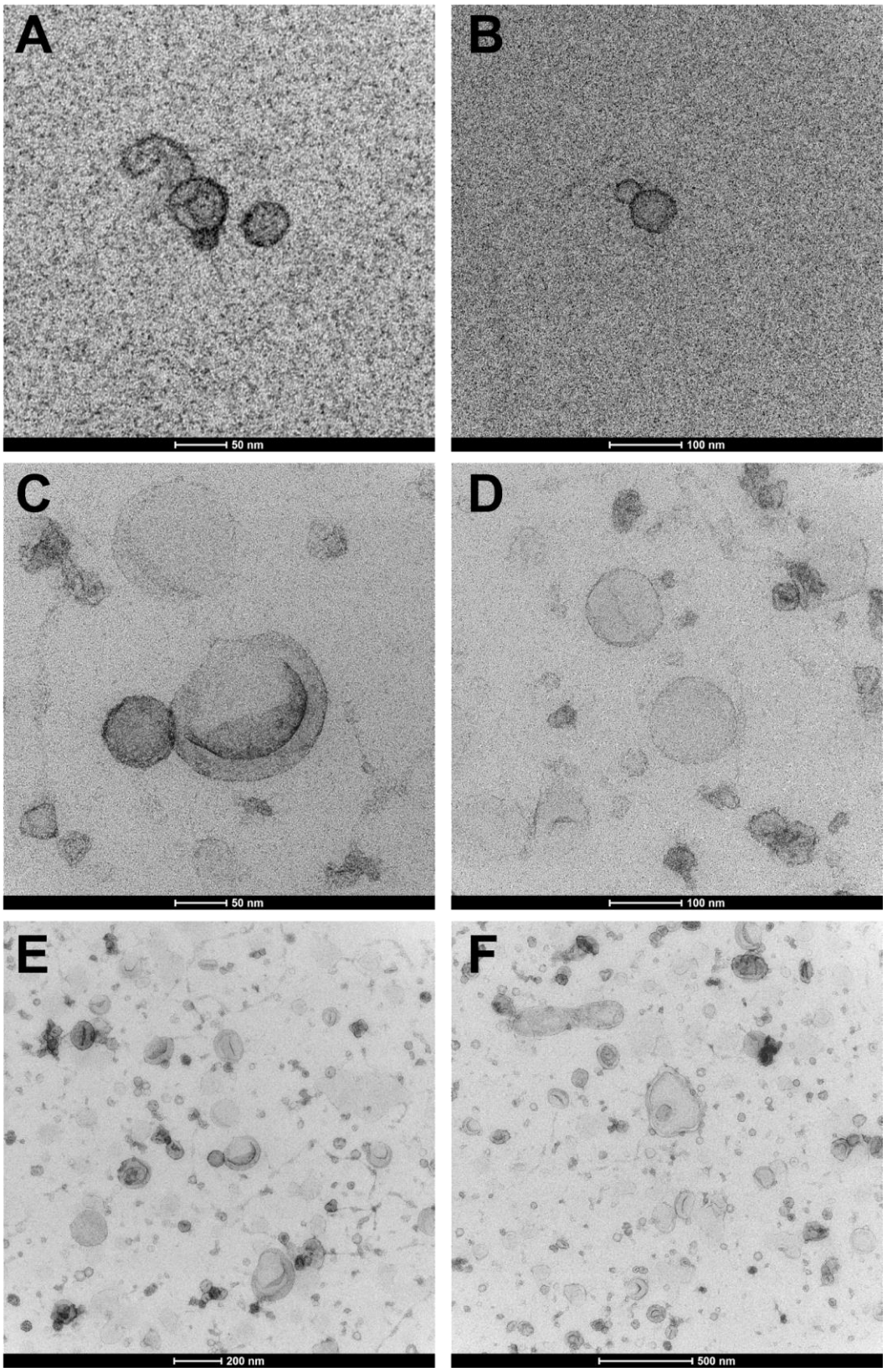

Figure 4.3. Representative transmission electron micrographs of 100k extracellular vesicles from WT and FGFR3-KO MSCs. EVs isolated from WT (A, B) and FGFR3-KO (C-F) MSCs. Scale bars as indicated on individual panels.

4.2 Functional effects of extracellular vesicles/conditioned medium

4.2.1 FGFR3-KO conditioned medium increases migration of WT cells

WT MSCs were used for a scratch wound assay, and either FGFR3-KO-derived EVs, conditioned media (CM), or EV-negative conditioned media (EV-ve CM), were applied. Individual cell metrics were tracked for 24 hours throughout wound healing.

CM and EV-ve CM significantly increased scratch closure, relative to an untreated control (Fig. 4.4A). EVs at a 1x, 5x, or 10x dose had no effect on closure. No treatment had a significant effect on track length relative to the control, however the 1x and 10x EV treatments had a significantly reduced track length compared to EV-ve CM (Fig. 4.4B). This may indicate antagonistic effects of EVs and the rest of the FGFR3-KO secretome. There were minor changes to the directness index across treatments (Fig. 4.4C). CM significantly increased the directness, whereas 5x EVs significantly decreased directness, relative to the control. This is one parameter which likely contributed to the increased wound healing percentage. Additionally, CM treated cells showed a significantly decreased thickness (Fig. 4.4D), and sphericity index, meaning they flatten more against the surface to which they are adhered. In contrast, 5x and 10x EV-treated cells show a significantly increased thickness and sphericity. This may indicate uptake of EVs is associated with cells pulling away from the growth surface and becoming more spherical. However, it is not clear whether these morphological changes are a direct result of the treatments, or a byproduct of differential migratory capacities as a result of treatments. Whether the CM treatment aids cell flattening, which aids migration, or vice versa, cannot be determined.

Increased velocity is likely the main factor contributing to the increased migration of CM and EV-ve CM treated MSCs. Both these treatments show significantly increased instantaneous velocity over the timecourse, particularly after 12 hours (Fig. 4.4E). The 5x EV dose shows a significantly decreased velocity, whereas 1x and 10x show a non-significant decrease, relative to the control.

These data suggest that the FGFR3-KO secretome, but not EVs, can promote MSC migration. This results from changes to MSC morphology, speed, and directness. Given its known regenerative properties, it was possible that improving scratch wound healing is a feature of MSC-CM in general. Thus, it was necessary to confirm that the FGFR3-KO secretome specifically is the driver of these changes.

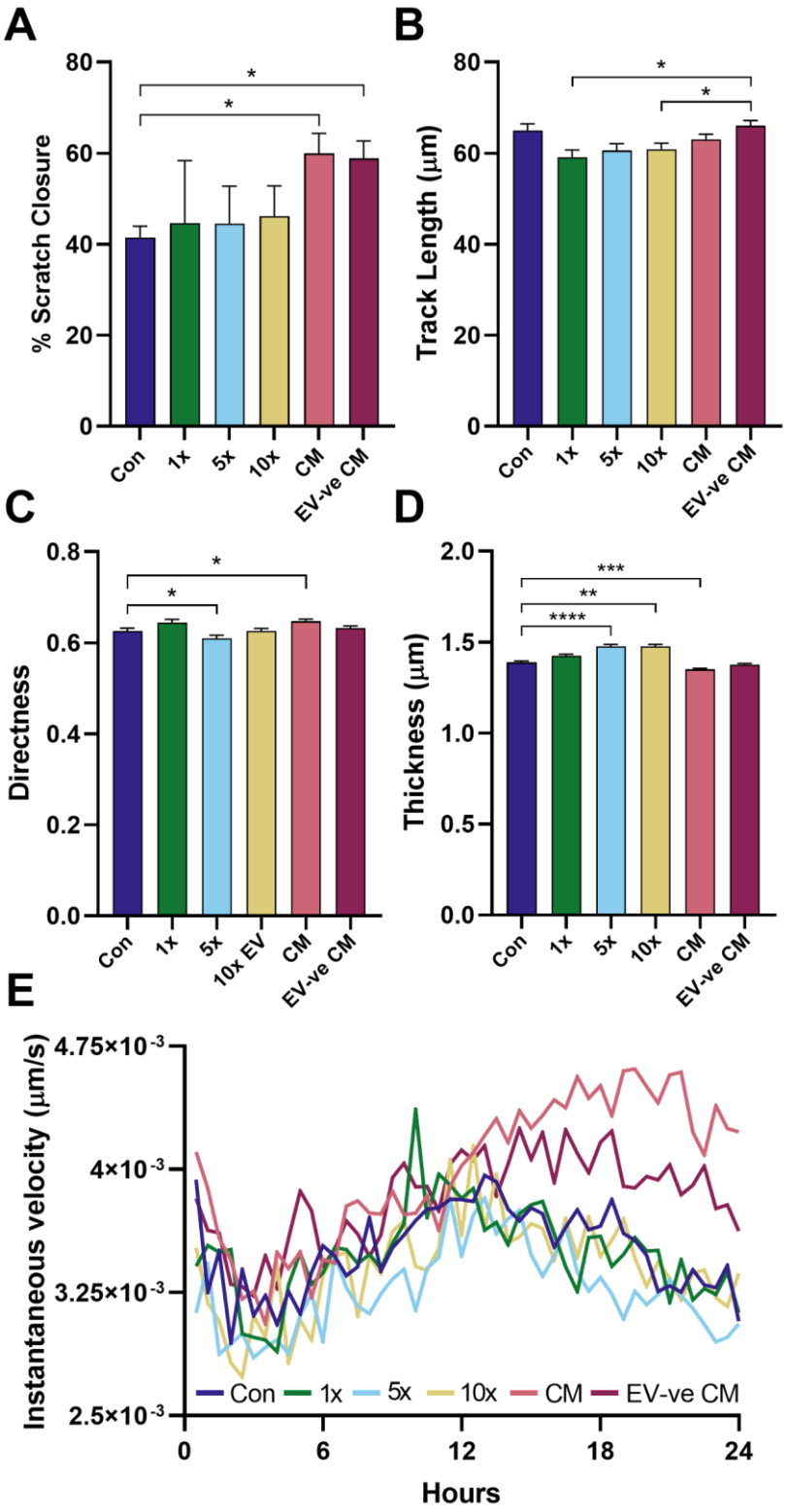

Figure 4.4. Cell migration metrics following scratch wounding of WT MSCs treated with components of the FGFR3-KO MSC secretome. Percentage scratch closure after 24 hours (A), total track length (B), directness index (C), and mean cell thickness (D). Instantaneous velocity throughout the timecourse (E). Bars show mean +SEM. Lines show means. **** = p <0.0001; ** = p < 0.01; * = p < 0.05, Tukey's multiple comparisons test (A), Dunn's multiple comparisons test (B- D).

4.2.2 FGFR3-KO, but not WT CM, improves scratch wound healing of WT MSCs

To confirm that the FGFR3-KO secretome specifically is causing the increase in migration, another scratch wound assay was performed, using WT CM as a control. FGFR3-KO MSCs themselves were also used as a positive control, to understand if WT MSCs treated with FGFR3-KO CM can recapitulate the wound healing capacity of the mutant cells.

WT cells treated with WT CM showed an increased average scratch closure, but this is insignificant relative to the untreated control ($p = 0.0769$) (Fig. 4.5). In contrast, WT cells treated with FGFR3-KO CM showed a 2.4-fold increase in scratch closure, significantly higher than that of both the untreated and WT-CM treated controls. In fact, treatment with FGFR3-KO CM conferred wound healing equivalent to that of FGFR3-KO cells themselves $p = 0.8476$).

In section 3.5.2, it was reported WT cells show a higher track speed and length than FGFR3-KO cells during migration (Fig. 3.21). It may be that WT cells treated with FGFR3-KO CM maintain these capabilities, whilst also gaining characteristics of FGFR3-KO cells that contribute to increased gap closure, such as increased area and altered collective cell migration. This was difficult to assess, because serum free media was used for all treatments, and it appears WT cells lose their typical arc-shaped migration patterns without the addition of FBS. This may simply be due to reduced migration in the absence of FBS, meaning insufficient distance is covered to see a prominent arc. However, the distribution of cells seemed more scattered, unlike the usual follow-the-leader style of MSC migration. Both cell lines also undergo morphological changes in the absence of FBS, becoming narrow and spindly in appearance. Regardless of the mechanism, it is clear that FGFR3-KO CM is a potent promoter of wound healing.

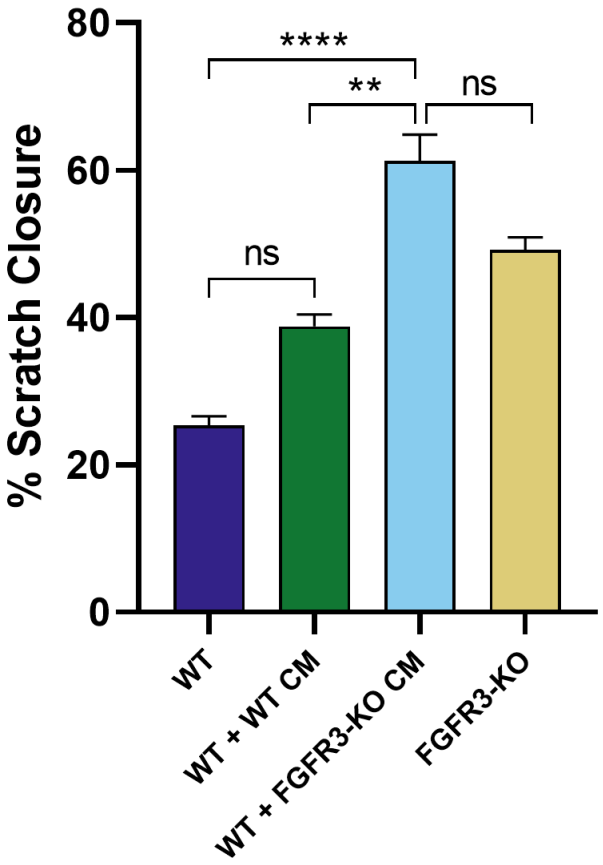

Figure 4.5. The effect of WT and FGFR3-KO conditioned media (CM) on WT MSC wound healing, compared to FGFR3-KO MSC healing. **** = $p < 0.0001$; ** = $p < 0.01$; ns = $p > 0.05$; Dunn's multiple comparisons test. Bars show mean +SEM.

4.2.3 The effect of conditioned media and fetal bovine serum on migration of MSCs

Collective migration patterns were lost in the absence of FBS supplementation to culture medium, indicating a role of FBS in MSC migration. The extent to which WT and FGFR3-KO MSCs depend on FBS for migration was assessed by further scratch wound assays. CM treatments supplemented with FBS were also used, to understand the interaction between these factors. Further, each of these treatments was applied to FGFR3-KO MSCs. Since FGFR3-KO CM improves WT migration, it was hypothesised WT CM has the potential to reduce FGFR3-KO migration.

As before, FGFR3-KO CM, but not WT CM, significantly improved WT MSC migration in the absence of serum (Fig. 4.6). With FBS supplementation, there was a 2-fold increase in wound healing relative to the serum free control. However, FBS supplementation negated the effect of CM, as neither CM had a significant effect relative to the FBS supplemented control.

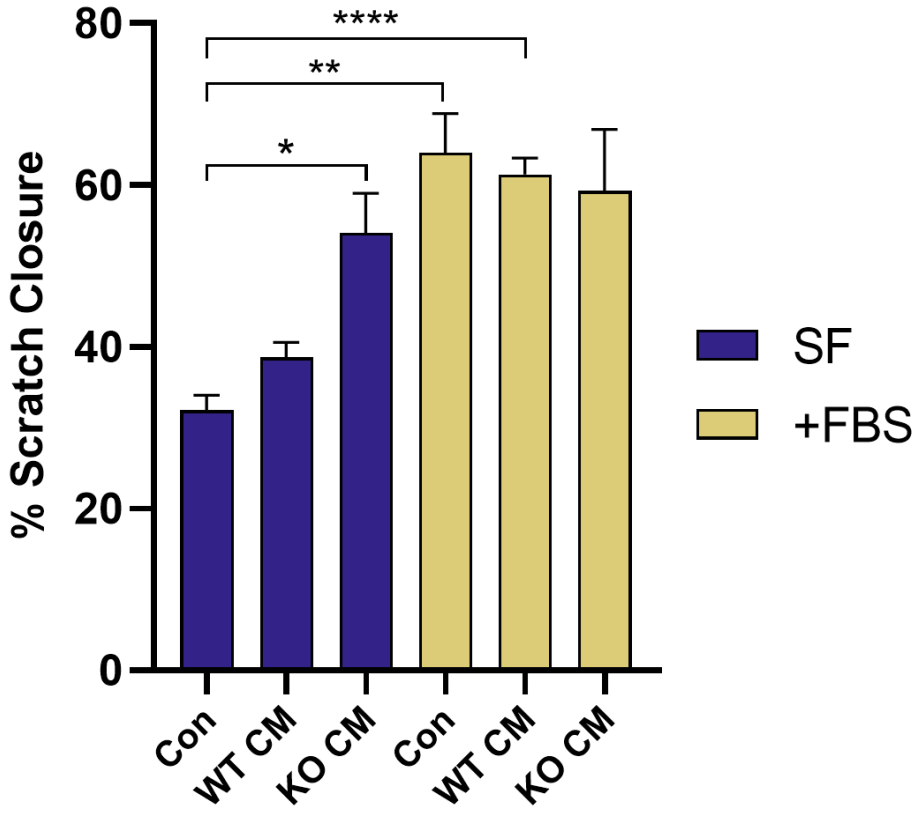

Figure 4.6. The effect of conditioned media (CM) and fetal bovine serum (FBS) on wound healing of WT MSCs. Percentage wound closure 24 hours following scratch wounding, where WT MSCs were treated with CM derived from WT or FGFR3-KO MSCs, with (+FBS) or without (SF) serum supplementation. **** = $p < 0.0001$; ** = $p < 0.01$; * = $p < 0.05$; Dunnett's T3 multiple comparisons test. Bars show mean +SEM.

When applied to FGFR3-KO MSCs, neither WT or FGFR3-KO CM treatments had a significant effect on wound healing, regardless of FBS supplementation (Fig. 4.7). FBS supplementation significantly improved wound healing. The full extent to which FBS improves migration may be clouded by the fact that a number of wells had 100% wound healing in the presence of FBS after 24 hours. This also left little room for discrimination between the effect of CM treatments in the presence of FBS. Repeating the experiment for a shorter time course would allow more accurate quantification of the differences in wound healing capacities.

From these results, it is clear FBS promotes migration of both WT and FGFR3-KO MSCs. FGFR3-KO CM can improve the migration of WT MSCs, but not FGFR3-KO MSCs. WT CM has no impact on migration of either MSC.

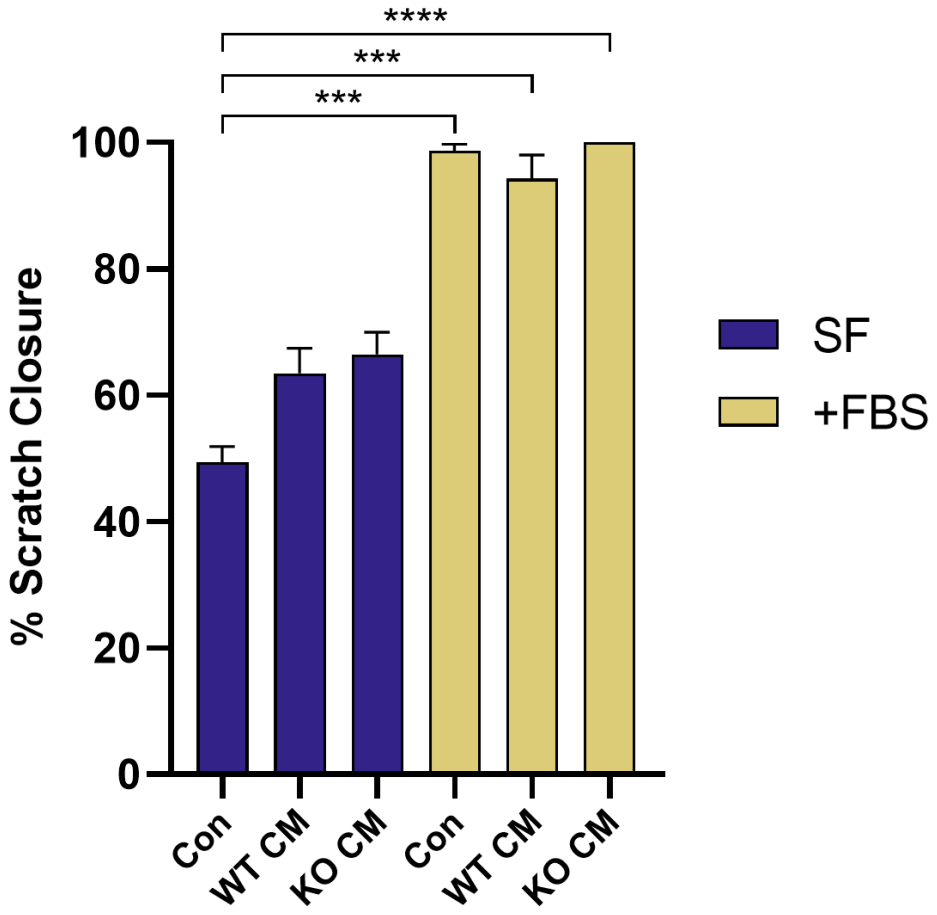

Figure 4.7. The effect of conditioned media (CM) and fetal bovine serum (FBS) on wound healing of FGFR3-KO MSCs. Percentage wound closure 24 hours following scratch wounding, where FGFR3-KO MSCs were treated with CM derived from WT or FGFR3-KO MSCs, with (+FBS) or without (SF) serum supplementation. **** = $p < 0.0001$; *** = $p < 0.001$; Dunn's multiple comparisons test. Bars show mean +SEM.

4.3 The effect of the MSC secretome on MSC proliferation and morphology

Next, WT and FGFR3-KO MSCs were treated with either CM derived from WT or from FGFR3-KO MSCs. Proliferation was assessed using alamar blue cell viability assay, but at no time point did any CM treatment have a significant effect on viable cell numbers (Fig. 4.8A). This indicates that the FGFR3-KO secretome can increase migration of WT MSCs, but that it is not sufficient to drive the increased proliferation seen in FGFR3-KO MSCs. The increased proliferation rate in these cells may instead be driven by changes to intracellular signalling pathways, as discussed earlier.

Cell morphology was also analysed following CM treatment to elucidate if the secretome contributes to the differential cell shape between the lines. WT cells showed a significant increase in cell area when treated with their own CM (Fig. 4.8B). This may indicate that whilst proliferation is not increased, WT CM can promote MSC growth. However, without assessing cell volume, it is not possible to conclude if growth is promoted, since the increase in area may be caused by a decreased sphericity index. This increase in area was not accompanied by any significant change to length:width ratio or roundness, indicating cells get larger without any change in shape (Fig. 4.8C, D). FGFR3-KO CM had no impact on WT MSC area or shape. However, treating FGFR3-KO MSCs with either WT or KO CM caused a significant decrease in cell area, especially when treated with WT CM. Again, it cannot be concluded if this decrease in cell area was driven by an overall decrease in cell volume. However, it appears that CM treatment curbs the extreme spreading phenotype seen in FGFR3-KO MSCs. Indeed, their roundness is decreased when treated with their own CM. Combined with the migratory experiments, these data indicate that both WT and FGFR3-KO MSCs are sensitive to CM, though in contrasting ways. Unlike in the migratory experiments, where FGFR3-KO CM promoted WT MSC migration to the same level as that of FGFR3-KO MSCs, it is clear no CM treatment is able to confer a change in proliferation or morphology such that WT cells behave like FGFR3-KOs, or vice versa.

The effect of FGFR3-KO EVs on WT MSC proliferation was also assessed. A preliminary experiment using varying EV doses showed little effect of any dosage at day 2. At day 3, there was a dose-dependent decrease in viable cell numbers. Cells treated with 10x EVs had a 31% lower fluorescence than the control. However, the EVs present in cell culture medium from FBS may be causing aggregation of the EVs added. Additionally, during migratory experiments the presence of FBS masked the effects of CM. Due to the requirement of both cell lines on FBS for normal proliferation,

this experiment was repeated with EV-depleted FBS and the 10x EV treatment applied. There was no significant effect of this treatment, indicating that neither FGFR3-KO CM or EVs regulate proliferation in MSCs.

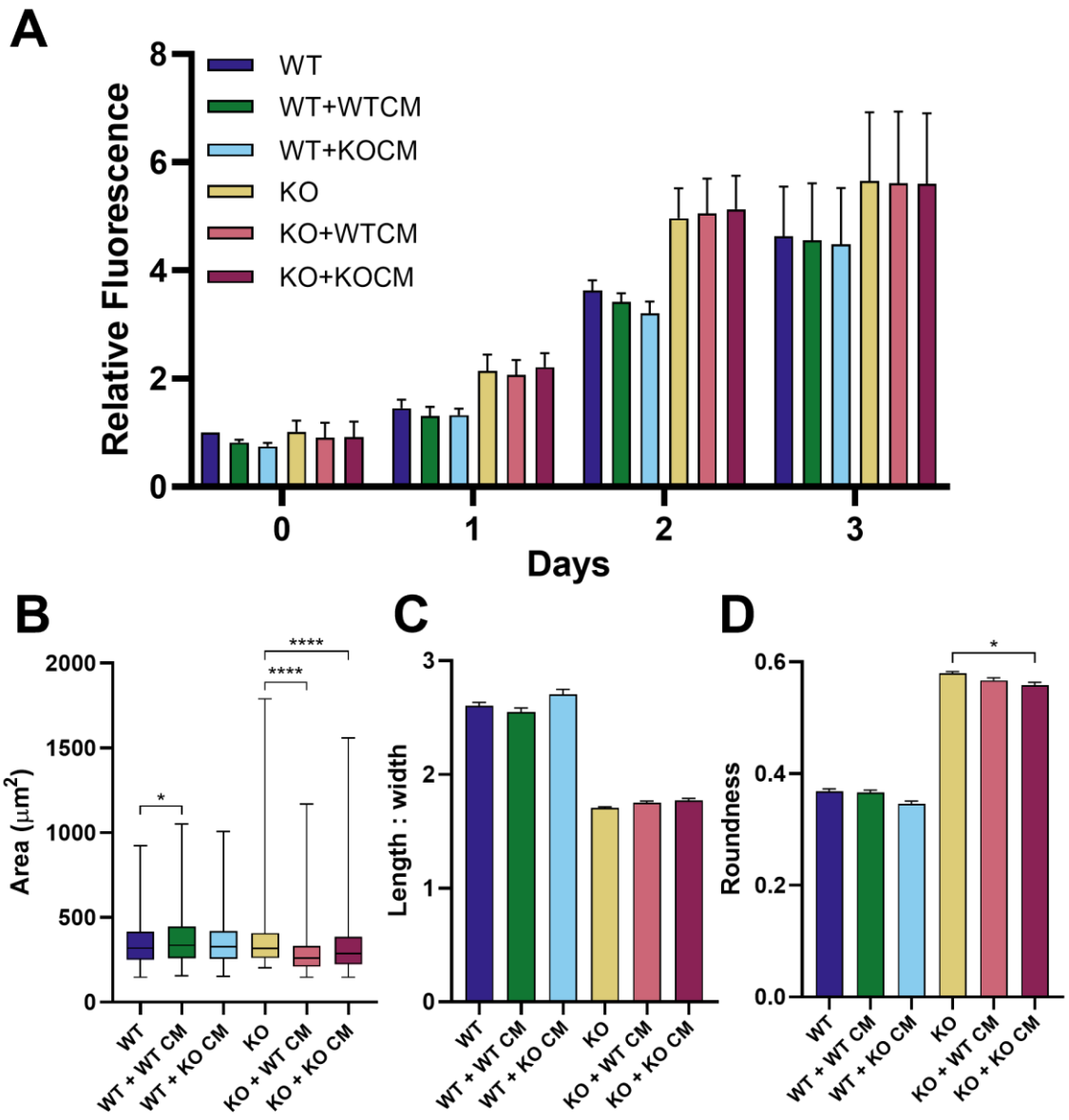

Figure 4.8. The effect of conditioned media (CM) on MSC morphology and proliferation. WT or FGFR3-KO (KO) MSCs were treated with CM derived from WT (+WT CM) or FGFR3-KO (+KO CM) MSCs, and alamar blue cell viability assay fluorescence readings taken at 600nm, shown relative to fluorescence of WT cells at day 0 (A). On day 2 of treatments, cell area (B), length: width ratio (C) and roundness (D) were calculated. Bars show mean +SEM, boxplots show 1-99 percentiles, and each quartile. No significant differences in A according to Tukey's multiple comparisons test. Significant differences relative to each untreated control shown for B-D, according to Dunn's multiple comparisons test: **** = $p < 0.0001$; * = $p < 0.05$.

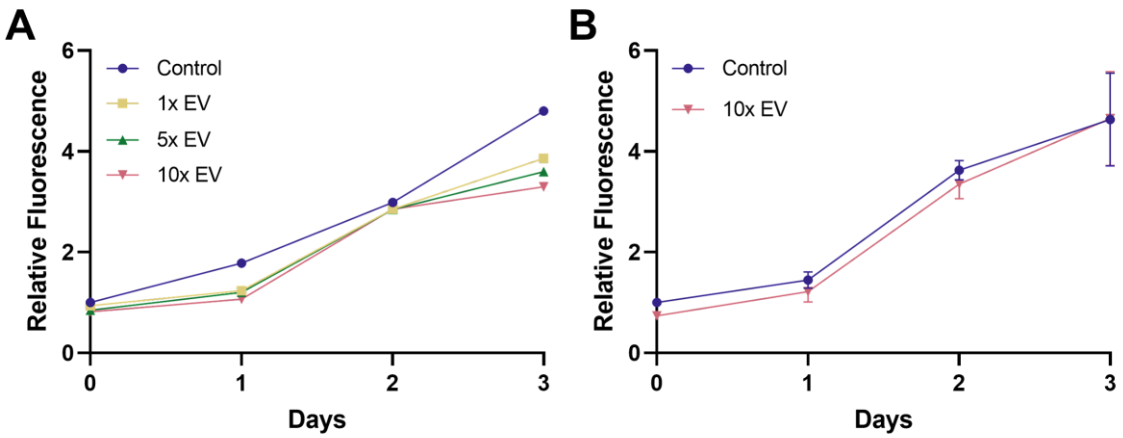

Figure 4.9. The effect of FGFR3-KO extracellular vesicles (EVs) on WT MSC proliferation. Alamar blue cell viability assay fluorescence readings 600nm, shown relative to fluorescence of WT cells at day 0. Mean ±SEM of 3 biological replicates shown for B, no significant differences according to Sidak's multiple comparisons test.

4.4 Survival and proliferation of MSCs without serum supplementation

During CM collections, MSCs are cultured in serum free media to avoid contamination with FBS EVs. Culture in serum free media typically causes growth arrest (Baserga, 1985), however it was noted that FGFR3-KO MSCs appeared to continue proliferating. As such, alamar blue viability assay was used to compare the growth of WT and FGFR3-KO MSCs in complete (10% FBS) and serum free (0% FBS) media.

As shown previously, in complete media, FGFR3-KOs show a significantly higher fluorescence than WT MSCs by day 2. By day 3, both WT and FGFR3-KO MSCs cultured in serum free media had a significantly lower fluorescence than their complete media counterparts (Fig. 4.10A). Interestingly, there was no significant difference at any timepoint between WT MSCs in complete media and FGFR3-KO MSCs in serum free. This indicates even in the absence of serum, FGFR3-KO MSCs proliferate at a similar rate to WT cells.

To understand if FGFR3-KO MSCs could maintain growth without serum, cells were cultured continuously in serum free media, and cell counts taken at each passage. WT MSCs showed no significant change in cell number over time, indicating a plateau of growth in the absence of serum (Fig. 4.10B). Cell number remained almost constant, suggesting a balance of cell proliferation and death. In contrast, FGFR3-KO MSCs showed a significant increase in cell number with time. When cells reached confluency, they were split equally into an additional culture flask, as indicated by arrows (Fig. 4.10B). This additional space to proliferate prompted a rapid increase in growth, which then slowed off as cells reached near-confluency once more. At day 21, cells were passaged more harshly to manage the exponential growth, but they struggled to recover from this sudden decrease in cell density. These data suggest that FGFR3-KOs can maintain proliferation on serum free media, with a population doubling time of as little as 32 hours. The true population doubling time may be even shorter, if an optimum seeding density and splitting ratio was devised. This increased survival and proliferation in the absence of serum may indicate an enriched secretome, containing anti-apoptotic factors that enable FGFR3-KO MSCs to survive.

Both WT and FGFR3-KO MSCs undergo dramatic morphological changes in the absence of serum (Fig. 4.10C-F). After 48 hours of culture on serum free media, WT MSCs became narrow, and spindle-like in shape, and appeared smaller in size. FGFR3-KO MSCs show a shift towards this narrow morphology, but there are still a number of rounded cells, and several with large lamellipodia.

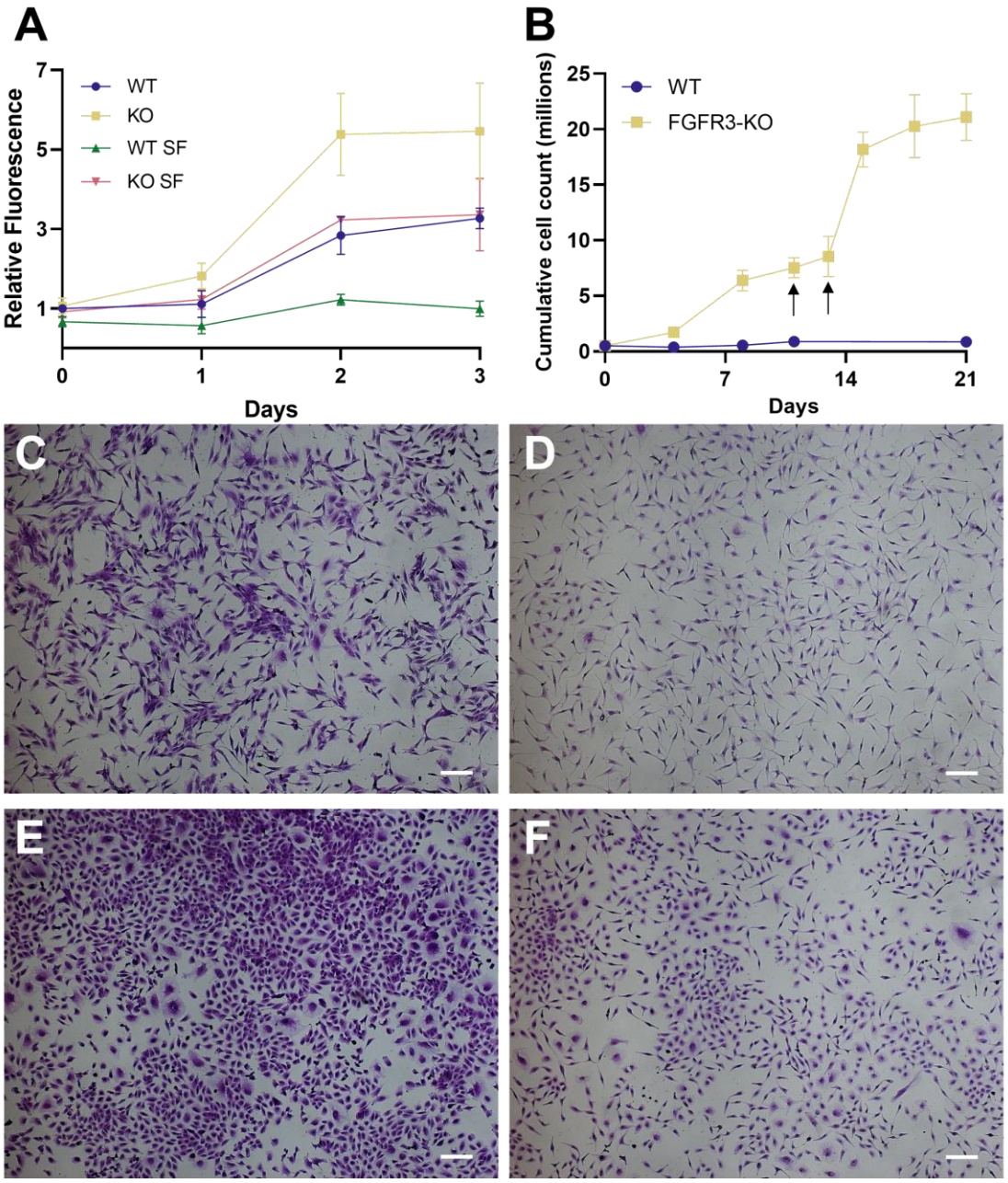

Figure 4.10. Proliferation and morphology of WT and FGFR3-KO MSCs on serum free (0% FBS) medium. Alamar blue cell viability assay (A) of WT and FGFR3-KO (KO) MSCs cultured in control or serum free (SF) medium. Fluorescence relative to WT MSCs at day 0. Cumulative cell count (B) of WT and FGFR3-KO MSCs, arrows indicating expansion into additional culture flasks. Points show means ±SEM. Brightfield images of crystal violet stained WT MSCs, cultured in complete (C) or SF (D) medium, and FGFR3-KO MSCs cultured in complete (E) or SF (F) medium. Scale bars = 200µm.

4.5 Summary

The results of this chapter suggest a drastically altered secretome of FGFR3-KO MSCs. Firstly, by an increase in EV size and yield. Second, due to the capability of FGFR3-KO CM, but not WT CM, to promote wound healing. Finally, the survival and proliferation of FGFR3-KO MSCs in the absence of serum may indicate that an enriched secretome is supporting their growth. Questions are raised that require further investigation, such as the mechanisms by which the above changes occur. Additionally, the effect of CM on cell size (volume) should be investigated, and the implications of the morphological changes caused by CM treatment require elucidation.

These results attribute novel roles to FGFR3 in MSCs that have not previously been discussed, and conclude a thorough characterisation of FGFR3-KO MSCs. Next, the implications of this data are discussed in the wider context of MSC biology, and the future directions for the study of, and therapeutic options for, FGFR3-related disorders.

Chapter 5: General Discussion

The overall aim of this study was to characterise the effect of an FGFR3 knockout mutation on MSC function. A thorough comparison of WT and FGFR3-KO MSCs, including analysis of cell behaviour, transcriptome, and secretome, elucidated the many roles of FGFR3 in MSCs. This chapter discusses these results, their implications, and their application for future research.

5.1 FGFR3 regulates proliferation of Mesenchymal Stromal Cells

The first key result was that FGFR3-KO MSCs had an equivalent clonogenic capacity to WT MSCs, forming colonies of the same size, and at the same efficiency. Therefore, FGFR3 is not essential for the adherence or survival of MSCs at low densities, in line with previous results that primary MSCs from $FGFR3^{-/-}$ mice are clonogenic (Valverde-Franco et al., 2003). However, FGFR3-KO MSCs produced denser colonies, indicating an increased proliferation rate, which was confirmed by cell metabolic activity assays and population doubling time calculations. FGFR3-KOs had a significantly faster population doubling time of 18.6 hours, compared to 25.0 hours for WT MSCs, suggesting FGFR3 normally functions to inhibit MSC proliferation. This is in accordance with a previous study showing FGFR3 is a inhibitor of proliferation in BMSCs (Su et al., 2010). However, it contradicts the notion that FGFR3's growth-inhibitory effect in achondroplasia is caused by cell arrest unique to proliferating chondrocytes (Wang et al., 2001). Instead, these results suggest that FGFR3 mutations may impact the skeletal system throughout adulthood by regulating MSC proliferation. If these results are corroborated in embryonic MSCs, it would indicate that FGFR3 mutations affect skeletal development from the earliest stage, prior to chondrocyte differentiation.

5.2 FGFR3 regulates morphology of Mesenchymal Stromal Cells

Regulation of the actin cytoskeleton in MSCs is a function that hasn't been previously attributed to FGFR3 signalling. However, the data here show FGFR3 knockout to dramatically impact MSC morphology. FGFR3-KO MSCs were consistently rounded in morphology, and sporadically enlarged in area, with wide-spreading lamellipodia. This was accompanied by remodelling of the cytoskeletal transcriptome. Arp3 drives the formation of branched actin filaments, and therefore lamellipodia (Suraneni et al., 2012), but was not found to be enriched at the lamellipodia of FGFR3-KO MSCs. This

lack of staining is an indication that differential Arp3 localisation and/or activity is not the driver of this rounded cell shape. During MSC culture, it is typical for cells to extend lamellipodia briefly before retracting the protrusions (Zimmermann and Falcke, 2014; Ryan et al., 2017). Therefore, the persistence of lamellipodia in FGFR3-KO MSCs may not be a result of increased formation of lamellipodia, but rather an inability to retract them. Myosin 9 (Myosin IIA/ MYH9) acts downstream of active FGF signalling, and causes lamellipodial retraction (Betapudi, 2010; Sai and Ladher, 2008). The transcript for MYH9 itself, and its activator, myosin light chain kinase (MLCK), are both downregulated in FGFR3-KO MSCs, indicating reduced MYH9 activity and thus may be responsible for an inability to attenuate lamellipodial extension. MYH9 can act downstream of a number of mediators, including Rho and Cdc42, as well as Rac (Tapon, 1997)

The role of Rac in FGFR3-KO MSCs was investigated due to its function upstream of Arp3, MYH9, and many other cytoskeletal proteins (Ten Klooster et al., 2006; Burridge and Wennerberg, 2004). However, no change in morphology was observed upon inhibition of Rac activation with NSC23766 for either WT or FGFR3-KO MSCs; both had non-significant differences in roundness and length:width ratio. Interestingly, inhibition of Rac caused a decrease in WT cell area but an increase in FGFR3-KO area. This may be due to altered sphericity or differences in cell growth, though there were no significant differences in the dependence of either cell line on Rac for cell survival. The exact link between FGFR3 and morphology requires further elucidation, with MYH9 a plausible candidate for the rounded phenotype in FGFR3-KO MSCs. A possible mechanistic explanation is shown in Fig. 5.1.

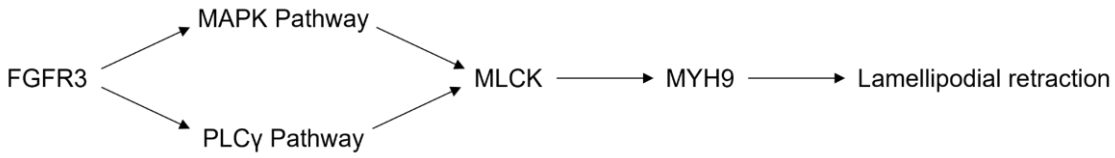

Figure 5.1. A hypothesis linking FGFR3 to lamellipodial dynamics. With the loss of FGFR3, lamellipodial retraction is diminished, generating an FGFR3-KO MSC with broad, extended lamellipodia.

5.3 FGFR3 regulates migratory behaviour of Mesenchymal Stromal Cells

Lamellipodia play a crucial role along the leading edge during migration, and mechanical force generated through actomyosin filaments is required for efficient migration (Mayor and Etienne-Manneville, 2016). Therefore, the extension of broad lamellipodia, and the altered expression of transcripts belonging to actomyosin and actin filament bundles, may predispose FGFR3-KO MSCs to a migratory phenotype. Additionally, transcripts for chemokines and proteases, including CXCL8 and 12, and MMPs 1, 2, and 11, were upregulated in FGFR3-KOs. Indeed, FGFR3-KO MSCs closed a higher percentage of both scratch wounds, and non-wounded gaps, compared to WT MSCs.

A number of differences between WT and FGFR3-KO MSCs were reversed during the migratory timecourse. First, FGFR3-KO MSCs showed fewer cell division events, suggesting either they lose their accelerated proliferation rate in response to a migratory stimulus, or that WT MSCs facilitate gap closure by accelerating their proliferation. Second, FGFR3-KO MSCs showed a significantly greater cell area than WT MSCs during migration, despite having a smaller area when not undergoing migration. This was accompanied by a significantly lower sphericity, but no difference in cell volume compared to WT MSCs. Thus, FGFR3-KO MSCs flatten against the growth surface to spread further, aiding their coverage of the gap.

As well as differences in individual cell behaviour, collective cell migration appears disrupted in FGFR3-KO MSCs. Collective cell migration has previously been shown to be dependent on FGF signalling during gastrulation (Sun and Stathopoulos, 2018), morphogenesis of the zebrafish lateral line, (Dries et al., 2020), and development of the inner ear (Sai and Ladher, 2008). However, none of these studies have specifically linked FGFR3 to collective cell migration. One key factor facilitating collective cell migration is the cell:cell interactions between leaders and followers. These interactions rely on adherens junctions maintained mainly by cadherins (Bazellières et al., 2015), and neural cadherin (cadherin 2) is significantly downregulated in FGFR3-KO MSCs. Impaired cadherin function has been shown to cause leader cells to detach from the collective sheet/ cluster and migrate separately, aiding an invasive migratory phenotype (Camand et al., 2012). Further, altered morphology and actomyosin filaments in FGFR3-KO MSCs may disrupt leader-follower dynamics, since collective migration relies on traction forces transmitted through acto-myosin cables (Reffay et al., 2014). Additionally, disruption to HSPGs in lateral line morphogenesis results in failed collective migration, due a reduction in local retention of FGF ligands and reduced FGF

signalling (Venero Galanternik et al., 2015). Thus, the altered expression of transcripts encoding HSPGs and HSPG synthesis enzymes in FGFR3-KO MSCs likely disrupts their migration patterns. The independent migration of FGFR3-KO cells may be responsible for the pathogenesis of CATSHL syndrome, one symptom of which is hearing loss. Further, the combination of disrupted migration patterns and increased proliferation in FGFR3-KO MSCs may drive the elongated, malformed skeletal structures seen in CATSHL patients and $FGFR3^{-/-}$ mice (Deng et al., 1996; Toydemir et al., 2006).

5.4 FGFR3 removal may impact the wider FGF signalling landscape

The lack of altered expression to any FGF or FGFR transcripts suggests the changes in this study are solely attributed to FGFR3, rather than disrupted signalling through any of its homologues. However, expression levels of FGF ligands or their receptors are not the only mechanism by which signalling output is determined. FGFRs are known to form both homo- and heterodimers (Plotnikov et al., 1999), and thus the loss of FGFR3 may cause different dimerisation pairings to occur, therefore triggering different intracellular signalling cascades. FGFRs face competition with one another for recruitment of downstream mediator molecules, and thus FGFR3 removal may not necessarily cause an overall decrease in FGF signalling, but rather a shift towards signalling through other receptors (Kondo et al., 2007). Similarly, despite differing affinities for ligand-binding, FGFRs also compete for FGF ligands (Yamagishi and Okamoto, 2010; Chellaiah et al., 1994). Therefore, with the removal of FGFR3 as a competitor, different ligand-receptor pairings may occur, with overactive signalling through FGFRs 1, 2 and 4 to be expected.

The reduction of extracellular HSPGs such as perlecan and aggrecan in FGFR3-KO MSCs may further potentiate this activation, due to a reduction in sequestration of ligands in the extracellular space. However, HSPGs also serve to present ligands to FGFRs, and maintain a stable FGF-FGFR complex, so the reduction in HSPG expression may in fact decrease signalling through other receptors. Whatever the effect, the remodelling of the HSPG landscape in FGFR3-KO MSCs will undoubtedly have knock-on effects on wider FGF signalling in these cells. As well as this, HSPGs have functions independent of regulating FGF signalling, for example both perlecan and aggrecan are essential for normal cartilage development (Arikawa-Hirasawa et al., 1999; Kiani et al., 2002). Their decreases in expression, and the dysregulation to other

matrix components such as collagens, may predispose FGFR3-KO MSCs to nullipotency.

5.5 FGFR3 is required for differentiation of Mesenchymal Stromal Cells

Previously, FGFR3-KO MSCs were determined to be incapable of differentiating down osteo- or adipogenic lineages (Carstairs, 2017), and this project investigated their capability to undergo chondrogenesis. The data here indicate that FGFR3 is essential for chondrogenic differentiation of MSCs *in vitro*. A similar loss of function mutation in a zebrafish model for CATSHL syndrome indicated that chondrogenesis can occur without FGFR3, but is severely disrupted, leading to disorganised arrangements and variable sizes of chondrocytes (Sun et al., 2020). During chondrogenesis, Sox9 levels peak in early differentiation before falling again (Ng et al., 1997), and persistent expression of Sox9 is associated with a block in chondrocyte differentiation at the prehypertrophic stage (Shung et al., 2012). Previously, WT MSC chondrogenic pellets have been shown to follow this pattern, with high Sox9 levels at day 7 and 14, and low levels by day 21 (Carstairs, 2017). FGFR3-KO MSC pellets, however, showed the highest expression of Sox9 at day 21.

Another potential cause for the lack of chondrogenesis in FGFR3-KOs is the downregulation of Snail1 to nearly zero expression. Snail1 and Snail2 (Slug) function downstream of FGFR3, and are both downregulated in FGFR3-KOs, which was unexpected given that in single knockout models, loss of one Snail gene causes upregulation of the other in order to compensate (Chen and Gridley, 2013). There is therefore some redundancy in their activity, but together they are essential for chondro- and osteogenesis. Additionally, transcriptomic data indicated an increase in activity of Wnt signalling in FGFR3-KO MSCs. This is in accordance with a recent study in which FGFR3-deficient zebrafish mimicked a CATSHL phenotype, partially through elevated Wnt signalling (Sun et al., 2020).

The results in this project suggest FGFR3 is required for chondrogenic differentiation of MSCs, but in the achondroplasia group of disorders, activated FGFR3 causes a decrease in endochondral ossification as a result of decreased chondrocyte proliferation and differentiation. There is wide agreement that the role of FGFR3 depends on the stage of development, and expression of FGFR3 varies in level throughout the chondrogenic differentiation process (Peters et al., 1993; Delezoide et al., 1998), suggesting that some stages of differentiation are more dependent on

FGFR3 than others. In FGFR3-KO MSCs, competency to commit to the chondrogenic lineage may be lost, even if subsequent differentiation stages would be possible without FGFR3 signalling. Chondrogenesis begins with the condensation of MSCs, and requires maintenance of cell:cell interactions, which is dependent on the precise modulation of neural cadherin levels (Tuli et al., 2003). As discussed previously, neural cadherin expression is downregulated in FGFR3-KOs. Accordingly, FGFR3-KO pellets showed an increased fragility in comparison to WT pellets, and therefore may be unable to differentiate due to the gene expression changes caused by FGFR3 loss, rather than due to an inactivation of FGFR3 signalling itself. Confirmation of these observations and mechanistic studies *in vivo* are required to fully elucidate the pathogenesis of FGFR3-related skeletal dysplasias.

5.6 FGFR3 regulates the secretome of Mesenchymal Stromal Cells

These observations provided a variety of reasons to investigate the FGFR3-KO MSC secretome. The MSC secretome regulates cell behaviours including proliferation, differentiation, and migration, which are all dysregulated in FGFR3-KO MSCs. There was also significant enrichment for transcripts encoding extracellular proteins amongst both the upregulated and downregulated transcripts. Additionally, the composition and structure of the cytoskeleton regulates extracellular vesicle (EV) release (Beghein et al., 2018; Catalano and O'Driscoll, 2020), so the quantity or properties of any EVs released by the FGFR3-KOs is likely to be affected by their morphological changes.

The MSC secretome has much therapeutic potential, with studies showing regenerative and anti-inflammatory effects in a variety of disease models, including skeletal disorders, as introduced in section 1.5. Thus, understanding if FGFR3-KO MSC behaviour is driven by its secretome, and if the WT secretome can correct this behaviour, could aid developmentof therapeutic strategies.

First, EVs from WT and FGFR3-KO MSCs were characterised, and FGFR3-KO EVs were found to be more abundant in yield, and larger in size. To date, no literature has found a link between FGFR3, or indeed FGF signalling, and EV biogenesis. Whether there is a mechanism by which loss of FGFR3 disrupts the secretory pathway, or whether the altered morphology of the cells indirectly drives EV release, is unclear. Overall, FGFR3-KOs secreted 2.87-fold more EVs per million cells than WT MSCs. This may be driven by a combination of increased EV release, and decreased uptake, leading to a larger yield in conditioned medium. In all three fractions, FGFR3-KO EVs

showed a shift towards larger diameters than WT EVs. TEM images highlighted the heterogeneity of these populations, with vast diversity in EV size within the 100k fraction alone. That said, more repeats are needed for both the NTA and TEM to determine the significance of these results, particularly in the case of the WT TEM, which yielded few images due to difficulty locating particles in on the grid. The particles yielded from EV isolations are referred to as EVs throughout this study, but the presence of other particles such as apoptotic bodies, and non-vesicular contaminants such as lipoproteins, cannot be excluded. Further experiments, including western blotting to confirm the presence of EV markers such as Alix, CD9 and CD63, as well as the absence of exclusion markers such as GP96 (Kowal et al., 2016), should be conducted to define the nature of the isolated particles. The International Society for Extracellular Vesicles suggests that the presence of at least 3 expected EV proteins should be validated in at least a semi-quantitative manner, for example by Western blot, flow cytometry, or mass spectrometry (Lötvall et al., 2014). Going forward, to build upon the results of this study, the isolates must be defined as EVs in this way.

5.7 Functional effects of the WT and FGFR3-KO MSC secretome

Despite this shift in EV size and yield, there appeared no bioactivity of FGFR3-KO EVs when applied to WT MSCs in either migration or proliferation assays. Nevertheless, their potential should not be dismissed, as there are weaknesses in all exosomal isolation methods (Xu, R. et al., 2016), and the exact contents and purity of isolates in this study requires further investigation. A different approach to EV dosage may also result in bioactivity. In this study, for a 1x dosage, cells were treated with a dosage theoretically equivalent to the number of EVs that they themselves produce in a 24 hour timeframe. Differential rates of EV production between the cell lines were not accounted for, therefore skewing these dosages for experiments where FGFR3-KO EVs were applied to WT MSCs. Particle number or protein concentration would provide a more standardised way to dose cells.

Additionally, before asserting no effect of the EVs, the interaction (if any) of EVs with the cells should be confirmed. There is inherent competition between native EVs and those introduced in these experiments, and it has not been confirmed the methods used here are sufficient to allow EV internalisation or binding. Fluorescent labelling of EVs could be used to monitor their interaction with cells, therefore confirming if EVs truly have no effect, or if they simply have not been delivered to the cell surface. Finally, the storage of conditioned media (CM) prior to EV isolation may have

contributed to reducing the bioactivity or yield of EVs, due to the failure to remove cell debris prior to freezing- it is possible EVs may have aggregated amongst this debris and been lost during isolation. The presence of dead cells in CM may have negative effects on bioactivity, however it is noted that as of 2018, no studies have reported effects of CM storage conditions on EV stability or bioactivity (Jeyaram and Jay, 2018). Additionally, Jeyaram and Jay review studies on EVs isolated from several biofluids (blood, urine, semen) which retain their stability and bioactivity even after the biofluid was stored unprocessed for several months, up to several years. Whilst the effect of storage cannot be discounted- as improper storage can alter EV morphology, quantity, and contents- it seems unlikely short term freezing of unprocessed CM would drop EV bioactivity to zero.

Both complete CM and EV-negative CM (EV-ve CM) derived from FGFR3-KOs significantly increased scratch wound healing of WT MSCs. The cells from these treatment groups showed a number of changes compared to the untreated control, including an increased directness, decreased cell thickness, and increased instantaneous velocity. Increasing the wound healing of WT MSCs was a function unique to FGFR3-KO CM, as application of WT CM had no significant effect on healing. Once again, this supports evidence that FGFR3-KO MSCs have an altered secretome. Previous studies show that whilst MSC-CM can promote wound healing, it is dependent on the presence of particular factors in the secretome, such as CXCL12 (SDF-1), which belongs to the Extracellular Vesicle cellular component GO term, as well as HGF and CCL2 (MCP-1) (Shen et al., 2015). Transcripts for both CXCL12 and HGF were significantly upregulated in FGFR3-KO MSCs, and therefore may contribute to the healing effect of FGFR3-KO CM. CCL2 was downregulated in FGFR3-KOs, but it is likely there are many other proteins that regulate the effect of CM, beyond these three.

Neither WT nor FGFR3-KO CM significantly promoted wound healing of FGFR3-KO MSCs. This, combined with the result that neither CM had an effect on proliferation of either cell line, indicates that FGFR3-KO MSCs are not sensitive to the WT MSC secretome. As such, using the MSC secretome as a therapy for FGFR3 disorders may yield ineffective results. That said, aberrant differentiation is a key component of dysplasia pathologies, and this project did not examine if the WT MSC secretome could restore the tripotency of FGFR3-KO MSCs.

5.8 FGFR3-KO MSCs proliferate in the absence of serum supplementation

Bringing together migration and proliferation experiments elucidates the role of FBS in WT and FGFR3-KO MSCs. Supplementation of media with FBS during scratch wound experiments promoted healing of both cell lines, though the extent to which FGFR3-KO MSCs increased migration may be clouded by several wells reaching 100% wound coverage before imaging. Neither CM had a significant effect on either cell line's migration with the addition of FBS, suggesting that FBS masks the effect of the FGFR3-KO secretome, or simply that cells were already migrating at their maximum capability. Again, FGFR3-KO MSCs reaching 100% healing leaves for little discrimination between CM treatments when supplemented by FBS, and thus a shorter timecourse would be useful to confirm this conclusion. Since FBS is capable of masking the effect of CM on migration, it may be that FBS also masks the effect of EVs/CM on proliferation, and therefore these treatments should be repeated in serum free media and proliferation reassessed.

WT MSCs are entirely dependent on FBS for proliferation, and showed no significant increase in viable cell number or cumulative cell count during proliferation timecourses. Although FGFR3-KO MSCs showed a slower increase in viable cell number in the absence of serum compared to FGFR3-KO MSCs in the presence of serum, they still showed a significant increase in growth over the 3 day timecourse. In fact, over 3 days, FGFR3-KO MSCs in the absence of serum demonstrated proliferation equivalent to WT MSCs in the presence of serum. Over 21 days, FGFR3-KO MSCs showed sustained proliferation in the absence of serum, with a population doubling time of 32 hours at their fastest. This is less than double their normal population doubling time of 18.6 hours. WT MSCs, on the other hand, took 10.8 days- 259.2 hours- to undergo one population doubling in the absence of serum, compared to a normal population doubling time of 25 hours. This shows the striking difference in the dependence on FBS supplementation for growth between the cell lines, and may be indicative of the FGFR3-KO secretome being self-sustaining. Nonetheless, both WT and FGFR3-KOs showed morphological changes in the absence of serum, characterised by a decrease in size and roundness, although FGFR3-KO MSCs with extended lamellipodia still remained.

5.9 Conclusions and future directions

Altogether, the removal of FGFR3 causes a shift towards a fast-growing, migratory, non-differentiating MSC with resistance to serum starvation. This is striking given that in a variety of cell types and tissues, FGFR3 is considered an oncogene, and such behaviours are gained upon activating FGFR3 mutations rather than knockout (Dieci et al., 2013; Helsten et al., 2016). Ectopic FGFR3 expression in B cells, for example, promotes proliferation and decreases their dependence on external mitogenic stimuli for growth (Plowright et al., 2000; Li et al., 2001). Therefore, the results of this project suggest a unique function of FGFR3 in MSCs. The role of FGFR3 in skeletal progenitors has been often overlooked in favour of studying its function in differentiated cells such as chondrocytes, but these results highlight the importance of FGFR3 in MSCs.

There is undoubtedly interplay between the altered behaviours in FGFR3-KO MSCs, such that it is difficult to determine which effects are a direct result of FGFR3 loss, and which are secondary, indirect effects. As discussed above, for example, cytoskeleton composition and structure affects EV release. Therefore, the increased EV yield from FGFR3-KO MSCs may be a consequence of cytoskeletal changes, rather than being due to a role of FGFR3 in the secretory pathway. These complex interactions between different cell behaviours are summarised in Fig. 5.2.

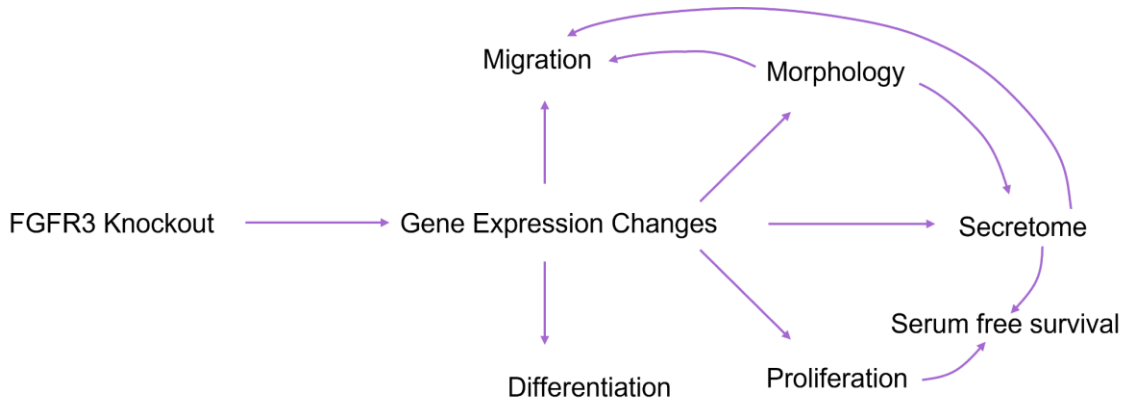

Figure 5.2. A summary of the cell behaviours impacted by removal of FGFR3 in MSCs and how these interact with one another.

As discussed throughout this chapter, a number of additional investigations would further our understanding of the wide-ranging effects of FGFR3 removal. Additionally, the specificity of the FGFR3 knockout should be confirmed. Restoring FGFR3 expression and showing restoration of WT behaviours would confirm the effectiveness of the CRISPR modification. Mechanistic links between FGFR3 and the phenotypes found in FGFR3-KO MSCs have been proposed based on existing literature and changes in transcript expression, but the role of these pathways should be confirmed by specific inhibition of putative regulators. Elucidating the regulators of these changes could provide therapeutic targets for CATSHL syndrome and other skeletal dysplasias.

Appendices

Supplementary Table 1. Notable genes with significantly increased expression in FGFR3-KO MSCs compared to WT.

Expression values are in fragments per kilobase million (FPKM) with genes displayed in descending order of log2 fold change.

Gene	Alternative gene name(s)	WT FPKM	FGFR3-KO FPKM	Log2 Fold Change	Q Value
MMP1	matrix metallopeptidase 1	9.6807	137.386	3.82698	0.00386
WNT5A	wingless-type MMTV integration site family, member 5A	3.88487	22.007	2.50202	0.00386
SOX9	SRY (sex determining region Y)-box 9	1.89073	8.63933	2.19198	0.00386
CXCL8	chemokine (C-X-C motif) ligand 8	16.2835	64.1532	1.97811	0.00386
TGFBR2	transforming growth factor, beta receptor II (70/80kDa)	18.5831	71.3693	1.94131	0.00386
TGFBR3	transforming growth factor, beta receptor III	2.34826	7.49133	1.67363	0.00386
FZD8	frizzled class receptor 8	16.1209	51.1987	1.66718	0.00386
MMP11	matrix metallopeptidase 11	4.01558	10.7522	1.42095	0.00386
CXCL12	chemokine (C-X-C motif) ligand 12	187.032	408.558	1.12726	0.00386
CD82	CD82 molecule	3.44016	7.47519	1.11964	0.01345
RND3	Rho family GTPase 3	51.9246	107.725	1.05287	0.00386
MMP2	matrix metallopeptidase 2	209.665	424.583	1.01796	0.00386
TWIST2	twist family bHLH transcription factor 2	27.2969	54.9548	1.00951	0.00386

Supplementary Table 2. Notable genes with significantly decreased expression in FGFR3-KO MSCs compared to WT.

Expression values are in fragments per kilobase million (FPKM) with genes displayed in descending order of log2 fold change.

Gene	Alternative gene name(s)	Y201 FPKM	FGFR3-KO FPKM	Log2 Fold Change	Q Value
ACAN	aggrecan	166.185	0.67039	-7.9536	0.00386
SNAI1	snail family zinc finger 1	8.42918	0.07849	-6.7467	0.04924
ACTA2	actin, alpha 2, smooth muscle, aorta	788.323	28.9517	-4.7671	0.00386
COL15A1	collagen, type XV, alpha 1	7.8741	0.5336	-3.8833	0.00386
PODN	podocan	15.8445	1.1786	-3.7488	0.00386
COL4A1	collagen, type IV, alpha 1	124.814	9.56315	-3.7062	0.00386
ELN	elastin	137.292	10.6966	-3.682	0.00386
DKK3	dickkopf WNT signaling pathway inhibitor 3	8.46895	0.96117	-3.1393	0.0073
LUM	lumican	13.6388	1.85012	-2.882	0.00386
CTGF	connective tissue growth factor	25.1534	322.256	-2.4346	0.00386
COL4A2	collagen, type IV, alpha 2	178.282	34.9657	-2.3502	0.00386

COL12A1	collagen, type XII, alpha 1	29.9021	6.68071	-2.1622	0.00386
SNAI2	snail family zinc finger 2	95.0643	22.1335	-2.1027	0.00386
COL5A1	collagen, type V, alpha 1	103.153	24.3305	-2.0839	0.00386
RHOB	ras homolog family member B	84.7711	22.7324	-1.8988	0.00386
MYL9	myosin, light chain 9, regulatory	312.021	92.5225	-1.7538	0.00386
BGN	biglycan	598.86	177.878	-1.7513	0.00386
COL16A1	collagen, type XVI, alpha 1	17.2986	5.6177	-1.6226	0.00386
COL5A2	collagen, type V, alpha 2	101.732	33.6797	-1.5948	0.00386
COL5A1	collagen, type V, alpha 1	76.8592	26.8642	-1.5165	0.00386
MYLK	myosin light chain kinase	8.90043	3.15724	-1.4952	0.01632
ADAMTS2	ADAM metallopeptidase with thrombospondin type 1 motif, 2	69.3168	24.6129	-1.4938	0.00386
AGRN	agrin	28.8162	10.831	-1.4117	0.00386
HSPG2	heparan sulfate proteoglycan 2	58.2907	22.0096	-1.4051	0.00386
POSTN	periostin, osteoblast specific factor	361.313	136.445	-1.4049	0.04065
RAC2	ras-related C3 botulinum toxin substrate 2 (rho family, small GTP binding protein Rac2)	19.4946	7.43916	-1.3899	0.00386

List of Abbreviations

ADAMTS: A disintegrin and metalloproteinase with thrombospondin motifs

Arp3: Actin related protein 3

BMSC: Bone marrow stromal cell

CATSHL: Campodactyly, tall stature, and hearing loss

CFU-F: Fibroblast colony forming units

CM: Conditioned media

DAPI: 4′,6-diamidino-2-phenylindole

ECM: Extracellular matrix

EV: Extracellular vesicle

EV-ve CM: Extracellular vesicle-negative conditioned media

FBS: Foetal bovine serum

FGF: Fibroblast growth factor

FGFR: Fibroblast growth factor receptor

FGFR3-KO: Fibroblast growth factor receptor 3 knockout

HSPG: Heparan sulfate proteoglycan

hTERT: Human telomerase reverse transcriptase

JAK/STAT: Janus kinase- signal transducer and activator of transcription

MAPK: Mitogen-activated protein kinase

MLCK: Myosin light chain kinase

MMP: Matrix metalloproteinase

MSC: Mesenchymal stromal cell

NTA: Nanoparticle tracking analysis

PI3K: Phosphoinositide 3-kinase

PLCγ: Phospholipase C gamma

SADDAN: Severe achondroplasia with developmental delay and acanthosis nigricans

TEM: Transmission electron microscopy

TGFβ: Transforming growth factor beta

WT: Wild type

References

Akai, J., Halley, P. A. and Storey, K. G. (2005). FGF-dependent Notch signaling maintains the spinal cord stem zone. *Genes & development*, 19 (23), pp.2877–2887.

Akiyama, H. et al. (2002). The transcription factor Sox9 has essential roles in successive steps of the chondrocyte differentiation pathway and is required for expression of Sox5 and Sox6. *Genes & development*, 16 (21), pp.2813–2828.

Andreu, Z., & Yáñez-Mó, M. (2014). Tetraspanins in extracellular vesicle formation and function. *Frontiers in immunology*, 5, p.442. https://doi.org/10.3389/fimmu.2014.00442

Arikawa-Hirasawa, E. et al. (1999). Perlecan is essential for cartilage and cephalic development. *Nature genetics*, 23 (3), pp.354–358.

Baffour, S. A. et al. (2015). Biological Functions of Plasma Membrane-Derived Extracellular Vesicles and Their Role in Diseases. *Journal of Cells*, pp. 33–42. doi: 10.18488/journal.97/2015.1.2/97.2.33.42.

Baserga, R. (1985). *The Biology of Cell Reproduction*. Harvard University Press.

Bazellières, E. et al. (2015). Control of cell-cell forces and collective cell dynamics by the intercellular adhesome. *Nature cell biology*, 17 (4), pp.409–420.

Beghein, E. et al. (2018). Cortactin and fascin-1 regulate extracellular vesicle release by controlling endosomal trafficking or invadopodia formation and function. *Scientific Reports*, 8 (1). [Online]. Available at: doi:10.1038/s41598-018-33868-z.

Behr, B. et al. (2010). Fgf-9 is required for angiogenesis and osteogenesis in long bone repair. *Proceedings of the National Academy of Sciences of the United States of America*, 107(26), pp. 11853–11858.

Bellus, G. A. et al. (1995). Achondroplasia is defined by recurrent G380R mutations of FGFR3. *American journal of human genetics*, 56(2), pp. 368–373.

Betapudi, V. (2010). Myosin II motor proteins with different functions determine the fate of lamellipodia extension during cell spreading. *PloS one*, 5 (1), p.e8560.

Biancone, L. et al. (2012). Therapeutic potential of mesenchymal stem cell-derived microvesicles. *Nephrology Dialysis Transplantation*, pp. 3037–3042. doi: 10.1093/ndt/gfs168.

Bortolotti, F. et al. (2015). In vivo therapeutic potential of mesenchymal stromal cells depends on the source and the isolation procedure. *Stem cell reports*, 4(3), pp. 332–339.

Braga, V. M. M. et al. (1997). The Small GTPases Rho and Rac Are Required for the

Establishment of Cadherin-dependent Cell–Cell Contacts. *Journal of Cell Biology*, 137 (6), pp.1421–1431. [Online]. Available at: doi:10.1083/jcb.137.6.1421.

Bretscher, M. S. and Aguado-Velasco, C. (1998). Membrane traffic during cell locomotion. *Current Opinion in Cell Biology*, 10 (4), pp.537–541. [Online]. Available at: doi:10.1016/s0955-0674(98)80070-7.

Burridge, K. and Wennerberg, K. (2004). Rho and Rac take center stage. *Cell*, 116 (2), pp.167–179.

Camand, E. et al. (2012). N-cadherin expression level modulates integrin-mediated polarity and strongly impacts on the speed and directionality of glial cell migration. *Journal of cell science*, 125 (Pt 4), pp.844–857.

Caplan A. I. (2017). Mesenchymal Stem Cells: Time to Change the Name! *Stem cells translational medicine*, 6(6), 1445–1451. doi:10.1002/sctm.17-0051

Carstairs, A. (2017). *Development of in vitro skeletal disease models using CRISPR/Cas9 genome editing in immortalised mesenchymal stem cells*. PhD, University of York.

Catalano, M. and O'Driscoll, L. (2020). Inhibiting extracellular vesicles formation and release: a review of EV inhibitors. *Journal of extracellular vesicles*, 9 (1), p.1703244.

Chellaiah, A. T. et al. (1994). Fibroblast growth factor receptor (FGFR) 3. Alternative splicing in immunoglobulin-like domain III creates a receptor highly specific for acidic FGF/FGF-1. *Journal of Biological Chemistry*, 269 (15), pp.11620–11627. [Online]. Available at: doi:10.1016/s0021-9258(19)78170-8.

Chen, C. S. et al. (1997). Geometric control of cell life and death. *Science*, 276 (5317), pp.1425–1428.

Chen, E. Y. et al. (2013). Enrichr: interactive and collaborative HTML5 gene list enrichment analysis tool. *BMC bioinformatics*, 14, p.128.

Chen, Y. and Gridley, T. (2013). Compensatory regulation of the Snai1 and Snai2 genes during chondrogenesis. *Journal of bone and mineral research: the official journal of the American Society for Bone and Mineral Research*, 28 (6), pp.1412–1421.

Chuang, P.-T., Kawcak, T. 'nay and McMahon, A. P. (2003). Feedback control of mammalian Hedgehog signaling by the Hedgehog-binding protein, Hip1, modulates Fgf signaling during branching morphogenesis of the lung. *Genes & development*, 17 (3), pp.342–347.

Collins, C. and Nelson, W. J. (2015). Running with neighbors: coordinating cell migration and cell-cell adhesion. *Current opinion in cell biology*, 36, pp. 62–70.

Dale, J. K. et al. (2006). Oscillations of the snail genes in the presomitic mesoderm coordinate segmental patterning and morphogenesis in vertebrate somitogenesis. *Developmental cell*, 10 (3), pp.355–366.

Delezoide, A. L. et al. (1998). Spatio-temporal expression of FGFR 1, 2 and 3 genes during human embryo-fetal ossification. *Mechanisms of development*, 77 (1), pp.19–30.

Deng, C. et al. (1996). Fibroblast Growth Factor Receptor 3 Is a Negative Regulator of Bone Growth. *Cell*, 84 (6), pp.911–921. [Online]. Available at: doi:10.1016/s0092-8674(00)81069-7.

Dieci, M. V. et al. (2013). Fibroblast growth factor receptor inhibitors as a cancer treatment: from a biologic rationale to medical perspectives. *Cancer discovery*, 3 (3), pp.264–279.

Dries, R. et al. (2020). Cell Proliferation and Collective Cell Migration During Zebrafish Lateral Line System Development Are Regulated by Ncam/Fgf-Receptor Interactions. *Frontiers in cell and developmental biology*, 8, p.591011.

Elfenbein, A. et al. (2012). Syndecan 4 regulates FGFR1 signaling in endothelial cells by directing macropinocytosis. *Science signaling*, 5(223), p. ra36.

Eswarakumar, V. P., Lax, I. and Schlessinger, J. (2005). Cellular signaling by fibroblast growth factor receptors. *Cytokine & growth factor reviews*, 16(2), pp. 139–149.

Floss, T., Arnold, H. H. and Braun, T. (1997). A role for FGF-6 in skeletal muscle regeneration. *Genes & development*, 11(16), pp. 2040–2051.

Frutos, C. A. de et al. (2007). Snail1 Is a Transcriptional Effector of FGFR3 Signaling during Chondrogenesis and Achondroplasias. *Developmental Cell*, 13 (6), pp.872–883. [Online]. Available at: doi:10.1016/j.devcel.2007.09.016.

Graves, L. E. et al. (2004). Proinvasive properties of ovarian cancer ascites-derived membrane vesicles. *Cancer research*, 64(19), pp. 7045–7049.

Helsten, T. et al. (2016). The FGFR Landscape in Cancer: Analysis of 4,853 Tumors by Next-Generation Sequencing. *Clinical cancer research: an official journal of the American Association for Cancer Research*, 22(1), pp. 259–267.

Horwitz, E. M., Gordon, P. L. and Koo, W. K. K. (2002). Isolated allogeneic bone marrow-derived mesenchymal cells engraft and stimulate growth in children with osteogenesis imperfecta: Implications for cell therapy of bone. *Proceedings of the National Academy of Sciences of the United States of America*, 99(13), pp. 8932-8937.

Hou, S. et al. (2007). The secreted serine protease xHtrA1 stimulates long-range FGF signaling in the early Xenopus embryo. *Developmental cell*, 13(2), pp. 226–241.

Hughes, S. E. (1997). Differential Expression of the Fibroblast Growth Factor Receptor (FGFR) Multigene Family in Normal Human Adult Tissues. *Journal of Histochemistry & Cytochemistry*, pp. 1005–1019.

Hunter, A. G. et al. (1998). Medical complications of achondroplasia: a multicentre patient review. *Journal of medical genetics*, 35(9), pp. 705–712.

Inada, M. et al. (2004). Critical roles for collagenase-3 (Mmp13) in development of growth plate cartilage and in endochondral ossification. *Proceedings of the National Academy of Sciences of the United States of America*, 101(49), pp. 17192–17197.

James, S. et al. (2015). Multiparameter Analysis of Human Bone Marrow Stromal Cells Identifies Distinct Immunomodulatory and Differentiation-Competent Subtypes. *Stem cell reports*, 4(6), pp. 1004–1015.

Ji, H. et al. (2014). Deep sequencing of RNA from three different extracellular vesicle (EV) subtypes released from the human LIM1863 colon cancer cell line uncovers distinct miRNA-enrichment signatures. *PloS one*, 9(10), e110314. doi:10.1371/journal.pone.0110314

Kanehisa, M. and Sato, Y. (2020). KEGG Mapper for inferring cellular functions from protein sequences. *Protein science: a publication of the Protein Society*, 29 (1), pp.28–35.

Kato, M. et al. (1998). Physiological degradation converts the soluble syndecan-1 ectodomain from an inhibitor to a potent activator of FGF-2. *Nature medicine*, 4(6), pp. 691–697.

Kiani, C. et al. (2002). Structure and function of aggrecan. *Cell research*, 12 (1), pp.19–32.

Kim, S.-Y. et al. (2012). Mesenchymal stem cell-conditioned media recovers lung fibroblasts from cigarette smoke-induced damage. *American journal of physiology. Lung cellular and molecular physiology*, 302 (9), pp.L891–L908.

Kondo, T. et al. (2007). Epigenetically controlled fibroblast growth factor receptor 2 signaling imposes on the RAS/BRAF/mitogen-activated protein kinase pathway to modulate thyroid cancer progression. *Cancer research*, 67 (11), pp.5461–5470.

Kowal, J. et al. (2016). Proteomic comparison defines novel markers to characterize heterogenous populations of extracellular vesicle subtypes. *Proceedings of the National Academy of Sciences of the United States of America,* 113(8). [Online]. Available at: doi: 10.1073/pnas.1521230113.

Krakow, D. (2015). Skeletal dysplasias. *Clinics in perinatology*, 42(2), pp. 301–19, viii.

Kriebel, P. W. et al. (2018). Extracellular vesicles direct migration by synthesizing and releasing chemotactic signals. *The Journal of cell biology*, 217(8), pp. 2891–2910.

Kronenberg, H. M. (2004). Twist genes regulate Runx2 and bone formation. *Developmental cell*, 6 (3), pp.317–318.

Li, Z. et al. (2001). The myeloma-associated oncogene fibroblast growth factor receptor 3 is transforming in hematopoietic cells. *Blood*, 97 (8), pp.2413–2419.

Lin, X. et al. (1999). Heparan sulfate proteoglycans are essential for FGF receptor signaling during Drosophila embryonic development. *Development* , 126 (17),

pp.3715–3723.

Linsenmayer, T. F. et al. (1991). Collagen types IX and X in the developing chick tibiotarsus: analyses of mRNAs and proteins. *Development*, pp. 191–196. doi: 10.1242/dev.111.1.191.

Lötvall, J. et al. (2014). Minimal experimental requirements for definition of extracellular vesicles and their functions: a position statement from the International Society for Extracellular Vesicles. *Journal of extracellular vesicles*, 3, 26913. doi:10.3402/jev.v3.26913

Lu, P. et al. (2011). Extracellular Matrix Degradation and Remodeling in Development and Disease. *Cold Spring Harbor Perspectives in Biology*, 3 (12), pp.a005058–a005058. [Online]. Available at: doi:10.1101/cshperspect.a005058.

Majumdar, M. K. et al. (2000). Human marrow-derived mesenchymal stem cells (MSCs) express hematopoietic cytokines and support long-term hematopoiesis when differentiated toward stromal and osteogenic lineages. *Journal of hematotherapy & stem cell research*, 9(6), pp. 841–848.

Marolt Presen, D. et al. (2019). Mesenchymal Stromal Cell-Based Bone Regeneration Therapies: From Cell Transplantation and Tissue Engineering to Therapeutic Secretomes and Extracellular Vesicles. *Frontiers in bioengineering and biotechnology*, 7, p. 352.

Matsuo, Y. et al. (2009). CXCL8/IL-8 and CXCL12/SDF-1α co-operatively promote invasiveness and angiogenesis in pancreatic cancer. *International Journal of Cancer*, 124 (4), pp.853–861. [Online]. Available at: doi:10.1002/ijc.24040.

Mayor, R. and Etienne-Manneville, S. (2016). The front and rear of collective cell migration. *Nature Reviews Molecular Cell Biology*, 17 (2), pp.97–109. [Online]. Available at: doi:10.1038/nrm.2015.14.

McQuin, C. et al. (2018). CellProfiler 3.0: Next-generation image processing for biology. *PLoS biology*, 16 (7), p.e2005970.

Mejillano, M. R. et al. (2004). Lamellipodial Versus Filopodial Mode of the Actin Nanomachinery. *Cell*, 118 (3), pp.363–373. [Online]. Available at: doi:10.1016/j.cell.2004.07.019.

Meyer, M. et al. (2012). FGF receptors 1 and 2 are key regulators of keratinocyte migration in vitro and in wounded skin. *Journal of cell science*, 125(Pt 23), pp. 5690–5701.

Miki, T. et al. (1992). Determination of ligand-binding specificity by alternative splicing: two distinct growth factor receptors encoded by a single gene. *Proceedings of the National Academy of Sciences of the United States of America*, 89(1), pp. 246–250.

Mukherjee, A. et al. (2005). Co-ordination of TGF-β and FGF signaling pathways in bone organ cultures. *Mechanisms of Development*, 122 (4), pp.557–571. [Online]. Available at: doi:10.1016/j.mod.2004.11.006.

Murakami, S. et al. (2004). Constitutive activation of MEK1 in chondrocytes causes Stat1-independent achondroplasia-like dwarfism and rescues the Fgfr3-deficient mouse phenotype. *Genes & development*, 18 (3), pp.290–305.

Nauta, A. J. and Fibbe, W. E. (2007). Immunomodulatory properties of mesenchymal stromal cells. *Blood*, pp. 3499–3506. doi: 10.1182/blood-2007-02-069716.

Ng, L. J. et al. (1997). SOX9 binds DNA, activates transcription, and coexpresses with type II collagen during chondrogenesis in the mouse. *Developmental biology*, 183 (1), pp.108–121.

Nowroozi, N. et al. (2005). Sustained ERK1/2 but not STAT1 or 3 activation is required for thanatophoric dysplasia phenotypes in PC12 cells. *Human Molecular Genetics*, 14 (11), pp.1529–1538. [Online]. Available at: doi:10.1093/hmg/ddi161.

Ogata, K. et al. (2018). Secretomes of mesenchymal stem cells induce early bone regeneration by accelerating migration of stem cells. *Journal of Oral and Maxillofacial Surgery, Medicine, and Pathology*, 30(5), pp. 445–451.

Oka, K. et al. (2007). The role of TGF-beta signaling in regulating chondrogenesis and osteogenesis during mandibular development. *Developmental biology*, 303 (1), pp.391–404.

Ornitz, D. M. and Marie, P. J. (2015). Fibroblast growth factor signaling in skeletal development and disease. *Genes & Development*, pp. 1463–1486.

Osugi, M. et al. (2012). Conditioned media from mesenchymal stem cells enhanced bone regeneration in rat calvarial bone defects. *Tissue engineering. Part A*, 18(13-14), pp. 1479–1489.

Parri, M. and Chiarugi, P. (2010). Rac and Rho GTPases in cancer cell motility control. *Cell communication and signaling: CCS*, 8, p. 23.

Perantoni, A. O. et al. (2005). Inactivation of FGF8 in early mesoderm reveals an essential role in kidney development. *Development*, pp. 3859–3871. doi: 10.1242/dev.01945.

Peters, K. et al. (1993). Unique expression pattern of the FGF receptor 3 gene during mouse organogenesis. *Developmental biology*, 155 (2), pp.423–430.

Plotnikov, A. N. et al. (1999). Structural basis for FGF receptor dimerization and activation. *Cell*, 98 (5), pp.641–650.

Plowright, E. E. et al. (2000). Ectopic expression of fibroblast growth factor receptor 3 promotes myeloma cell proliferation and prevents apoptosis. *Blood*, 95 (3),pp.992–998.

Qi. X. et al. Exosomes Secreted by Human-Induced Pluripotent Stem Cell-Derived Mesenchymal Stem Cells Repair Critical-Sized Bone Defects through Enhanced Angiogenesis and Osteogenesis in Osteoporotic Rats. *Int J Biol Sci*, 12(7) p.836-49.

Qin. Y. et al. Bone marrow stromal/stem cell-derived extracellular vesicles regulate osteoblast activity and differentiation *in vitro* and promote bone regeneration in vivo. *Scientific Reports* 6(21961). doi:10.1038/srep.21961.

Raucci, A. et al. (2004). Activation of the ERK1/2 and p38 mitogen-activated proteinkinase pathways mediates fibroblast growth factor-induced growth arrest of chondrocytes. *The Journal of biological chemistry*, 279 (3), pp.1747–1756.

Reffay, M. et al. (2014). Interplay of RhoA and mechanical forces in collective cell migration driven by leader cells. *Nature cell biology*, 16 (3), pp.217–223.

Revest, J.-M. et al. (2001). Fibroblast Growth Factor Receptor 2-IIIb Acts Upstream of Shh and Fgf4 and Is Required for Limb Bud Maintenance but Not for the Induction of Fgf8, Fgf10, Msx1, or Bmp4. *Developmental Biology*, pp. 47–62. doi: 10.1006/dbio.2000.0144.

Rojas, M. et al. (2005). Bone Marrow–Derived Mesenchymal Stem Cells in Repair of the Injured Lung. *American journal of respiratory cell and molecular biology*, 33(2), pp. 145–152.

Rostovskaya, M. and Anastassiadis, K. (2012). Differential expression of surface markers in mouse bone marrow mesenchymal stromal cell subpopulations with distinct lineage commitment. *PloS one*, 7(12), p. e51221.

Rousseau, F. et al. (1994). Mutations in the gene encoding fibroblast growth factor receptor-3 in achondroplasia. *Nature*, pp. 252–254. doi: 10.1038/371252a0.

RStudio Team. (2020). *RStudio: Integrated Development for R*. [Online]. Available at: http://www.rstudio.com/.

Ryan, G. L. et al. (2017). Cell protrusion and retraction driven by fluctuations in actin polymerization: A two-dimensional model. *Cytoskeleton* , 74 (12), pp.490–503.

Safaei, R. et al. (2005). Abnormal lysosomal trafficking and enhanced exosomal export of cisplatin in drug-resistant human ovarian carcinoma cells. *Molecular cancer therapeutics*, 4(10), pp. 1595–1604.

Sagar, R. et al. (2018). Fetal Mesenchymal Stromal Cells: an Opportunity for Prenatal Cellular Therapy. *Current stem cell reports*, 4(1), pp. 61–68.

Sagaradze, G. et al. (2019). Conditioned Medium from Human Mesenchymal Stromal Cells: Towards the Clinical Translation. *International journal of molecular sciences*, 20 (7). [Online]. Available at: doi:10.3390/ijms20071656.

Sai, X. and Ladher, R. K. (2008). FGF signaling regulates cytoskeletal remodeling during epithelial morphogenesis. *Current biology: CB*, 18 (13), pp.976–981.

Schindelin, J. et al. (2012). Fiji: an open-source platform for biological-image analysis. *Nature methods*, 9 (7), pp.676–682.

Segura, E. et al. (2007). CD8+ dendritic cells use LFA-1 to capture MHC-peptide complexes from exosomes in vivo. *Journal of immunology* , 179(3), pp. 1489–1496.

Shabbir, A. et al. (2015). Mesenchymal Stem Cell Exosomes Induce Proliferation and Migration of Normal and Chronic Wound Fibroblasts, and Enhance Angiogenesis In Vitro. *Stem cells and development*, 24 (14), pp.1635–1647.

Shen, C. et al. (2015). Conditioned medium from umbilical cord mesenchymal stem cells induces migration and angiogenesis. *Molecular medicine reports*, 12 (1), pp.20–30.

Shimokawa, K. et al. (2011). Cell surface heparan sulfate chains regulate local reception of FGF signaling in the mouse embryo. *Developmental cell*, 21(2), pp.257–272.

Shung, C.-Y. et al. (2012). Disruption of a Sox9-β-catenin circuit by mutant Fgfr3 in thanatophoric dysplasia type II. *Human molecular genetics*, 21 (21), pp.4628–4644.

Siclari, V. et al. (2013). Mesenchymal progenitors residing close to the bone surface are functionally distinct from those in the central bone marrow. *Bone*, *53*(2), 575–586. https://doi.org/10.1016/j.bone.2012.12.013.

Stenderup et al. (2003). Aging is associated with decreased maximal lifespan and accelerated senescence of bone marrow stromal cells. *Bone*, 33(6), p.919-26.

Su, N. et al. (2010). Gain-of-function mutation in FGFR3 in mice leads to decreased bone mass by affecting both osteoblastogenesis and osteoclastogenesis. *Human molecular genetics*, 19 (7), pp.1199–1210.

Su, N., Jin, M. and Chen, L. (2014). Role of FGF/FGFR signaling in skeletal development and homeostasis: learning from mouse models. *Bone research*, 2, p. 14003.

Sun, J. and Stathopoulos, A. (2018). FGF controls epithelial-mesenchymal transitions during gastrulation by regulating cell division and apicobasal polarity. *Development* , 145 (19). [Online]. Available at: doi:10.1242/dev.161927.

Sun, X. et al. (2020). *Fgfr3* mutation disrupts chondrogenesis and bone ossification in zebrafish model mimicking CATSHL syndrome partially via enhanced Wnt/β-catenin signaling. *Theranostics*, 10 (16), pp.7111–7130.

Suraneni, P. et al. (2012). The Arp2/3 complex is required for lamellipodia extension and directional fibroblast cell migration. *The Journal of cell biology*, 197 (2), pp.239–251.

Szklarczyk, D. et al. (2019). STRING v11: protein-protein association networks with increased coverage, supporting functional discovery in genome-wide experimental datasets. *Nucleic acids research*, 47 (D1), pp.D607–D613.

Tapon, N. (1997). Rho, Rac and Cdc42 GTPases regulate the organization of the actin cytoskeleton. *Current Opinion in Cell Biology*, 9 (1), pp.86–92. [Online]. Available at: doi:10.1016/s0955-0674(97)80156-1.

Tauro, B. J. et al. (2013). Two distinct populations of exosomes are released from LIM1863 colon carcinoma cell-derived organoids. *Molecular & cellular proteomics*, 12(3), 587–598. doi:10.1074/mcp.M112.021303

Tavormina, P. L. et al. (1995). Thanatophoric dysplasia (types I and II) caused by distinct mutations in fibroblast growth factor receptor 3. *Nature genetics*, 9(3), pp. 321–328.

Tavormina, P. L. et al. (1999). A novel skeletal dysplasia with developmental delay and acanthosis nigricans is caused by a Lys650Met mutation in the fibroblast growth factor receptor 3 gene. *American journal of human genetics*, 64(3), pp. 722–731.

Ten Klooster, J. P. et al. (2006). Interaction between Tiam1 and the Arp2/3 complex links activation of Rac to actin polymerization. *Biochemical Journal*, 397 (1), pp.39–45.

Toydemir, R. M. et al. (2006). A novel mutation in FGFR3 causes camptodactyly, tall stature, and hearing loss (CATSHL) syndrome. *American journal of human genetics*, 79 (5), pp.935–941.

Tuli, R. et al. (2003). Transforming Growth Factor-β-mediated Chondrogenesis of Human Mesenchymal Progenitor Cells Involves N-cadherin and Mitogen-activated Protein Kinase and Wnt Signaling Cross-talk. *Journal of Biological Chemistry*, 278 (42), pp.41227–41236. [Online]. Available at: doi:10.1074/jbc.m305312200.

Turner, N. and Grose, R. (2010). Fibroblast growth factor signalling: from development to cancer. *Nature Reviews Cancer*, pp. 116–129. doi: 10.1038/nrc2780.

Valverde-Franco, G. et al. (2003). Defective bone mineralization and osteopenia in young adult FGFR3-/- mice. *Human Molecular Genetics*, pp. 271–284. doi: 10.1093/hmg/ddh034.

Venero Galanternik, M., Kramer, K. L. and Piotrowski, T. (2015). Heparan Sulfate Proteoglycans Regulate Fgf Signaling and Cell Polarity during Collective Cell Migration. *Cell reports*, 10 (3), pp.414–428.

Verheyden, J. M. et al. (2005). Conditional inactivation of Fgfr1 in mouse defines its role in limb bud establishment, outgrowth and digit patterning. *Development* , 132(19), pp. 4235–4245.

Vu, T. H. et al. (1998). MMP-9/Gelatinase B Is a Key Regulator of Growth Plate Angiogenesis and Apoptosis of Hypertrophic Chondrocytes. *Cell*, pp. 411–422. doi: 10.1016/s0092-8674(00)81169-1.

Wang, Q. et al. (2001). Differential regulation of endochondral bone growth and joint development by FGFR1 and FGFR3 tyrosine kinase domains. *Development* , 128 (19), pp.3867–3876.

Weil, B. R. et al. (2009). Mesenchymal stem cells enhance the viability and proliferation of human fetal intestinal epithelial cells following hypoxic injury via paracrine mechanisms. *Surgery*, 146 (2), pp.190–197.

Wickham, H. (2016). *ggplot2: Elegant Graphics for Data Analysis*. Springer.

Wilkie, A. (1997). Craniosynostosis: genes and mechanisms. *Human Molecular Genetics*, pp. 1647–1656. doi: 10.1093/hmg/6.10.1647.

Wöhrle, S. et al. (2011). FGF receptors control vitamin D and phosphate homeostasis by mediating renal FGF-23 signaling and regulating FGF-23 expression in bone. *Journal of bone and mineral research: the official journal of the American Society for Bone and Mineral Research*, 26(10), pp. 2486–2497.

Wysoczynski, M. et al. (2019). Pro-Angiogenic Actions of CMC-Derived Extracellular Vesicles Rely on Selective Packaging of Angiopoietin 1 and 2, but Not FGF-2 and VEGF. *Stem cell reviews and reports*, 15 (4), pp.530–542.

Xu, J. et al. (2016). Human fetal mesenchymal stem cell secretome enhances bone consolidation in distraction osteogenesis. *Stem cell research & therapy*, 7(1), pp. 1–12.

Xu, R., Greening, D. W., Zhu, H. J., Takahashi, N., & Simpson, R. J. (2016). Extracellular vesicle isolation and characterization: toward clinical application. *The Journal of clinical investigation*, 126(4), p.1152–1162. doi:10.1172.JCI81129.

Yamagishi, M. and Okamoto, H. (2010). Competition for ligands between FGFR1 and FGFR4 regulates Xenopus neural development. *The International journal of developmental biology*, 54 (1), pp.93–104.

Yan, D. and Lin, X. (2009). Shaping morphogen gradients by proteoglycans. *Cold Spring Harbor perspectives in biology*, 1(3), p. a002493.

Yáñez-Mó, M. et al. (2015). Biological properties of extracellular vesicles and their physiological functions. *J Extracell Vesicles*. 14(4) p.27066. doi: 10.3402/jev.v4.27066.

Yu, K. and Ornitz, D. M. (2008). FGF signaling regulates mesenchymal differentiation and skeletal patterning along the limb bud proximodistal axis. *Development*, pp. 483–491. doi: 10.1242/dev.013268.

Zhang, K. et al. (2013). The collagen receptor discoidin domain receptor 2 stabilizes SNAIL1 to facilitate breast cancer metastasis. *Nature cell biology*, 15 (6), pp.677–687.

Zhang, S. et al. (2016). Exosomes derived from human embryonic mesenchymal stem cells promote osteochondral regeneration. *Osteoarthritis and cartilage*, 24(12), 2135–2140. doi:10.1016/j.joca.2016.06.022.

Zimmermann, J. and Falcke, M. (2014). Formation of Transient Lamellipodia. *PLoS ONE*, 9 (2), p.e87638. [Online]. Available at: doi:10.1371/journal.pone.0087638.